Final Report

Geoid Recovery
using Geophysical Inverse Theory
Applied to Satellite to Satellite Tracking Data

NASA Contract NAS5-99123

Principal Investigator

E.M.Gaposchkin

August 2000

Mathematical Geosciences Inc.
Lexington MA 02421

Final Report

Geoid Recovery
using Geophysical Inverse Theory
Applied to Satellite to Satellite Tracking Data

NASA Contract NAS5-99123

Principal Investigator

E.M.Gaposchkin

August 2000

Mathematical Geosciences Inc.
Lexington MA 02421

Abstract

This report describes a new method for determination of the geopotential, or the equivalent geoid. It is based on Satellite-to-Satellite Tracking (SST) of two co-orbiting low earth satellites separated by a few hundred kilometers. The analysis is aimed at the GRACE Mission, though it is generally applicable to any SST data. It is proposed that the SST be viewed as a mapping mission. That is, the result will be maps of the geoid or gravity, as contrasted with determination of spherical harmonics or Fourier coefficients. A method has been developed, based on Geophysical Inverse Theory (GIT), that can provide maps at a prescribed (desired) resolution and the corresponding error map from the SST data. This computation can be done area by area avoiding simultaneous recovery of all the geopotential information. The necessary elements of potential theory, celestial mechanics, and Geophysical Inverse Theory are described, a computation architecture is described, and the results of several simulations presented. Centimeter accuracy geoids with 50 to 100 km resolution can be recovered with a 30 to 60 day mission.

Table of Contents

I   Introduction

This analysis is focused on the Gravity Recovery and Climate Experiment (GRACE) mission, to map the earth's gravity field, or geopotential. The GRACE mission concept was based on extensive experience with dynamic satellite geodesy, using well established methods and with the confidence based on very good results. Though there is no doubt that the existing methods will satisfy the mission requirements, we propose here an alternative methodology for analyzing the mission data that can provide a different type of result, some analysis advantages, and possibly lower analysis cost. The basic objective is to determine regional geoid maps, directly from the satellite-to-satellite (SST) tracking data, without recourse to global spherical harmonic solutions. Regional maps could be produced based on 30 to 60 days of mission data, allowing investigation of temporal changes with monthly variation.

This report lays out the methodology for this mapping analysis, providing the necessary elements of potential theory, orbital mechanics, and estimation theory. It is apparent that with 0.5 µ/sec SST data, centimeter accuracy geoid heights, with 50 to 100 km spatial resolution and monthly temporal resolution, can be recovered. Though, there are still details to work out, this objective can be met.

The concept of a Satellite-to-Satellite Tracking (SST) mission is simply to calculate the gravitational force acting on a spacecraft from changes in its measured velocity. The satellite itself is the sensor, and its velocity, the observable. This is pictured notionally as follows. Consider a satellite in orbit around the earth approaching a region of excess mass. As the satellite approaches, it is accelerated toward the mass, and after passing the mass, it is decelerated. By measuring the time history of the velocity variation, an estimate of the magnitude and position of the mass excess can be deduced. Or course, the actual situation is much more complex for several reasons: the structure of the earth's mass distribution is very complicated, other forces act on the satellite, only one component of the satellite velocity is measured from another satellite, and the observations contain errors. In the SST concept, the second satellite could be very high, say in geosynchronous orbit or on another planet – the high-low configuration. Alternatively, the second satellite could be in the same low orbit, trailing the first low satellite – the low-low configuration. In the low-low case, the second satellite would experience similar velocity changes, but at a later time.

SST tracking has been realized in a number of missions. The earliest example of Doppler tracking a satellite from a point not on the body being studied is the mapping of the lunar gravity field by means of lunar orbiters tracked from the earth [*Muller and Sjogren*, (1968)]. Since this remarkable success, there have been notable Doppler tracking experiments for earth satellites: the tracking of Geos-3 from the ATS geosynchronous satellite. These are examples of the high-low configuration. There have since been numerous examples of tracking around Mars, Venus, and Eros: also examples of the high-low configuration.

A number of analytical strategies have been employed. The most common is to treat the

-3-

SST data in the same way as other tracking data, and determine spherical harmonic coefficients of the body under consideration by variants of the method of least squares: an estimation problem in a finite-dimensional vector space of parameters. There are significant computational issues with global solutions [*Bettadpur et al.*, (1992)]. In any case, these solutions would benefit from the high accuracy of the SST tracking data, but do not make any use of the unique geometry of the SST data. These ideas have been applied to estimating gravity anomalies [*Vonbun et al.*, (1978)]. Alternatively, the analysis can be done as a mapping of the acceleration field at the satellite's altitude [*Muller and Sjogren*, (1968)]. Studies have also been done on mapping the acceleration of potential at the earth's surface [*Colombo*, (1981) ; *Rummel*, (1975) ; *Rummel et al.*, (1978)]. Studies of recovery of fourier coefficients at satellite altitude have also been made [*Kaula*, (1982)].

The analysis described in the sequel employs a generalized inverse theory (GIT) [*Backus and Gilbert*, (1967) ; *Backus and Gilbert*, (1968) ; *Backus and Gilbert*, (1970) ; *Backus*, (1968)] to convert the observed velocity measurements to a mapping of surface values of geoid height. The ill-posed boundary-value problem and the unstable downward-continuation problem [*Bullard and Cooper*, (1948a)] are addressed in a way that the additional assumptions used to obtain the solutions are clearly identified and an error estimate is found. On the way to this end, a semi-analytical solution of the problem of calculating satellite perturbations caused by the anomalous potential will be formulated. Such a solution provides insight into the proposed measurement mapping, and significant computational economies. It gives a direct way to calculate analytically partial derivatives for the observable (velocity) with respect to the desired end product (the geoid). The analytical solution also allows the kernel function in the generalized inversion to be calculated directly.

II   Background

It is seen to be obligatory in this section to provide a prolix, far ranging, penetrating, and relevant review of the scientific objectives and uses of the analysis to be described in the sequel as well as a similar critical -- in the classical sense -- review of the past work. Since there are a number of carefully written reports available,[*anon.*, (1979); *anon.*, (1997); *Kaula*, (1970); *Nerem et al.*, (1995 Aug 10)] this discussion will be limited to a few remarks on the method.

Before, October 4, 1957, individual surface gravity measurements were made and essentially local gravity or geoid maps produced. Attempts to produce global gravity, or geoid, models from these data produced rather simple ones. Tracking of artificial earth satellites very soon produced significant improvement in knowledge of the global gravity field. The difference was that satellites provided a global sensor, that allowed measurement of large scale features of the geoid. In the succeeding years, analysis of tracking data has produced remarkable results, all based on using the integrating property of satellite motion. Combining the large scale information, from satellite tracking, with the small scale information from surface measurements -- surface gravity or more recently satellite altimetry -- has produced combined models of remarkable resolution and accuracy. This has required development and refinement of algorithms and orbit computation methods for determination of spherical harmonic representations, which will be referred to as classical satellite geodesy..

Satellites provided two significant advantages. First, orbital motion samples large scale, long wavelength, features of the geoid. Second, satellites can quickly sample the geoid everywhere. The idea that a satellite samples the geoid everywhere was first dramatically shown, not for the earth, but for the moon by Muller and Sjorgen [*Muller and Sjogren*, (1968)] with observation of MASCON's. Though the geometry is quite different -- the lunar orbiter was observed from the earth where this analysis has two co-orbiting earth satellites, one tracking the other -- the principle is the same: viz that instantaneous relative velocity changes are due to the difference in potential of the two satellites. So, to proceed in a rigorous way, one needs a mathematical formalism for: a) the potential mapping, b) the relation between potential and satellite velocity, and c) an estimation procedure. The estimation procedure chosen, Geophysical Inverse Theory Spectral Expansion Method (GITSEM), seems to make fewer assumptions about the form of the model, defining representation basis functions derived only from the observation geometry. It also provides a rigorous method of solving the downward continuation problem. The end result is intended to be a direct mapping of the satellite-to-satellite (SST) tracking measurement to geoid maps -- the choice of geoid maps or gravity anomalies being quite arbitrary. The method can be used for any size map, including a global one, though in this case there seems to be little advantage of the method compared with a spherical harmonic expansion. In addition, a rigorous error estimate is also available.

The view represented in this analysis, is to build on the results already available from classical satellite geodesy geopotential solutions. At present our knowledge of the low degree and order terms in the spherical harmonic model of the geopotential is quite good. We will

assume that up to a certain degree and order, a reference field can be adopted. In fact, the theory and implementation allows one to calculate local corrections to this model if needed. For example, in this analysis a reference field to degree and order 40 and another to degree and order 90 were used. The derived map is then a correction to this reference model.

III   Elements of Potential Theory

The underlying mathematical framework of Geophysical Inverse Theory is based on potential theory. There are two facets of this discussion: 1) The solution of the boundary value problem in Geodesy, and 2) The downward continuation problem. There is an extensive literature on both of these topics ([*Heiskanen and Moritz*, (1967); *Jekeli*, (1981); *Moritz*, (1980,1989)]), and so we limit ourselves to a few remarks to define the notation and relations used in this analysis.

From classical potential theory [*Kellog*, (1953)], the geopotential, $\Psi(r,\varphi,\lambda)$, – depending on the spherical coordinates r, the distance from the origin i.e. the center of mass of the earth, φ, the geocentric latitude measured from the equator, and λ, the longitude measured from an arbitrary point on the equator [*IAU*, (1983)] – is harmonic in free space, i.e. is a solution of Laplaces equation in three dimensional space exterior to all attracting masses, has continuous second derivatives, and is regular at r=∞. Therefore, Ψ is analytic. There are a number of issues of principle concerning other masses (the earth's atmosphere, The Sun, Moon, planets, galaxies etc.) that we treat with various approximations, viz, the atmosphere is modeled as an equivalent surface layer, the sun, moon, and planets are moved to ∞ by removing their tidal potential, and the remainder of the universe is regarded has having a negligible effect. Therefore, given the values of the potential everywhere on a known surface enclosing all the earth's attracting masses (the Dirichlet boundary value problem), Ψ is uniquely determined everywhere outside that surface.

If we chose the surface to be a sphere of radius R, centered at the earths center of mass, then Ψ is given by Poissons Integral Formula [*Heiskanen and Moritz*, (1967), p35; *Jeffreys and Jeffreys*, (1956,p221)]

$$\Psi(r,\varphi,\lambda) = \frac{R(r^2 - R^2)}{4\pi} \int_{\lambda=0}^{2\pi} \int_{\varphi'=-\pi/2}^{\pi/2} \frac{\Psi(R,\varphi',\lambda')\cos\varphi' d\varphi' d\lambda'}{\rho^3} \tag{3.1}$$

where, ρ, the distance from the integration point on the sphere (R,φ',λ') to the sample point (r,φ,λ) is given by

$$\rho^2 = r^2 + R^2 - 2rR\cos\psi \tag{3.2}$$

and
$$\cos\psi = \sin\varphi\sin\varphi' + \cos\varphi\cos\varphi'\cos(\lambda - \lambda')_1 \tag{3.3}$$

---

[1]N.B. We have written these expressions in terms of the latitude, φ, whereas they are often written in terms of the colatitide, $\theta=\pi/2-\varphi$. In this report we will freely use both conventions, strictly adhering to this notation.

For example, R can be chosen to be: a) just below a satellite orbit, or b) small enough to just enclose all the attracting mass (6384403m).

Poissons Integral Formula makes no assumption about the mathematical form of Ψ, only that it be harmonic and regular at infinity. However for both theoretical and practical applications, much use is made of spherical harmonics: solutions of Laplaces equation by separation of variables. Now Laplaces equation in spherical coordinates is:

$$r^2 \frac{\partial^2 \Psi}{\partial r^2} + 2r \frac{\partial \Psi}{\partial r} + \frac{\partial^2 \Psi}{\partial \varphi^2} - \tan \varphi \frac{\partial \Psi}{\partial \varphi} + \frac{1}{\cos^2 \varphi} \frac{\partial^2 \Psi}{\partial \lambda^2} = 0 . \tag{3.4}$$

Assume than one can write Ψ as:

$$\Psi = R(r)P(\varphi)\Gamma(\lambda) . \tag{3.5}$$

Introducing the constants $n(n+1)$ and m^2 (m and n turn out to be integers) we find:

$$R(r) = \begin{vmatrix} r^n \\ r^{-(n-1)} \end{vmatrix} , \tag{3.6}$$

$$P(\phi) = P_{nm}(\sin \varphi) \tag{3.7}$$

the ubiquitous Legendre functions, and

$$\Gamma(\lambda) = \begin{vmatrix} \cos m\lambda \\ \sin m\lambda \end{vmatrix} . \tag{3.8}$$

Conventional usage is to call n the degree of the Legendre function and m the order of the Legendre function. The combination $P_{nm}(\sin \varphi)\begin{vmatrix} \cos m\lambda \\ \sin m\lambda \end{vmatrix}$ are sometimes referred to as surface

spherical harmonics and $\begin{vmatrix} r^n \\ 1/r^{n+1} \end{vmatrix} \begin{vmatrix} P_{nm}(\sin \varphi)\begin{vmatrix} \cos m\lambda \\ \sin m\lambda \end{vmatrix}\end{vmatrix}$ are sometimes referred to as solid

spherical harmonics. It has also common to denote the surface harmonics as:

$$Y_{nm} = P_{nm}(\sin \varphi)\begin{vmatrix} \cos m\lambda \\ \sin m\lambda \end{vmatrix} \tag{3.9}$$

The functions Y_{nm} are orthogonal. That is when integrated over the sphere:

$$\iint_\sigma \begin{vmatrix} P_{nm}(\sin \varphi)\cos m\lambda P_{sr}(\sin \varphi)\cos m\lambda d\sigma = 0 \\ P_{nm}(\sin \varphi)\sin m\lambda P_{sr}(\sin \varphi)\sin m\lambda d\sigma = 0 \\ P_{nm}(\sin \varphi)\cos m\lambda P_{sr}(\sin \varphi)\sin m\lambda d\sigma = 0 \end{vmatrix} \begin{cases} s \neq n, or, r \neq m \\ s \neq n, or, r \neq m \\ always \end{cases} \tag{3.10}$$

with

$$d\sigma = \cos \varphi d\varphi d\lambda \tag{3.11}$$

It is convenient to define fully normalized Legendre functions $\overline{P}_{nm}(\sin \varphi)$ such that the integral

-8-

over the sphere is:

$$\iint_\sigma \left(\overline{P}_{nm}(\sin \varphi) \begin{vmatrix} \cos m\lambda \\ \sin m\lambda \end{vmatrix} \right)^2 d\sigma = 4\pi. \tag{3.12}$$

We have:

$$\overline{P}_{nm}(\sin \varphi) \begin{vmatrix} \cos m\lambda \\ \sin m\lambda \end{vmatrix} = \sqrt{(2 - \delta_{m0})(2n+1)\frac{(n-m)!}{(n+m)!}} P_{nm}(\sin \varphi) \begin{vmatrix} \cos m\lambda \\ \sin m\lambda \end{vmatrix} \tag{3.13}$$

with the familiar Dirac Delta function $\delta_{nm} = \begin{vmatrix} 0 \begin{cases} n \neq m \\ 1 \begin{cases} n = m \end{cases} \end{cases} \end{vmatrix}$. Formulae for calculation of $P_{nm}(\sin\varphi)$

can be found books on Mathematical Physics and Physical Geodesy. Great care must be given to accurate calculation for high degree and order functions and their derivatives.

It is easy to see that outside a sphere of radius R, enclosing all attracting masses, the most general solution, that is regular at ∞, can be written:

$$\Psi(r,\varphi,\lambda) = \frac{GM}{r} \sum_{n=0}^{\infty} \sum_{m=0}^{n} \left(\frac{R}{r}\right)^n \overline{P}_{nm}(\sin \varphi) \left[\overline{C}_{nm} \cos m\lambda + \overline{S}_{nm} \sin m\lambda \right], R \leq r \leq \infty. \tag{3.14}$$

where G is Newtons Gravitational Constant (6.67423 ± 0.00009 x 10^{-8} cm^3/(gram sec^2), and M is the mass of the solid earth, ocean, and atmosphere, GM=$3.98600.44177\pm0.0000000010$ x 10^{20} cm^3/sec^2. Now if, as supposed with Poissons Integral formula, Ψ is known everywhere on the sphere r=R enclosing all attracting mass, then $\Psi(R,\varphi,\lambda)$ can be represented in terms of a surface harmonic series given by (3.14). The determined geopotential coefficients -- $\overline{C}_{nm}, \overline{S}_{nm}$ - then provide the representation of Ψ everywhere outside R.

The downward continuation error (DCE) is usually framed in terms of this representation. The DCE arises from the need to know Ψ at or near the earth's surface, a point where r≤R, and (3.14) diverges. In principle, one can obtain a series, using spherical surface harmonics, that represents Ψ, provided one assumes knowledge of the attracting mass distribution above the sphere of radius r.

$$\Psi^-(r,\varphi,\lambda) = \frac{GM}{r} \sum_{n=0}^{\infty} \sum_{m=0}^{n} \overline{P}_{nm}(\sin \varphi) \left[\overline{C}_{nm}^-(r) \cos m\lambda + \overline{S}_{nm}^- \sin m\lambda \right], 0 \leq r \leq R \tag{3.15}$$

It must be emphasized that the resulting representation, Ψ^- has potential coefficients that depend on r – the distance from the earth center of mass to the desired point: e.g. the earth surface or geoid – i.e. $\left| \frac{\overline{C}_{nm}^-(r)}{\overline{S}_{nm}^-(r)} \right|_{,r \leq R}$ [Jekeli, (1981) ,p36]. This is **not** a representation in solid spherical harmonics, and that the coefficients in (3.14) and (3.15) are not comparable for r≤R. Other than a representation of the potential for r<R, given knowledge of the coefficients $\overline{C}_{nm}^-(r), \overline{S}_{nm}^-(r)$. it is unclear how to use this representation.

In the practical application of (3.14) to satellite orbits, the infinite sum is truncated to

terms $n \leq \bar{n}$ for two reasons, one practical – it is impossible to numerically perform an infinite sum – and the other fundamental. The measurement(s) to be analyzed are of finite accuracy, and there is a point where higher degree and order terms have no sensible affect, and are therefore ignored[2]. Therefore, no matter what data analysis techniques are used, e.g. satellite perturbation analysis or direct mapping of acceleration of potential difference, the resulting geopotential is smoothed, or averaged, usually characterized by the limiting degree of spherical harmonic representation, i.e. $\Psi^{\bar{n}}$.

$$\Psi^{\bar{n}}(r,\varphi,\lambda) = \frac{GM}{r} \sum_{n=0}^{\bar{n}} \sum_{m=0}^{n} \left(\frac{R}{r}\right)^n \bar{P}_{nm}(\sin\varphi)\left[\bar{C}_{nm}\cos m\lambda + \bar{S}_{nm}\sin m\lambda\right], R \leq r \leq \infty \tag{3.16}$$

There is also the partial sum of (3.15), i.e.:

$$\Psi^{\sim\bar{n}}(r,\varphi,\lambda) = \frac{GM}{r} \sum_{n=0}^{\bar{n}} \sum_{m=0}^{n} \bar{P}_{nm}(\sin\varphi)\left[\bar{C}_{nm}^{\sim}(r)\cos m\lambda + \bar{S}_{nm}^{\sim}\sin m\lambda\right], 0 \leq r \leq R \tag{3.17}$$

Now for $r \geq R$, a spherical harmonic coefficient representation of Ψ has two sorts of errors: 1) errors of commission, i.e. errors in the coefficients themselves, and 2) errors of omission, i.e. errors due to ignoring the higher degree and order coefficients. If we let the true geopotential be $\hat{\Psi}$, and the true geopotential truncated be $\hat{\Psi}^{\bar{n}}$ we can define the error of commission as:

$$\varepsilon_c\left(\Psi^{\bar{n}}\right) = \hat{\Psi}^{\bar{n}} - \Psi^{\bar{n}} \tag{3.18}$$

and the error of omission as:

$$\varepsilon_o\left(\Psi\right) = \hat{\Psi} - \hat{\Psi}^{\bar{n}} = \frac{GM}{r} \sum_{n=\bar{n}+1}^{\infty} \sum_{m=0}^{n} \left(\frac{R}{r}\right)^n \bar{P}_{nm}(\sin\varphi)\left[\bar{C}_{nm}\cos m\lambda + \bar{S}_{nm}\sin m\lambda\right], R \leq r \leq \infty \tag{3.19}$$

Now the error of commission is compounded by the present practice of evaluating (3.16), for r<R to obtain smoothed values at the earth's surface [*Bullard and Cooper*, (1948b)]. which is convergent everywhere. However, the errors in the coefficients are amplified by $(R/r)^n$ for each order. If we contemplate fields of degree 360, then the error amplification of the degree 360 terms for a geopotential representation derived from data on a satellite at 450km altitude would be $((6378+450)/6378)^{360} = 4.6\times10^{10}$. For degree 180 the amplification is only 2.14×10^4. Errors of commission will grow very dramatically. Though one expects the higher degree and order coefficients to be smaller than the lower degree ones, (Kaula's rule of thumb [*Kaula*, (1966)]), they are also more difficult of determine, and consequently the uncertainties will be larger.

Second, we have the representation error: the difference between (3.16) and (3.17):

$$\varepsilon_r\left(\hat{\Psi}\right) = \hat{\Psi}^{\bar{n}} - \overline{\Psi}^{\sim\bar{n}} \tag{3.20}$$

---

[2]This assumes that the size of higher degree and order terms – as measured, for example, by the degree variances – continue to decrease, as models suggest [*Kaula*, (1966)]

which depends on the degree and order of series truncation. In a careful and detailed analysis Jekeli, [*Jekeli*, (1981)] has shown two critical results. Jekeli combines the error of representation (3.20) and the error of omission (3.19 suitably generalized for r<R as 3.17) as the downward continuation error – the error of commission is not included. Jekeli, with $\bar{n} = 300$, finds (tables 3 and 4) that the DCE largest near the poles $\sigma(\varepsilon_r)$ <0.090 mgals (0.290 mgals max) gravity anomaly and $\sigma(\varepsilon_r)$ <0.042 cm (0.14 cm max) geoid height. Second, by seeking anomalies averaged over a spherical cap of about 1.4 degrees (tables 6 and 7), the DCE – again largest at the poles, is estimated to be $\sigma(\varepsilon_r)$ <0.004 mgals (0.014 mgals max) gravity anomaly and $\sigma(\varepsilon_r)$ <0.0020 cm (0.0066 cm max) geoid height. Therefore the conclusion of Jekeli [*Jekeli*, (1981), p127] "The downward continuation errors depicted in tables 3 through 7 are completely insignificant with respect to anticipated measurement accuracies of 1 mgal and 10 cm in the gravity anomaly and geoid undulation, respectively." And, " .. the estimation of point or mean gravity anomalies and geoid undulations (height anomalies) using the outer series expansion to degree 300 anywhere on the earth's surface is practically unaffected by the divergence of the total series." This issue was discussed again [*Wang*, (1997)] who confirms Jekeli's analysis: viz " .. , the method of smoothed analytical downward continuation can be used to determine the earth's gravitational potential to any required accuracy."

The basic potential theory formalism has been presented, and the relevant formulae defined for use in this analysis. The downward continuation error of commission is controlled by suitable averaging, which is inevitable given a finite spacing of the data and a finite number of observations. Therefore we adopt the earth equatorial radius (R=6378137 m) for the reference sphere. We see that the essential problem of downward continuation is controlling the growth of numerical error of commission. We turn to data analysis methods that provide tools for this.

IV   Orbital Theory

In discussing the recovery of gravity anomalies, Δg, or geoid heights, N, with SST data, it is convenient to have analytical formulae relating satellite position and velocity (the state vector) to the desired quantity. Such formulae also enable the sensitivity, or partial derivatives of gravity anomalies and geoid heights to be more easily obtained. Otherwise, one must resort to costly numerical methods, with consequent loss of generality and insight. With this motivation, we proceed on two levels. First, some simple illustrative relations are obtained. Then a more complete treatment will be developed, for use with the actual data analysis.

Consider, first, the theorem of conservation of energy for the satellite orbit. Of course, drag and radiation pressure perturbations would have to be taken into account if the following relationships were used for analysis of actual data. Let the total potential be represented by Ψ, which for convenience, can be separated into a reference potential, $\mu/r+U$, and an anomalous potential, T, i.e.

$$\Psi = \frac{\mu}{r} + U + T \tag{4.1}$$

In the conventional physical geodesy notation, U is the normal potential corresponding to that of a reference ellipsoid. However, here we prefer to view it as a reference, or adopted potential, with T being the remaining (unmodeled) part that we seek[3]. If we write the kinetic energy as $\frac{1}{2}mv^2$, with the vector components of velocity along track (v_u), cross track (v_W), and radial (v_S), then

$$\frac{1}{2}\left(v_S^2 + v_u^2 + v_W^2\right) + \Psi = \text{constant} \tag{4.2}$$

For a satellite with small eccentricity, we can treat the along track velocity as the unperturbed velocity, v_o, which gives $v_u=v_o+\delta v_u$, $v_S=\delta v_S$, and $v_W=\delta v_W$. Therefore, to first order in small quantities, we have

---

[3]Some confusion is bound to occur because the anomalous potential, or disturbing function, is generally denoted by R in celestial mechanics, and T in geodesy. Also the sign convention for potential in physics is reversed from that in celestial mechanics and geodesy. Here the force $\vec{F} = \nabla\Psi = m\dfrac{d^2\vec{x}}{dt^2}$. Finally, for convenience in this section, we refer to the product GM=μ.

$$\delta v_u = T\!\!\Big/\!\!v_o \; .$$

(4.3)

This formula was first derived by Wolf [*Wolf*, (1969)] and subsequently used by many others. For small eccentricity satellites, equation (4.3) gives the change in along track velocity as a function of the potential in space (i.e. position and time) to about 10%, the errors arising from the change in radial distance owing to T interacting with $\mu/r+U$. Equation (4.3) is a direct mapping to the potential into the along track velocity, and could be used as a first approximation for inverting observations of δv_T to determine T.

For a more complete theory, following the treatment in Brouwer and Clemence [*Brouwer and Clemence*, (1961)], using the potential, Ψ, we can write the equations of motion as

$$\frac{d^2x}{dt^2} + \mu\frac{x}{r^3} = \frac{\partial(U+T)}{\partial x}$$

$$\frac{d^2y}{dt^2} + \mu\frac{y}{r^3} = \frac{\partial(U+T)}{\partial y}$$

$$\frac{d^2z}{dt^2} + \mu\frac{x}{r^3} = \frac{\partial(U+T)}{\partial z}$$

(4.4)

where $\mu = GM \approx 3.986 \times 10^{20}$ cm^{3}sec^{-2} and

$$r^2 = x^2 + y^2 + z^2$$

(4.5)

If the coordinates are r, u, and φ, where the longitude from the equator crossing in the orbit plane is $u=f+\omega$, (true anomaly, f, plus argument of perigee, ω), and φ is the latitude[4] then the equivalent differential equations of motion are:

$$\frac{d^2r}{dt^2} - r\cos^2\varphi\left(\frac{du}{dt}\right)^2 - r\left[\frac{d\varphi}{dt}\right]^2 + \frac{\mu}{r^2} = \frac{\partial(U+T)}{\partial r}$$

$$\frac{d}{dt}\left(r^2\cos^2\varphi\frac{du}{dt}\right) = \frac{\partial(U+T)}{\partial u}$$

(4.6)

$$\frac{d}{dt}\left(r^2\frac{d\varphi}{dt}\right) + r^2\sin\varphi\cos\varphi\left(\frac{du}{dt}\right)^2 = \frac{\partial(U+T)}{\partial\varphi}$$

---

[4]The derivation is general. Below, the orbit plane will be used as a reference, and perturbations in along track (δu), cross track (δw) and radius (δr) will be developed. In this case the latitude, φ, will become the cross track, w, component.

-13-

To obtain an expression for the potential, U+T, as a function of position (and time), we begin by assuming that the potential on the earth's surface at r=R is $(U+T)_{\text{ten}}(R,\varphi,\lambda)$, where R is the radius of the earth and λ is the longitude. To express T in an inertial system appropriate for equation (4.4) or (4.6), we have $(U+T)_{\text{inert}}(R,\varphi,\lambda-\hat{\theta}(t))$, where $\hat{\theta}(t)$ is the sidereal angle at the time in question. For the moment we ignore the effects of a moving equator [*Gaposchkin*, (1973)].

Following the discussion in section III, since $(U+T)(R,\varphi,\lambda)$ given on a sphere is the Dirichlet boundary condition for Laplace's equation external to the sphere r=R, we can use the basic results from potential theory to obtain T at any point in space outside this sphere, see section III. Therefore we can expand T in terms of orthonormal base functions (associated Legendre polynomials) as

$$(U+T)(R,\varphi,\lambda) = \frac{GM}{R}\sum_{n=2}^{n=\infty}\sum_{m=0}^{m=n}\overline{P}_{nm}(\sin\varphi)\left[\overline{C}_{nm}\cos m\lambda + \overline{S}_{nm}\sin m\lambda\right] \qquad (4.7)$$

which, using the properties of solutions of Laplace's equation in spherical harmonics, can be upward continued as

$$(U+T)(r,\varphi,\lambda) = \frac{GM}{r}\sum_{n=2}^{n=\infty}\sum_{m=0}^{m=n}\left(\frac{R}{r}\right)^{n}\overline{P}_{nm}(\sin\varphi)\left[\overline{C}_{nm}\cos m\lambda + \overline{S}_{nm}\sin m\lambda\right] \qquad (4.8)$$

Alternatively, since U+T is harmonic in space, we can use Poission's integral to obtain

$$(U+T)(r,\varphi,\lambda) = \frac{R(r^{2}-R^{2})}{4\pi}\int_{\lambda'=0}^{2\pi}\int_{\varphi'=-\pi/2}^{\pi/2}\frac{(U+T)(R,\varphi',\lambda')}{\rho^{3}}\cos\varphi'\,d\varphi'\,d\lambda' \qquad (4.9)$$

where ρ is the distance between the integration point R,φ',λ' and the sample point r,φ,λ; it is often written as

$$\rho^{2} = r^{2} + R^{2} - 2rR\cos\psi \qquad (4.10)$$

ψ being the central angle, which can be expressed

$$\cos\psi = \sin\varphi\cos\varphi'| + \cos\varphi\cos\varphi'\cos(\lambda-\lambda') . \qquad (4.11)$$

Now, assume the motion of the satellite is given in two parts: i.e.

$$x = x_o + \delta x$$

$$y = y_o + \delta y \tag{4.12}$$

$$z = z_o + \delta z$$

where x_o, y_o, and z_o satisfy

$$\frac{d^2 x_o}{dt^2} + \mu \frac{x_o}{r_o^3} = \frac{\partial U}{\partial x_o}$$

$$\frac{d^2 y_o}{dt^2} + \mu \frac{y_o}{r_o^3} = \frac{\partial U}{\partial y_o} \tag{4.13}$$

$$\frac{d^2 z_o}{dt^2} + \mu \frac{z_o}{r_o^3} = \frac{\partial U}{\partial z_o}$$

and $r = r_o + \delta r$. We also have

$$d(U + T) = \frac{\partial(U + T)}{\partial x} dx + \frac{\partial(U + T)}{\partial y} dy + \frac{\partial(U + T)}{\partial z} dz$$

$$d(U + T) = \frac{\partial(U + T)}{\partial r} dr + \frac{\partial(U + T)}{\partial u} du + \frac{\partial(U + T)}{\partial \varphi} d\varphi \tag{4.14}$$

and

$$r \frac{\partial(U + T)}{\partial r} = x \frac{\partial(U + T)}{\partial x} + y \frac{\partial(U + T)}{\partial x} + z \frac{\partial(U + T)}{\partial x}. \tag{4.15}$$

Now, multiplying (4.4) by 2dx, 2dy, and 2dz respectively, adding, and integrating the result we have

$$\left(\frac{dx}{dt}\right)^2 + \left(\frac{dy}{dt}\right)^2 + \left(\frac{dz}{dt}\right)^2 - \frac{2\mu}{r} + \frac{\mu}{a} = 2 \int d(U + T) \tag{4.16}$$

where μ/a is an arbitrary constant of integration. This is chosen such that

$$\left(\frac{dx_o}{dt}\right)^2 + \left(\frac{dy_o}{dt}\right)^2 + \left(\frac{dz_o}{dt}\right)^2 - \frac{2\mu}{r_o} + \frac{\mu}{a} = 2 \int dU \tag{4.17}$$

is satisfied. In terms of polar coordinates (4.16) becomes

$$\left(\frac{dr}{dt}\right)^2 + r^2 \cos^2 \varphi \left(\frac{du}{dt}\right)^2 + r^2 \left(\frac{d\varphi}{dt}\right)^2 - \frac{2\mu}{r} + \frac{\mu}{a} = 2\int d(U+T). \tag{4.18}$$

Again, multiplying (4.4) by x,y,and z respectively, adding, and using (4.15) we have

$$x\frac{d^2x}{dt^2} + y\frac{d^2y}{dt^2} + z\frac{d^2z}{dt^2} + \frac{\mu}{r} = r\frac{\partial(U+T)}{\partial r} \tag{4.19}$$

or in polar coordinates

$$r\frac{d^2r}{dt} - r^2 \cos^2 \varphi \left(\frac{du}{dt}\right)^2 - r^2 \left(\frac{d\varphi}{dt}\right)^2 + \frac{\mu}{r} = r\frac{\partial(U+T)}{dr}. \tag{4.20}$$

Adding (4.18) and (4.20) we have

$$\frac{1}{2}\frac{d^2r^2}{dt^2} - \frac{\mu}{r} + \frac{\mu}{a} = 2\int d(U+T) + r\frac{\partial(U+T)}{\partial r}. \tag{4.21}$$

Now using r=r$_o$+δr, and subtract the reference orbit

$$\frac{1}{2}\frac{d^2r_o^2}{dt^2} - \frac{\mu}{r_o} + \frac{\mu}{a} = 2\int dU + r\frac{\partial U}{\partial r_o} \tag{4.22}$$

to first order in small quantities δr and T we have

$$\frac{d^2(r_o\delta r)}{dt^2} + \frac{\mu}{r_o^3}r_o\delta r = 2\int dT + r_o\frac{\partial T}{\partial r} + \delta r\frac{\partial U}{\partial r} = Q_r. \tag{4.23}$$

We also have

$$\frac{d^2\delta x}{dt^2} + \frac{\mu}{r_o^3}\delta x = \frac{\partial T}{\partial x} + \mu\left(\frac{1}{r_o^3} - \frac{1}{r^3}\right)x = Q_x$$

$$\frac{d^2\delta y}{dt^2} + \frac{\mu}{r_o^3}\delta y = \frac{\partial T}{\partial y} + \mu\left(\frac{1}{r_o^3} - \frac{1}{r^3}\right)y = Q_y$$

$$\frac{d^2\delta z}{dt^2} + \frac{\mu}{r_o^3}\delta z = \frac{\partial T}{\partial z} + \mu\left(\frac{1}{r_o^3} - \frac{1}{r^3}\right)z = Q_z$$

(4.24)

Now, a solution to (4.23) and (4.24), due to Hansen, can be found ([*Brouwer and Clemence*, (1961)] chapter XIII) for the perturbations in radial (δr), along track (δu) and cross track (δw) and can be written:

$$\delta r = \int X \sin[f - f']df'$$

$$\delta u = \int\left[\int Y df - 2\frac{\delta r}{r}\right]df$$

$$dw = \int Z \sin[f - f']df'$$

(4.25)

where

$$X = \frac{r^3}{\mu p}Q_r = \frac{r^3}{\mu p}\left[2\int dT + r\frac{\partial T}{\partial r} + \delta r\frac{\partial U}{\partial r}\right]$$

$$Y = \frac{r^2}{\mu p}\frac{\partial T}{\partial u}$$

$$Z = \frac{r^2}{\mu p}\frac{\partial T}{\partial w}$$

(4.26)

where $\mu=GM=n_o^2 a_o^3$ and $p=a(1-e^2)$. Here, the integration variable is the true anomaly, f, but for practical numerical implementation, we will use time as the variable of integration, using

$$df = n\left(\frac{a}{r}\right)^2\sqrt{1-e^2}\,dt \approx ndt$$

(4.27)

In equation (4.26) we interpret dT as

$$dT = \frac{\partial T}{\partial r}dr + \frac{\partial T}{\partial u}du + \frac{\partial T}{\partial w}dw$$

(4.28)

-17-

i.e. the integral along the satellite path. Therefore $\int dT = \Delta T$, the difference in potential from a reference point on the orbit to the point of interest.

Now, we measure relative velocity, and can obtain the perturbation in velocity – in radial, across track, and along track direction – as:

$$\delta v_r = \frac{d}{dt}\delta r = \frac{n}{(1-e^2)^{3/2}}\left(\frac{a}{r}\right)^3\left\{\int_{f_o}^{f} X\cos(f-f')df'-X\sin(f-f_o)\right\}$$

$$\delta v_u = r\frac{d}{dt}\delta u = \frac{n}{(1-e^2)^{3/2}}\left(\frac{a}{r}\right)^3\left\{r\int_{f_o}^{f}Ydf-2\delta r\right\} \qquad (4.29)$$

$$\delta v_w = r\frac{d}{dt}\delta\varphi = \frac{n}{(1-e^2)^{3/2}}\left(\frac{a}{r}\right)^3\left\{\int_{f_o}^{f}Z\cos(f-f')df'-Z\sin(f-f_o)\right\}$$

For illustrative purposes, these expressions can be simplified for small eccentricity. Of course, in all numerical calculation, the full expressions (4.25) and (4.29) are used. The simplified expressions are:

$$X = \frac{1}{n^2a}\left[2\int dT + a\frac{\partial T}{\partial r} + \delta r\frac{\partial U}{\partial r}\right]$$

$$Y = \frac{1}{n^2a}\frac{\partial T}{\partial M} \qquad (4.30)$$

$$Z = \frac{1}{n^2a}\frac{\partial T}{\partial z}$$

Now

$$\delta r = \frac{2}{n^2a}\int X\sin(f-f')df' = \frac{2}{n^2a}\int\sin(f-f')\int dTdf' + \frac{1}{n^2}\int\left(\frac{\partial T}{\partial r} + \frac{\delta r}{a}\frac{\partial U}{\partial r}\right)\sin(f-f')df'$$

$$(4.31)$$

and

$$\delta v_r = n\left\{\int X\cos(M - M')dM' - X\sin(M - M_o)\right\}$$

$$\delta v_u = n\left\{\int YdM - 2\delta r\right\}$$

$$\delta v_w = na\left\{\int Z\cos(M - M')dM' - Z\sin(M - M_o)\right\} \qquad (4.32)$$

Equation (4.31) defines δr in terms of $(\delta r/a)(\partial U/\partial r)$, and can be solved by iteration, as $(\partial U/\partial r)$ is of the order 10^{-3}. Now we can rederive equation (4.3) using the second parts from equations (4.30) and (4.32)

$$\delta v_u = n\left(a\frac{1}{n^2 a^2}T - 2\delta r\right) = \frac{1}{na}T - 2n\delta r \qquad (4.33)$$

where we can make the identification $v_o = na$. Now the second term can be written

$$-n\delta r = -\frac{GM}{na^3}\delta r = -\frac{GM}{naa^2}\delta r = -\frac{GM}{v_o}\frac{\delta r}{a^2} = \frac{1}{v_o}\frac{d}{dr}\left(\frac{GM}{r}\right)\bigg|_{r=a}\delta r \qquad (4.34)$$

which is simply the change in velocity due to the perturbation, δr, with the central force term, as pointed out earlier.

We can now formulate the observable, $\Delta\dot\rho$. We have the satellites, P and Q, with position $\bar r_P, \bar r_Q$ and $\bar v_P, \bar v_Q$. The relative position between P and Q is

$$\bar\rho = \bar r_P - \bar r_Q, \qquad (4.35)$$

the distance between them is

$$\rho = \sqrt{\bar\rho \cdot \bar\rho}, \qquad (4.36)$$

and the relative velocity is

$$\dot\rho = \hat\rho \cdot (\bar v_P - \bar v_Q). \qquad (4.37)$$

Now, we suppose that we have a reference orbit, $\bar r_{Po}, \bar r_{Qo}, \bar v_{Po}, \bar v_{Qo}$, and the true orbit, $\bar r_P, \bar r_Q, \bar v_P, \bar v_Q$.

Figure 4.1   Geometry of Satellite Perturbations

The difference, or perturbation, to be modeled is $\delta\bar r_P, \delta\bar r_Q, \delta\bar v_P, \delta\bar v_Q$. Now consider the residual, or difference between the observed, assumed to be the true, relative velocity, and the relative velocity computed from the reference orbit

$$\Delta\dot\rho = \dot\rho - \dot\rho_o = \dot\rho - \hat\rho_o \cdot (\bar v_{Po} - \bar v_{Qo}) \qquad (4.38)$$
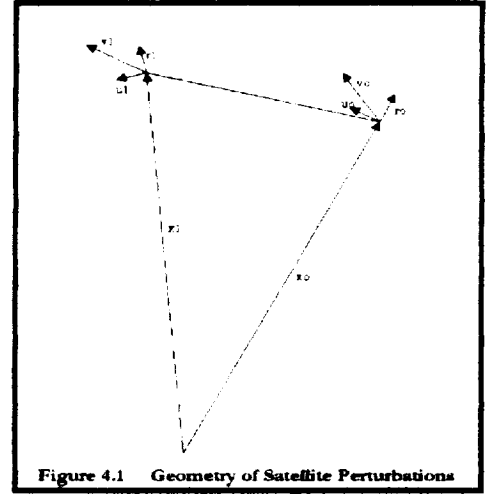
To define the algorithm for calculation of the perturbed position and velocity, $\bar{r}, \bar{v}$, from the unperturbed position and velocity, $\bar{r}_o, \bar{v}_o$, and the along track, δu, across track, δw, and radial perturbations, δr, (Figure 4.1).

We use the unit vectors

$$\hat{r} = \bar{r} \Big/ \sqrt{\bar{r} \cdot \bar{r}}$$

$$\hat{w} = \bar{r} \times \bar{v} \Big/ \sqrt{(\bar{r} \times \bar{v}) \cdot (\bar{r} \times \bar{v})} \qquad (4.39)$$

$$\hat{u} = \hat{w} \times \hat{r}$$

for the radial, cross track and along track directions. More precisely, the along track unit vector is normal to the radius vector, and not along the velocity vector, to be consistent with the definition of the along track perturbation. So we can write

$$\delta \frac{du}{dt} = \hat{u}_1 \cdot \bar{v}_1 - \hat{u}_o \cdot \bar{v}_o$$

$$\delta \frac{dw}{dt} = \hat{w}_1 \cdot \bar{v}_1 - \hat{w}_o \cdot \bar{v}_o \qquad (4.40)$$

$$\delta \frac{dr}{dt} = \hat{r}_1 \cdot \bar{v}_1 - \hat{r}_o \cdot \bar{v}_o$$

These relations lead to the perturbed velocity

$$\bar{v}_1 = \begin{bmatrix} \hat{u}_1 & \hat{w}_1 & \hat{r}_1 \end{bmatrix} \begin{bmatrix} \hat{u}_o^t \\ \hat{w}_o^t \\ \hat{r}_o^t \end{bmatrix} [\bar{v}_o] + \begin{bmatrix} \hat{u}_1 & \hat{w}_1 & \hat{r}_1 \end{bmatrix} \begin{bmatrix} \delta \dfrac{du}{dt} \\ \delta \dfrac{dw}{dt} \\ \delta \dfrac{dr}{dt} \end{bmatrix} \qquad (4.41)$$

Now, with two satellites (P,Q) at positions x_P and x_Q, the unperturbed satellite to satellite range ρ_o is

$$\rho_o = \sqrt{\left(\bar{x}_{Po} - \bar{x}_{Qo}\right) \cdot \left(\bar{x}_{Po} - \bar{x}_{Qo}\right)} \qquad (4.42)$$

from which we can obtain the unperturbed range rate

$$\frac{d\rho_o}{dt} = \dot{\rho}_o = \hat{\rho}_o \cdot \left(\dot{\bar{x}}_{Po} - \dot{\bar{x}}_{Qo} \right) \tag{4.42}$$

The corresponding perturbed range rate is

$$\hat{\rho}_1 = \hat{\rho}_1 \cdot \left(\dot{\bar{x}}_{P1} - \dot{\bar{x}}_{Q1} \right) \tag{4.42}$$

If we define

$$A_{Xi} = \begin{bmatrix} \hat{u}_{Xi} & \hat{w}_{Xi} & \hat{r}_{Xi} \end{bmatrix} \tag{4.43}$$

the perturbation in range rate, $\Delta\dot{\rho} = \dot{\rho}_1 - \dot{\rho}_o$, is

$$\Delta\dot{\rho} = \hat{\rho}_1 \cdot \left\{ A_{P1} A'_{Po} \dot{\bar{x}}_{Po} + A_{P1} \left[\delta u w r_P \right] - A_{Q1} A'_{Qo} \dot{\bar{x}}_{Qo} - A_{Q1} \left[\delta u w r_Q \right] \right\} - \hat{\rho}_o \cdot \left\{ \dot{\bar{x}}_{Po} - \dot{\bar{x}}_{Qo} \right\} \tag{4.44}$$

With this formalism, we give an example of this calculation. The full Cartesian equations of motion for perturbed (true) and unperturbed (reference) orbits are integrated, in this case with a 4th order Runge-Kutta integrator with variable step size error control, set at 10^{-16}, using 20 digit precision calculation. Both models include the quadrapole moment, J2. The twenty four equations of motion are integrated. The quadrature of (4.25) and (4.29) is done following the presumptive data to be obtained from the GRACE mission. We assume equal time spacing of the data, nominally 10 seconds, and use a modified Simpsons rule [*Hamming*, (1973)] quadrature formula. Using the unperturbed position and velocity, the six perturbation equations (4.25) and (4.29) are integrated. In fact the time spacing for the Simpsons rule was set to 1 sec, 2 sec, 5 sec, and 10 sec. The 10 sec quadrature interval had some error build up: for actual data analysis, the perturbations should be calculated with a 5 sec or smaller time step. This is not difficult, as the reference orbit can be obtained at any time resolution.

For illustrative purposes, two perturbing potential cases will be shown. The first, is a single geoid height anomaly in the subsatellite path, and the second is with two geoid height anomalies separated by 1 degree, ≈ 110 km, of equal size and opposite sign: a classical dipole. These will illustrate some important properties of the perturbations, to be used in developing the data analysis methods. Table 4.1 gives the initial orbit elements of the trajectories (the cartesian coordinates are used), and table 4.2 defines the anomalous potential.

Table 4.1 Initial Orbit Elements		
	Satellite P	Satellite Q
Epoch (MJD)	51478.000	51478.000
x (cm)	6.7743733337811697E+08	6.7743733337811697E+08
dx/dt (cm/sec)	-2.2620699340959200E+04	2.2620699340959200E+04
y (cm)	1.0462759319408060E+06	-1.0462759319408060E+06
dy/dt (cm/sec)	4.0121087168058562E+04	4.0121087168058562E+04
z (cm)	1.9964134070442688E+07	-1.9964134070442688E+07
dz/dt (cm/sec)	7.6555594831398176E+05	7.6555594831398176E+05
a (cm)	6.778E+08	6.778E+08
e	0.0001	0.0001
I (deg)	87.0	87.0
M (deg)	1.69	-1.69
Ω (deg)	0.0	0.0
ω (deg)	0.0	0.0

Table 4.2 Anomalous Potential				
Case	φ (deg)	λ (deg)	H (cm)	Size (km)
I	45.0	325.0	400.0	110.0
II	45.0	325.0	400.0	110.0
II	46.0	325.1	-400.0	110.0

Now, we let the unperturbed satellite position and velocity be $\bar{x}_{P_o}, \bar{v}_{P_o}$, and the

perturbed position and velocity be $\overline{x}_{P1}, \overline{v}_{P1}$. So in figure 4.2 we show the change in velocity[5],

$\delta v_P = v_{P1} - v_{Po}$ for satellite P for case I, and figure 4.3 shows the change in radius vector,

$\delta r_P = r_{P1} - r_{Po}$ for satellite P. These are obtained from numerical integration of the equations of motion. If the analytical theory for $\delta v_P, \delta r_P$ were plotted on the same graph, they would overlay the numerical result. Figure 4.4 shows the difference in the numerical and analytical theory for $\delta v_P, \delta r_P$. The rms difference between the numerical and

Figure 4.2

dv=vP1-vPo

Figure 4.3

dr=rP1-rPo

Figure 4.4

n*(dr[numerical]-dr[theory])

dv[numerical]-dv[theory]
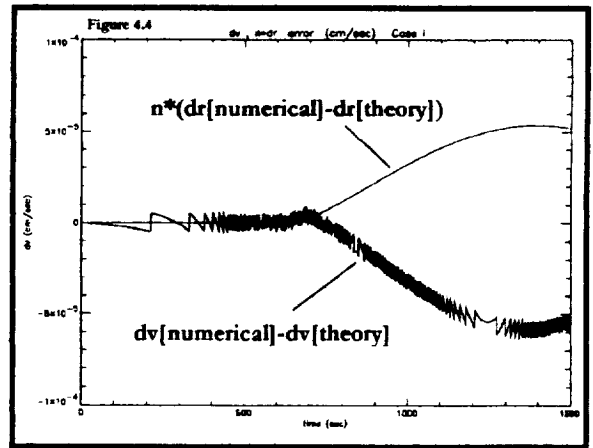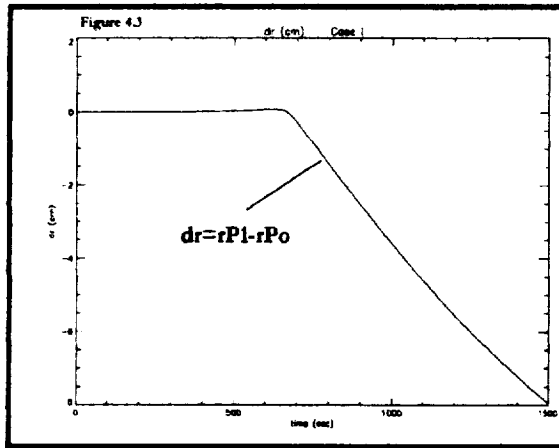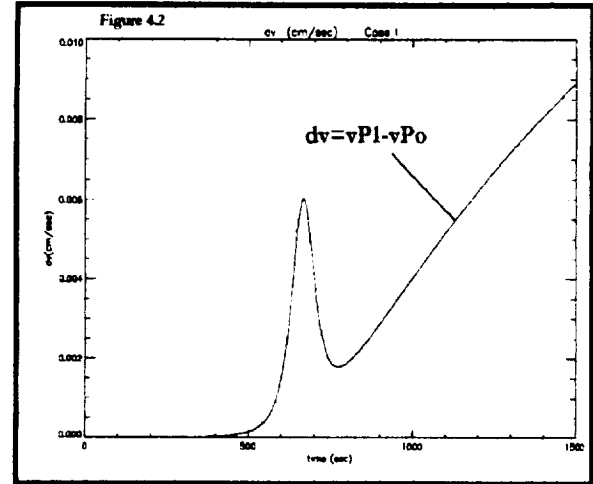
theoretical perturbations for the two curves is 2.4×10^{-5} (cm/sec) = 0.24 (μ/sec) and 0.019 cm. The long period structure in Figure 4.4 is an unmodeled interaction perturbation between δr and J2. With J2=0.0, the numerical and analytical theory agree to 10^{-10}. The high frequency δv noise is due to rounding error in data input to the plotting program, and not an orbital effect.
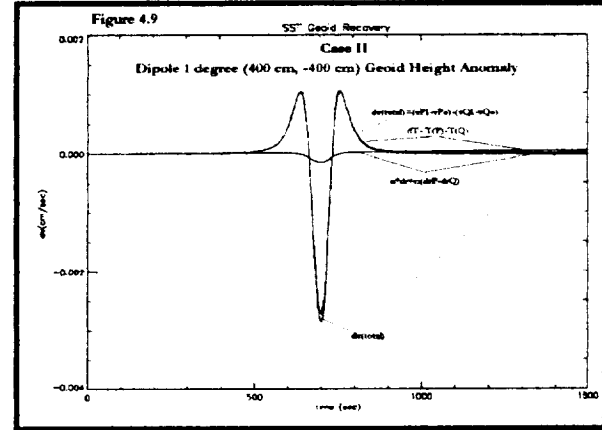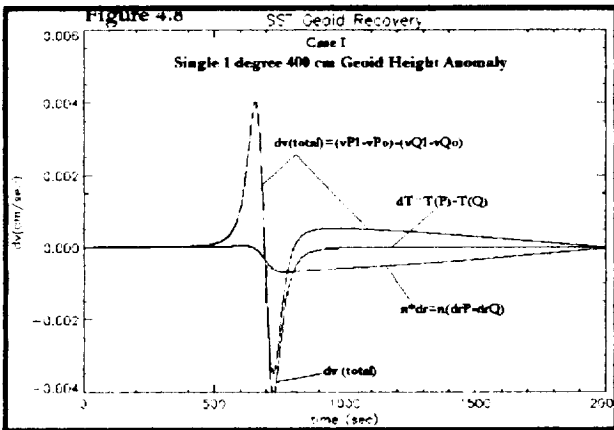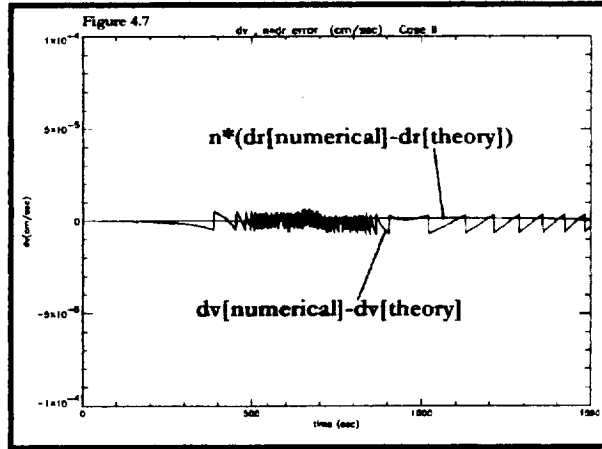
Figures 4.5,4.6,and 4.7 are the same quantities for case II, the dipole anomaly. The very small δr perturbation (0.18 cm maximum) results in negligible J2 interaction and long period terms. The reduced δr also results in smaller contribution to δv. For case II, the rms difference

---

[5] Strictly speaking we are plotting speed. Velocity is a vector quantity, and we measure and analyze a scalar quantity, the speed. However, common usage is to refer to this scalar quantity as velocity. In this discussion, vector quantities are always given as $\overline{x}$, or $\hat{x}$ for a unit vector, and scalar quantities as x.

Figure 4.5 — dv (cm/sec) Case I — dv=vP1-vPo

Figure 4.6 — dr (cm) Case I — dr=rP1-rPo
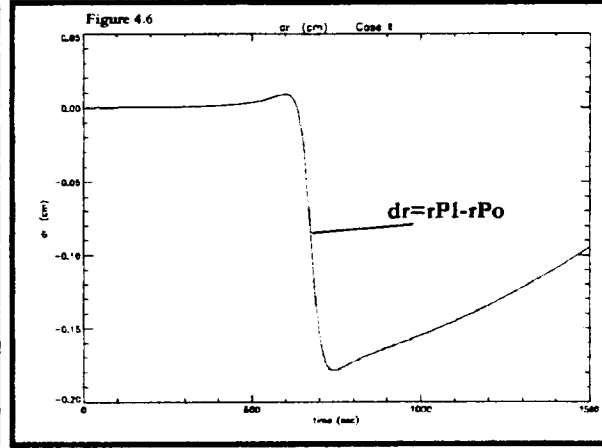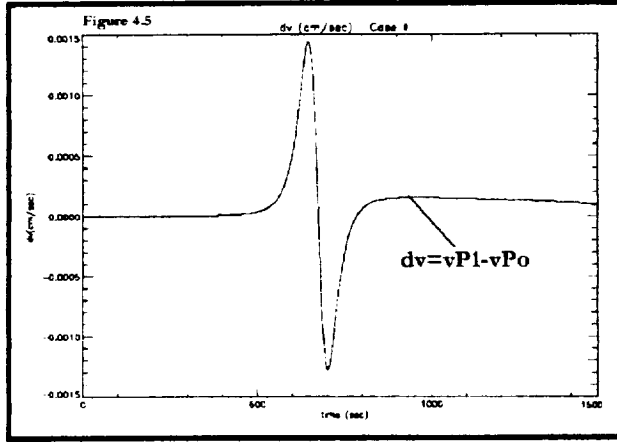
between the numerical and theoretical perturbations for the two curves is 2.7×10^{-6} cm/sec and 0.0006 cm. N.B. that 0.0006 cm gives 6.4×10^{-7} cm/sec contribution to the velocity.

We now illustrate the difference in velocity of two satellites, see table 4.1, separated by 400 km, at an altitude of 400 km. In figure 4.8 we show the difference in velocity

Figure 4.7 — dv , dr error (cm/sec) Case II — $n*(dr[numerical]-dr[theory])$ — $dv[numerical]-dv[theory]$

Figure 4.8 — SS Geoid Recovery — Case I — Single 1 degree 400 cm Geoid Height Anomaly — $dv(total)=(vP1-vPo)-(vQ1-vQo)$ — $dT \ T(P)-T(Q)$ — $n*dr=n(drP-drQ)$ — dv (total)

Figure 4.9 — SS Geoid Recovery — Case II — Dipole 1 degree (400 cm, -400 cm) Geoid Height Anomaly

for case I. Note that here we plot the difference in absolute velocity, not the rate of change in distance between P and Q. See section V for further discussion of this point. We also plot the difference in anomalous potential, ΔT, between P and Q, and the contribution of $n\Delta r = n(\delta r_p - \delta r_Q)$ to the difference in velocity. Recall that $\Delta v \approx \Delta T + n\Delta r$. The root mean square, rms, difference between the numerical and theoretical perturbations are 2.5×10^{-4} cm/sec in differential velocity and 0.0024 cm in differential radius (2.6×10^{-6} cm/sec as

velocity). Figures 4.9 shows the same quantities for Case II. For Case II, the rms difference between the numerical and theoretical perturbations are 2.9×10^{-5} cm/sec in differential velocity and 0.0002 cm in differential radius (2.3×10^{-7} cm/sec as velocity).

Jekeli [*Jekeli*, (1999)] has studied this issue using the energy conservation theorem with quite different objectives. He presents an expression for the corrections to Δv to obtain ΔT. In this case he proposes to measure these corrections "in situ" with the GPS receivers on the GRACE satellites. However, the requirements for the "in situ" measurements exceed the present GPS capability.

The simple simulation shown here demonstrates a number of facts.

1) First we see the, well known, sensitivity of relative velocity to the anomalous geopotential. Here we have postulated a rather large 1x1 degree 400 cm geoid anomaly.

2) The significant indirect effect of the radial perturbation on the relative velocity. To make best use of the relative velocity measurement, one must treat this indirect effect. The radial perturbation also has a significantly different time history (or fourier spectrum), with the presence of long period effects. This should compared with the potential difference, ΔT, contribution, which is more than 10 times larger, and is a local effect confined to the dimension of the anomaly. This will be discussed further in section V.

3) The efficacy of these formulae in calculating the perturbations, given the anomalous potential. One use of these equations could be to correct the observed velocity for the effects of an anomalous potential in an iterative procedure. The relative efficiency of such a calculation, requiring quadrature over the total anomalous potential field, compared with use of a spherical harmonic representation would have to be investigated.

V   Satellite to Satellite Tracking

To define the algorithm for calculation of the perturbed position, x_1, and velocity, v_1, from the unperturbed position, x_0, and velocity, v_0, and the along track, du, across track, dw, and radial perturbations, dr, (Figure 1).

If we use the unit vectors

$$\hat{r} = \bar{r} \Big/ \sqrt{\bar{r} \cdot \bar{r}}$$

$$\hat{w} = \bar{r} \times \bar{v} \Big/ \sqrt{(\bar{r} \times \bar{v}) \cdot (\bar{r} \times \bar{v})}$$

$$\hat{u} = \hat{w} \times \hat{r}$$

Figure 1   Geometry of Satellite Perturbations

for the radial, cross track and along track directions. More precisely, the along track unit vector is normal to the radius vector, and not along the velocity vector, to be consistent with the definition of the along track perturbation.

More precisely, the along track unit vector is normal to the radius vector, and not along the velocity vector, to be consistent with the definition of the along track perturbation. So we can write

$$\delta \frac{du}{dt} = \hat{u}_1 \cdot \bar{v}_1 - \hat{u}_o \cdot \bar{v}_o$$

$$\delta \frac{dw}{dt} = \hat{w}_1 \cdot \bar{v}_1 - \hat{w}_o \cdot \bar{v}_o \qquad (5.1)$$

$$\delta \frac{dr}{dt} = \hat{r}_1 \cdot \bar{v}_1 - \hat{r}_o \cdot \bar{v}_o$$

These relations lead to the perturbed velocity

$$\bar{v}_1 = \begin{bmatrix} \hat{u}_1 & \hat{w}_1 & \hat{r}_1 \end{bmatrix} \begin{bmatrix} \hat{u}_o' \\ \hat{w}_o' \\ \hat{r}_o' \end{bmatrix} [\bar{v}_o] + \begin{bmatrix} \hat{u}_1 & \hat{w}_1 & \hat{r}_1 \end{bmatrix} \begin{bmatrix} \delta \dfrac{du}{dt} \\ \delta \dfrac{dw}{dt} \\ \delta \dfrac{dr}{dt} \end{bmatrix} \qquad (5.2)$$
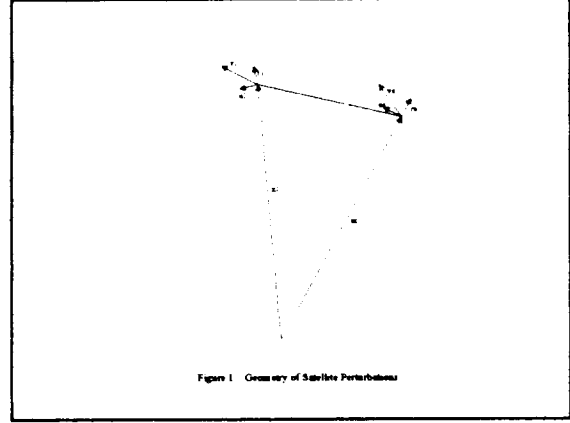
Now, with two satellites (P,Q) at positions x_P and x_Q, the unperturbed satellite to satellite range ρ_o is

$$\rho_o = \sqrt{\left(\bar{x}_{Po} - \bar{x}_{Qo}\right)\cdot\left(\bar{x}_{Po} - \bar{x}_{Qo}\right)} \tag{5.3}$$

from which we can obtain the unperturbed range rate

$$\frac{d\rho_o}{dt} = \dot{\rho}_o = \hat{\rho}_o\cdot\left(\dot{\bar{x}}_{Po} - \dot{\bar{x}}_{Qo}\right) \tag{5.4}$$

The corresponding perturbed range rate is

$$\dot{\rho}_1 = \hat{\rho}_1\cdot\left(\dot{\bar{x}}_{P1} - \dot{\bar{x}}_{Q1}\right) \tag{5.5}$$

If we define

$$A_{Xi} = \begin{bmatrix} \hat{u}_{Xi} & \hat{w}_{Xi} & \hat{r}_{Xi} \end{bmatrix} \tag{5.6}$$

the perturbation in range rate, $\Delta\dot{\rho} = \dot{\rho}_1 - \dot{\rho}_o$, is

$$\Delta\dot{\rho} = \hat{\rho}_1\cdot\left\{A_{P1}A'_{Po}\dot{\bar{x}}_{Po} + A_{P1}\left[\delta uwr_P\right] - A_{Q1}A'_{Qo}\dot{\bar{x}}_{Qo} - A_{Q1}\left[\delta uwr_Q\right]\right\} - \hat{\rho}_o\cdot\left\{\dot{\bar{x}}_{Po} - \dot{\bar{x}}_{Qo}\right\} \tag{5.7}$$

The basic observable desired is the difference in velocity, i.e. the intersatellite range rate is

$$\Delta v = \sqrt{\dot{\bar{x}}_P\cdot\dot{\bar{x}}_P} - \sqrt{\dot{\bar{x}}_Q\cdot\dot{\bar{x}}_Q} \tag{5.7}$$

where the SST measurement is give by (5.5). If we assume that the perturbation is along the velocity vector, then these are related by

$$\Delta\dot{\rho} = \cos(\theta_P)\sqrt{\dot{\bar{x}}_P\cdot\dot{\bar{x}}_P} - \cos(\theta_Q)\sqrt{\dot{\bar{x}}_Q\cdot\dot{\bar{x}}_Q} \cong \cos(\theta_P)v_Q - \cos(\theta_Q)v_Q \tag{5.8}$$

where

$$\cos(\theta_i) = \frac{(\bar{x}_P - \bar{x}_Q) \cdot \dot{\bar{x}}_i}{\rho v_i} \tag{5.9}$$

In the simulations performed here θ was of the order of 1.0 degrees, $\cos(\theta)=0.9998$. By correcting the observed range rate using

$$\Delta T = \Delta v \cong \Delta\dot{\rho} / \cos(\bar{\theta}) \tag{5.10}$$

where $\bar{\theta} = (\theta_P + \theta_Q) / 2$. This correction was applied in the following simulations, resulting in small improvements consistent with the small size of θ.

VI   Geophysical Inverse Theory

The two issues concerning the fundamental process of converting range-rate measurements at satellite altitudes to geoid heights at the earth's surface are: a) the solution of a boundary value problem in potential theory with incomplete data on an undefined surface, and b) the downward continuation of the potential to the earth's surface in a manner that keeps the errors within bounds. A related issue concerns the regularization of the data so as to account for the mass between the geoid and the external boundary.

Geophysical Inverse Theory (GIT) allows one to address these issues in one step.. The GIT motivation and theoretical framework was first introduced by [Backus and Gilbert, (1967); Backus and Gilbert, (1968); Backus and Gilbert, (1970)] and has had wide application. A good source for further developments and survey of applications and results, as well as the approach used here, the Spectral Expansion Method (SEM) can be found in [Parker, (1977)] and [Parker, (1994)]. Therefore, we provide a brief discussion of the approach, and some details of the implementation for the problem addressed in this study.

One central idea in GIT is to seek a representation of some geophysical quantity with a continuous function. The determination of a model with a finite number of parameters is a problem in statistics, e.g. least squares and is not Inverse Theory. In practice, for this continuous function, with a finite number of errorless observations, an infinite number of models can fit the data exactly. For selection of one of these models, GIT provides methods for finding the model that minimizes a norm, i.e. in some sense the model minimizes some property of the solution. This is also generalized to data with errors when one would not want to fit the data exactly anyway. There are many possible norms to chose: study of this is beyond the scope of our discussion. The norm, used here is to find the solution that minimizes the square of model integrated over the sphere, i.e. the so called L2 minimization. We will also introduce a seminorm minimization, introducing arbitrary functions into the solution space that will allow specific model parameters to be determined. Norm minimization is also a basic concept in Least Squares Collocation [Moritz, (1978)], and some comparison of the two methods is given in [Parker, (1994)].

The Geophysical Inverse Theory Spectral Expansion Method provides a means to incorporate error analysis, an arbitrary amount of smoothing, and a direct mapping of the observable – in this instance range rate, δv, converted to potential difference – to geoid height, N. As discussed in Section III, we can adopt a reference potential, U, including the principal oblateness and other low degree and order reference potential terms that we can assume known with sufficient accuracy. In addition we can safely assume a sphere of radius a_e=6378.137 km as the boundary surface for the boundary value problem. Finally we can assume the effects of mass between this reference surface and the observation are negligible. Furthermore, as discussed in section IV, the measurement of δv between satellites P and Q, can be processed in a precision orbit determination calculation using the reference potential, U, to obtain residuals, Δv. These residuals represent three factors: a) the potential difference, ΔT, between the satellites P and Q,

-29-

b) a perturbation, nδr, due to ΔT interacting with GM/r, and c) other orbital errors. By correcting for nδr, and filtering the other orbital errors, the residual, Δv, gives an estimate of ΔT=T(P)-T(Q).

In this work we consider the fundamental desiderata to be the geoid height, N, often referred to as geoid undulation, from the reference surface. To relate geoid height to geopotential we use Bruns formula [*Heiskanen and Moritz*, (1967), page 85)]

$$N = \frac{T}{\gamma} \tag{6.1}$$

where γ is gravity on the reference ellipsoid, strictly in this application it is gravity on the reference surface. Since we are concerned with small corrections to the geopotential, we use γ=978.0327 (cm/sec²)[6] to scale the geoid model, N, to geopotential, T.

The Poisson Integral Formula (3.1) and Bruns Formula (6.1) allows us to solve the forward problem, i.e. given a geoid model on a reference sphere, compute the potential at a point in space, P_i. outside the reference sphere This is of the form:

$$T(P_i) = \int_\sigma g(P_i,S)T(S)d\sigma_S = \gamma \int_\sigma g(P_i,S)N(S)d\sigma_s \tag{6.2}$$

The P_i is the position of the observation, S is on the reference sphere and $d\sigma_s$ is the surface element of integration on that sphere. The estimate of ΔT=T(P)-T(Q) is then written

$$\Delta T(P_i,Q_i) = \gamma \int_\sigma [g(P_i,S) - g(Q_i,S)]N(S)d\sigma_S = \gamma \int_\sigma G(P_i,Q_i,S)N(S)d\sigma_S \tag{6.3}$$

Anticipating the treatment of observation errors we can by use:

$$\Delta T_i' = \frac{\Delta T_i}{\sigma_i} \text{ and } G_{i'} = \frac{G_i}{\sigma_i} \tag{6.4}$$

where σ_i is the standard error of the observation ΔT_1.

Now, the functional (6.3) is linear in the unknown, N, and therefore we have a linear inverse problem. Assuming P_i does not lie on the reference sphere, (6.3) is also finite. With n values, or observations, we have ΔT_i $i = 1,2,...n$ there are n kernals in (6.3)

$$G_i(S) = G(P_i,Q_i,S) \quad i = 1,2,...n \tag{6.5}$$

Which are n functions of position, S. With a little thought one can see that these are linearly

---

[6] Geodetic convention defines the unit of 1.0 gal as 1.0 cm/sec².

independent, i.e. G_i is linearly independent from G_j if (P_i,Q_i) is not the same as (P_j,Q_j).
Therefore they could form **a** set of basis functions to represent the geoid height on the sphere,
i.e.

$$N(S) = \sum_{j=1}^{n} \alpha_j G_j(S) \tag{6.6}$$

One can show that this has the minimum norm [Parker, (1994),Chapter 1]. Substitution of (6.6)
in (6.3) resulting in the matrix equation for α_j.

$$\gamma\left[\Gamma_{ij}\right]\left[\alpha_j\right] = \left[\Delta T_i\right] \tag{6.7}$$

where Γ is a symmetric matrix, called the Gram matix, with elements

$$\Gamma_{ij} = \Gamma_{ji} = \int_\sigma G_i(S)G_j(s)d\sigma_S \tag{6.8}$$

This system of equations can be solved for α_j.

Now, the spectral expansion method, SEM, is introduced at this point, leading to great
computational simplification and functional utility. The positive definite matrix Γ can be
diagonalized with an orthogonal, eigenvector, matrix Θ with

$$\Theta'\Gamma\Theta = \Lambda \tag{6.9}$$

where

$$\Lambda = diag(\lambda_1,\lambda_2,\lambda_3,.....,\lambda_n), \lambda_1 \geq \lambda_2 \geq \lambda_3 \geq......\lambda_n \geq 0 \tag{6.10}$$

The matrix of eigenvectors, Θ, has the usual properties

$$\Theta'\Theta = \Theta\Theta' = I \tag{6.11}$$

the unit matrix $I=diag(1,1,1,....1)$. The eigenvalues, λ_j ,are often referred to as the spectrum of
the problem. This diagonal decomposition can be accomplished by methods such as described
in [Golub and Reinsch, (1971)]. We can now define another set of orthogonal base functions[7]

---

[7] The association of $1/\lambda_j$ with a_j follows [Parker, (1994)]. This change from associating
$1/\sqrt{\lambda_j}$ with both a_j and ψ_j, as in [Parker, (1977)] is quite arbitrary, and is used to facilitate the
seminorm minimization outlined below.

-31-

$$\psi_i(P) = \sum_j \Theta_{ji} G_j(P) \tag{6.12}$$

and write for the computed potential

$$T^c(P) = \sum_i a_i \psi_i(P) \tag{6.13}$$

where

$$a_i = \sum_j \Theta_{ji} \alpha_j \tag{6.14}$$

Substituting (6.9) and (6.14) in (6.7) we find

$$a_i = \frac{1}{\lambda_i} \sum_j \Theta_{ji} \Delta T_j . \tag{6.15}$$

The a_i are uncorrelated, i.e. are statistically independent, with the standard error of each coefficient $1/\lambda_i$, i.e.

$$\sigma_{a_i} = 1 / \lambda_i \tag{6.16}$$

These basis functions, (6.13) become more oscillatory as i increases, i.e. as λ_i decreases, and approaches +0, see below for some examples. Consequently, the standard error of the coefficients increases as i increases. The power of the SEM lies in using λ_j to select the desired solution. For example, by eliminating basis functions with high frequency oscillations – i.e. those functions with eigenvalues less than some minimum eigenvalue, λ_{min} – one can obtain a smoothed solution. Of course, not using the complete eigenfunction expansion, the model, (6.13) would not fit the data exactly. An alternative would be to add a constant, C, to each λ_j in (6.15), which has the effect of significantly reducing the effects of small eigenvalues on the model. So, in matrix notation we have

$$[a] = [\Lambda + CI]^{-1} [\Theta^t][\Delta T] \tag{6.17}$$

In the case were there are observation errors, using (6.4) in (6.7) and (6.8) leads to a new solution if the observation uncertainties are different for each observation. Otherwise, the standard deviation of each observation cancels, and the result is the same. This leads to considerable computational simplification in this analysis, as we can compute (6.7) once for a given data set, and analyze the effects of random errors by scaling Γ, and adding noise to ΔT.

In the case were there are observation errors we can compute a statistic for the data set

$$\chi^2 = \sum_{i=1}^{n} \left(\Delta T_i' - \Delta T_i'^c \right)^2 = n \qquad (6.18)$$

This can be used as the criterion for selecting λ_{min} or C. Having selected λ_{min} or C one now has the formal error of commission in the model

$$\sigma^2_{\Delta T(S)} = \sum_{i=1}^{n} \frac{1}{\lambda_i + C} \psi_i^2(S) \qquad (6.19)$$

where the obvious functions are removed based on selection of λ_{min}.

The orthogonal functions (6.12) used to represent the geoid are finite in number, and therefore define a limited functional representation of the geoid. For example they do not provide the same representation as the same number of spherical harmonics. The spirit of GIT is to let the data distribution define the representation. As an aside, it is the distribution of the data point positions (P,Q) that define the Gram matrix, (6.7), and not the actual data (ΔT), hence the representation.

There may be functions that, a priori, we wish to include in the representation. For example, a constant, low degree polynomial, or spherical harmonic, that would not be included in the basis (6.12). For example, if the reference potential field, U, has a long wavelength error that could be locally modeled by a low degree bivariate polynomial. By including such functions, one cannot obtain a minimum norm, but can achieve a subnorm minimization. We can accomplish this expansion of the basis functions as follows. Let us include in the representation, a linear function:

$$h(S) = \sum_{k=1}^{nK} b_k h_k(S) \qquad (6.20)$$

where the b_k are to be determined from the data. The model becomes

$$N(S) = \sum_{i=1}^{n} a_i \psi_i(S) + \sum_{k=1}^{nK} b_k h_k(S). \qquad (6.21)$$

Assuming that h_k and ψ_i are independent function of position, S, making the same substitutions as before, we have the system of equations to solve

$$\begin{bmatrix} \Delta + CI & \overline{A} \\ \overline{A}^t & 0 \end{bmatrix} \begin{bmatrix} a \\ b \end{bmatrix} = \begin{bmatrix} \Theta^t \Delta T \\ 0 \end{bmatrix} \qquad (6.22)$$

where the elements of the rectangular (n x nK) matrix are

$$A_{ij} = \int_\sigma h_i(S)G_j(S)d\sigma \qquad (6.23)$$

and

$$\left[\overline{A}\right] = \left[\Theta^t\right]\left[A\right]. \qquad (6.24)$$

As with (6.4) each element of (6.24) should be divided by the observation uncertainty when treating data containing errors. This system of equations has the solution

$$[b] = \left[\overline{A}^t \left(\Lambda + CI\right)^{-1}\overline{A}\right]^{-1}\overline{A}^t\left[\Lambda + CI\right]^{-1}\Theta^t\left[\Delta T\right] \qquad (6.25)$$

and

$$[a] = \left[\Lambda + CI\right]^{-1}\left[\Theta^t\left[\Delta T\right] - \overline{A}b\right] \qquad (6.26)$$

In the application here, we intend to use low degree polynomials, centered in the region of interest (φ_o, λ_o). These polynomial coefficients are used to account for errors in the reference potential model, U. The errors are assumed to be long wavelength variations, and can be suitably modeled with low degree polynomials in longitude and latitude. The polynomial variables would be φ-φ_o and λ-λ_o. Since the region of interest is of the order of a few degrees, (<0.2 radians) we choose the variables

$$\xi = \sin(\varphi - \varphi_o)$$
$$\eta = \sin(\lambda - \lambda_o) \qquad (6.27)$$

with the 21 polynomials $1, \xi, \eta, \xi^2, \xi\eta, \eta^2, \dots, \xi\eta^4, \eta^5$. This removes questions of definition in computing (6.23).

VII   Simulations

VII.1   Introduction

In previous sections, necessary elements of, Potential Theory (III), Orbit Theory (IV), and Geophysical Inverse Theory (VI) to analyze satellite to satellite tracking data for geoid determination have been reviewed. Now, some numerical experiments will be described that illustrate how these elements can be combined, and what sort of results may be expected. These numerical experiments will be progressively more complex and complete, in four stages. First will explore the nature of the eigenvalues and eigenfunctions that come from the singular value decomposition. This requires combining the elements of Potential Theory with Geophysical Inverse Theory. As seen in section VI, these results depend only on the physical geometry of the measurement, and are independent of the measurement itself. Second, some properties of the solution assuming a direct measurement of potential difference: accuracy, resolution, error propagation, and sensitivity can be shown. For these analyses, idealized geoid anomalies will be used: blocks with a dimension of 1.0 degree and 5.0 degrees will be combined. Third, an orbital simulation using a small number of idealized blocks is done, to illustrate geoid recovery using SST measurements. Finally a number of orbital simulations will be offered, with increasing complexity in the desired geoid, and other orbital effects. For these the geoid model will be the EGM96 [*Lemoine and al.*, (1998)] geopotential model. EGM96 is a complete model to degree and order
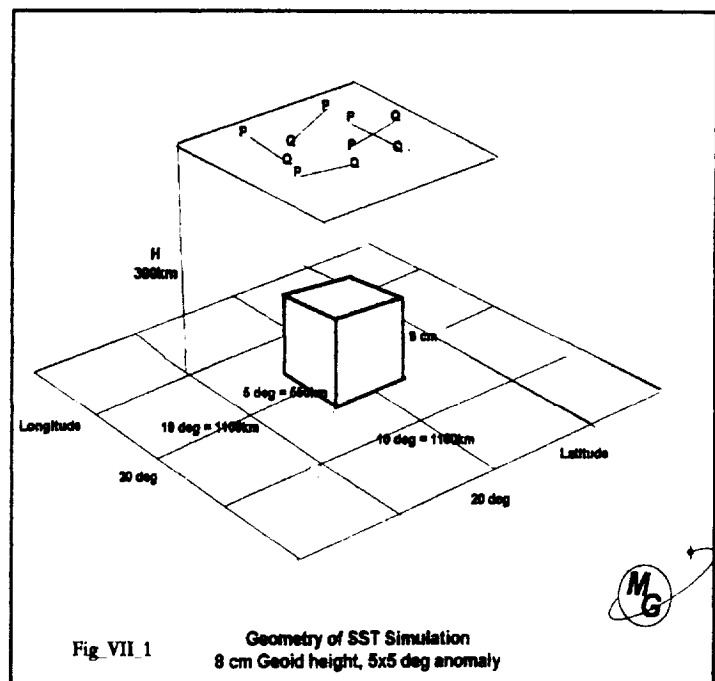
Fig_VII_1   Geometry of SST Simulation
8 cm Geoid height, 5x5 deg anomaly

360. For the illustrative proposes of these demonstrations, the EGM96 model will be truncated, at degree 70, 90 and 180. In addition other physical forces will be included: lunar and solar forces, ocean and solid body tides, atmospheric drag, solar radiation pressure, and earth albedo pressure. The focus of these last simulations will be to demonstrate the recovery of geoid information from satellite to satellite range rate, which involves correcting for the indirect effects (equation 4.33) in the presence of other force model errors, that can only approximately accounted for in the orbit fit. Exploration of the degradation of the recovered geoid in the presence of these other forces, is a much larger effort than was addressed here, but some limited cases will be shown.
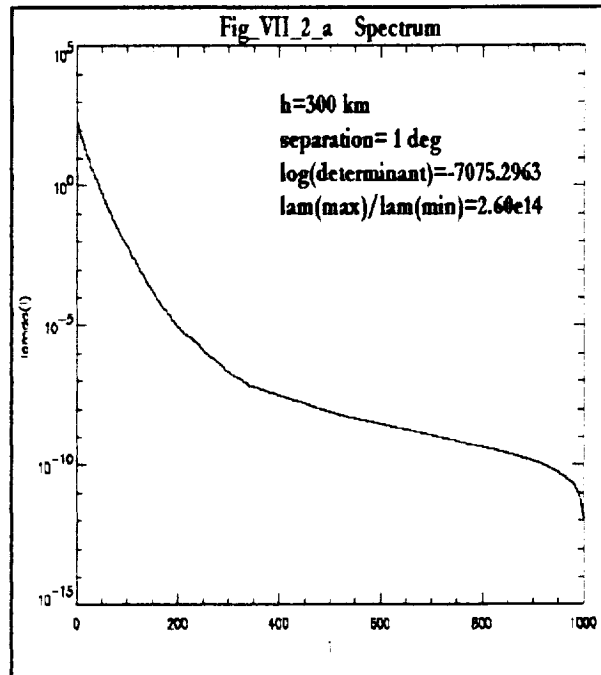
VII.2 Geometry of GIT

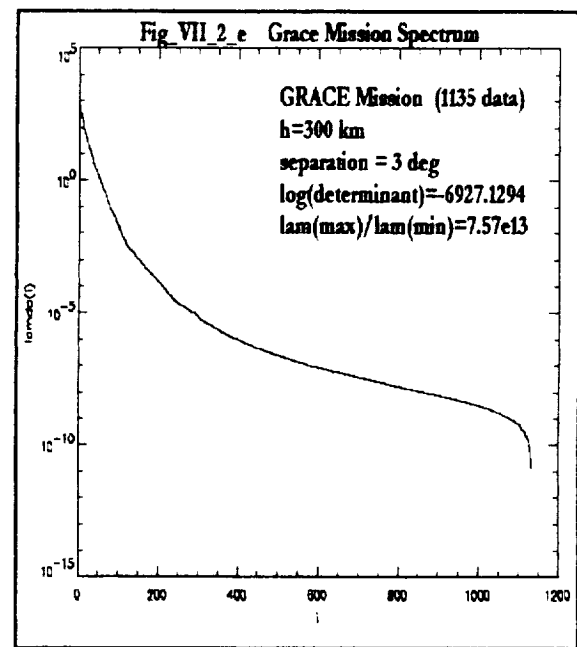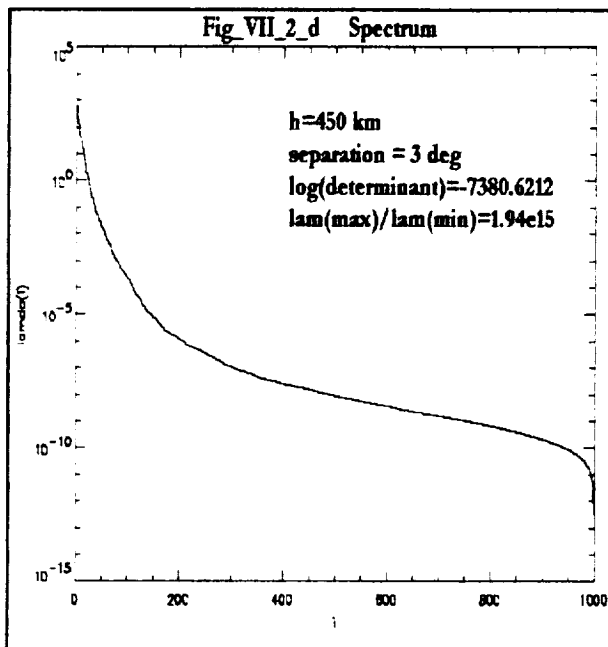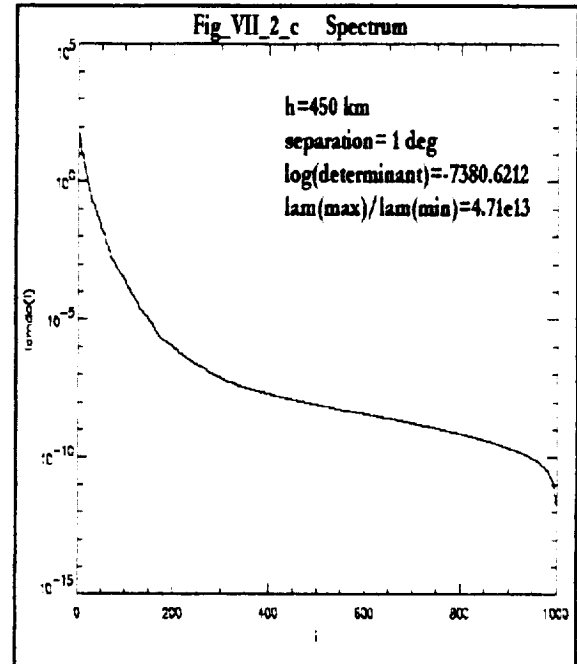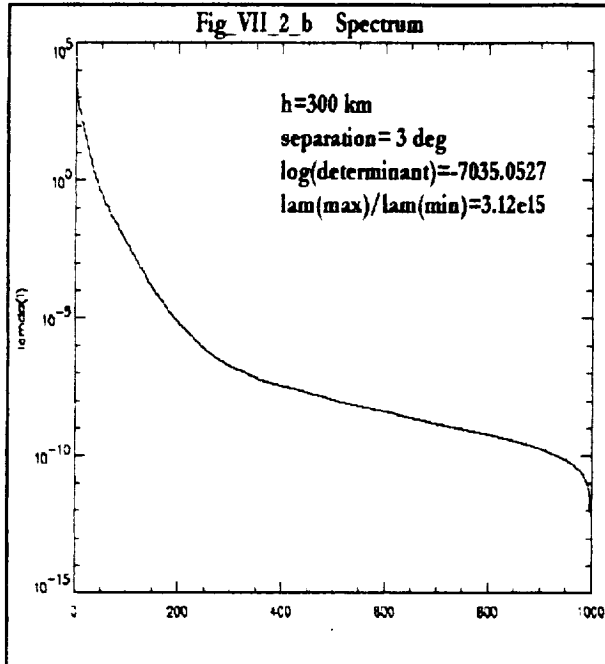A set of data is generated with the parameters given in Table VII_2_1.

Table VII_2_1 Parameters for Simulation	
Area Size	20°x20°
Geoid anomaly Size	5°x5°
Geoid anomaly amplitude	8 cm
Satellite Altitude	300 km - 450 km
Satellite Separation	1° - 3° (110 km - 330 km)
Number of Data Points	1000
Distribution of positions	Random
Distribution of orientation	Random

Figure VII_1 is a cartoon showing this configuration of data. Figures VII_2_a,b,c, and d shows the eigenvalues for this system, often referred to as the spectrum of the system, for various combinations of orbit configuration. The enormous range, 10^{14}, of the eigenvalues is evident. Note that the determinant of the system, the product of the eigenvalues, cannot be computed directly, as it is smaller than the minimum number represented in the computer (3.4×10^{-4932}). Of course the logarithm can be computed (-7075.2963). The Singular Value Decomposition of this system, can potentially be numerically inaccurate. The algorithm used is taken from [*Golub and Reinsch*, (1971)]. The orthogonality of the eigenvectors has been verified. However, with any linear vector space of this dimension, one must remain aware of possible numerical errors [*Hamming*, (1973) ; *Wilkinson and Reinsch*, (1971)]. For example, if the position of P or Q in an observation is the same as P or Q for another observation, the Gram matrix will not have independent elements. Though this is unlikely to ever to be exactly true, we have found that we must require all points P and Q be separated by more than a minimum distance. For large a system, n>1000, using a minimum distance of 20 km is satisfactory. For systems with n =

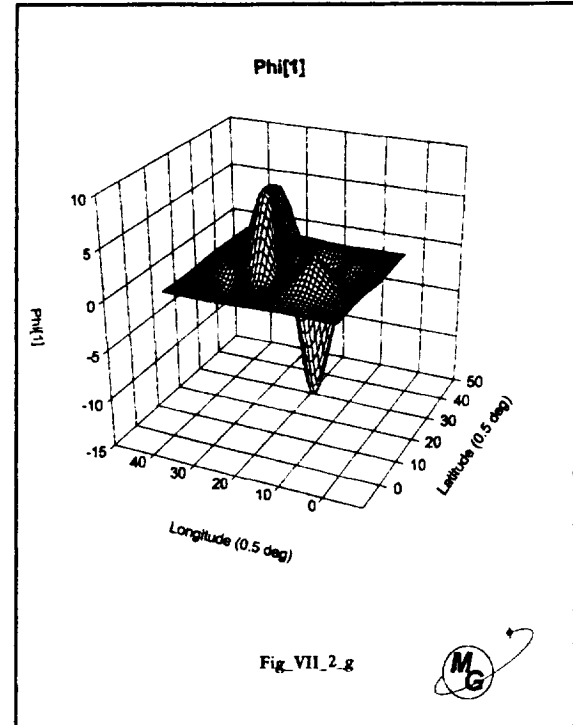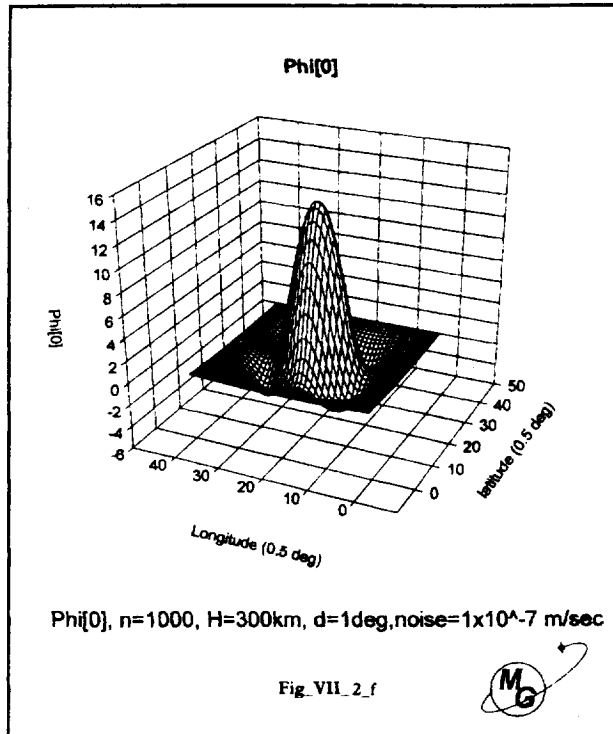Fig_VII_2_a Spectrum

h=300 km
separation= 1 deg
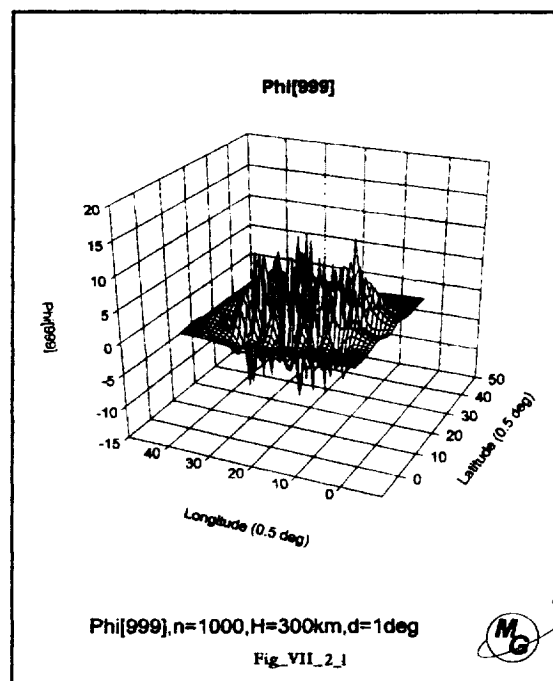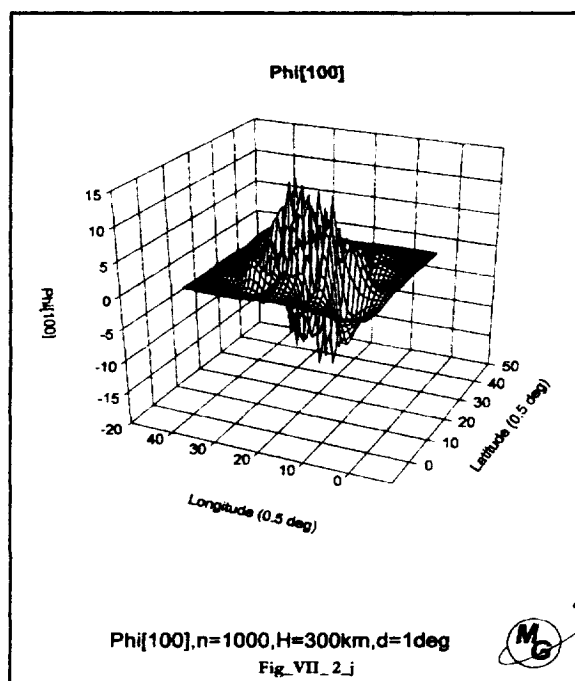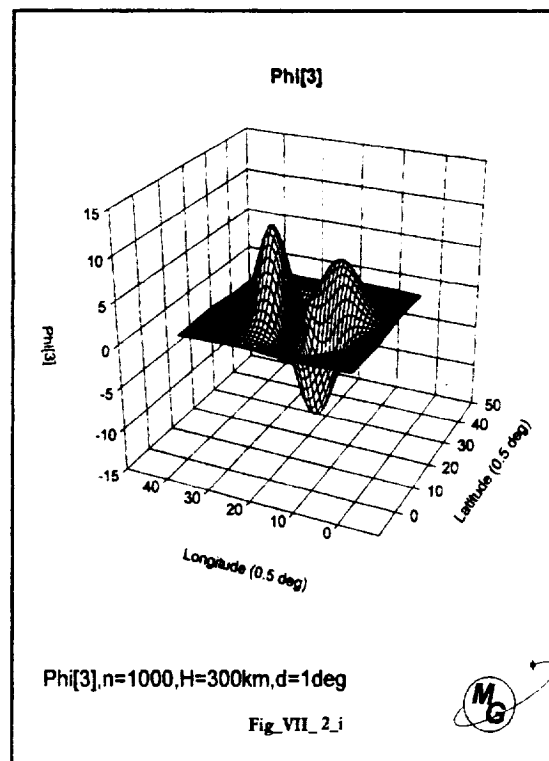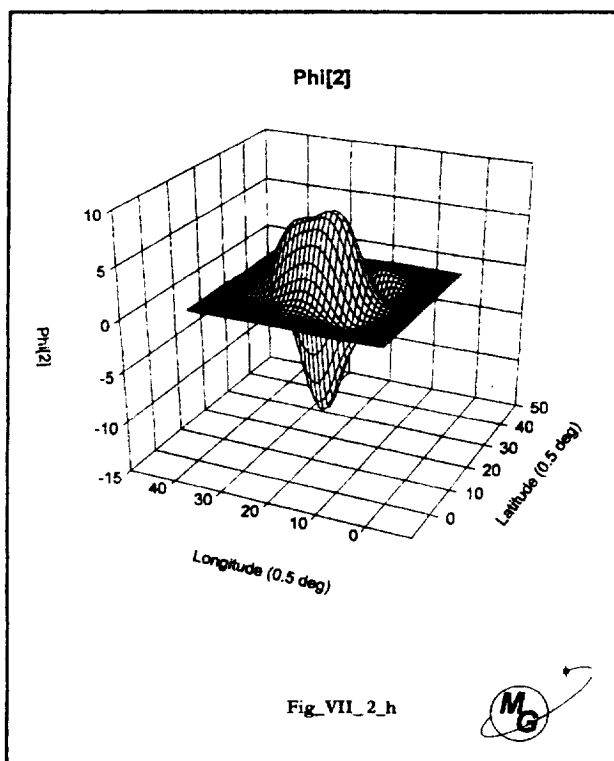log(determinant)=-7075.2963
lam(max)/lam(min)=2.64e14

several hundred, a minimum distance of 5 km works well. Figures VII_2_f,g,h,i,j, and l show a selection of the basis functions, Ψ_i, (6.11) computed from these data and eigenvectors. The eigenvectors and basis functions have been ordered with the decreasing values of the eigenvalues: $\lambda_1 \geq \lambda_2 \geq \lambda_3 \geq ... \geq \lambda_n \geq 0$. As expected from the general theory [*Parker*, (1994)] the Ψ_i

Fig_VII_2_b Spectrum

h=300 km
separation= 3 deg
log(determinant)=-7035.0527
lam(max)/lam(min)=3.12e15

Fig_VII_2_c Spectrum

h=450 km
separation= 1 deg
log(determinant)=-7380.6212
lam(max)/lam(min)=4.71e13

Fig_VII_2_d Spectrum

h=450 km
separation = 3 deg
log(determinant)=-7380.6212
lam(max)/lam(min)=1.94e15

Fig_VII_2_e Grace Mission Spectrum

GRACE Mission (1135 data)
h=300 km
separation = 3 deg
log(determinant)=-6927.1294
lam(max)/lam(min)=7.57e13

become more variable, oscillatory, as λ_i decreases in size. This supports the notion that by truncating the series of basis functions, Ψ_i, a certain smoothing is achieved by eliminating high frequency variations.
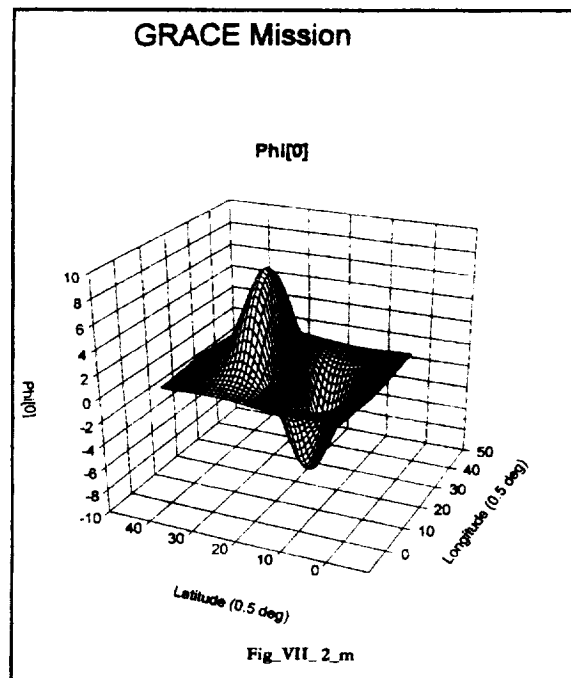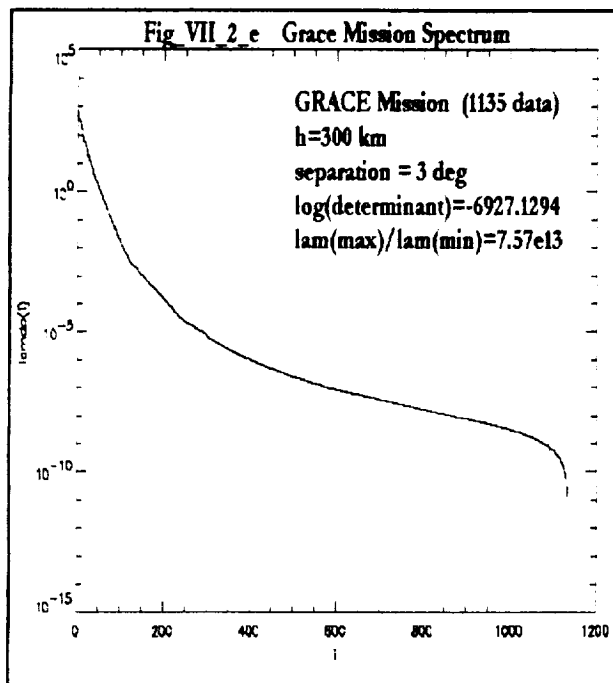

Phi[0], n=1000, H=300km, d=1deg,noise=1x10^-7 m/sec

Fig_VII_2_f

Fig_VII_2_g

Phi[2]

Fig_VII_2_h

Phi[3]

Phi[3],n=1000,H=300km,d=1deg

Fig_VII_2_i

Phi[100]

Phi[100],n=1000,H=300km,d=1deg

Fig_VII_2_j

Phi[999]

Phi[999],n=1000,H=300km,d=1deg

Fig_VII_2_l

The selection of random positions and orientations, would be expected to provide the best set of n data points. Since the target of this analysis is the GRACE mission, the physical orientation of the data in low and mid latitudes will be controlled by the satellite inclination (87°) – near the pole, of course, all orientations will be obtained. Therefore, this experiment is repeated with the parameters given in Table VII_2_2.

Table VII_2_2 Parameters for GRACE Simulation	
Area Size	20°x20°
Geoid anomaly Size	5°x5°
Geoid anomaly amplitude	8 cm
Satellite Altitude	400 km
Satellite Separation	3° (330 km)
Number of Data Points	1000
Distribution of positions	Random
Distribution of orientation	87°,183°

Figure VII_2_e shows the eigenvalues for this GRACE system. often referred to as the spectrum of the system. Table VII_2_3 summarizes the eigenvalues of the cases presented. With the GRACE data we see the same range, 10^{14}, of the eigenvalues is present as existed in the
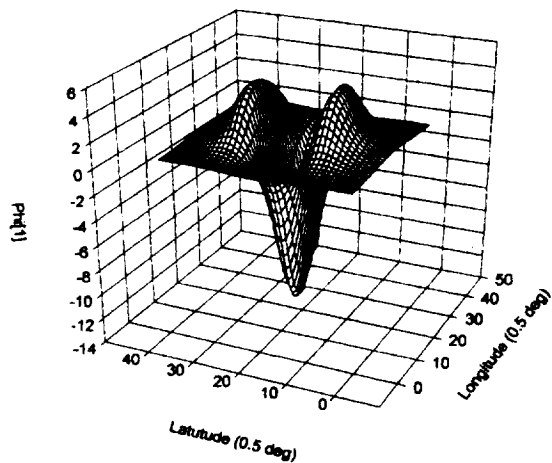
Table VII_2_3 Eigenvalue Summary				
h(km)	Separation (°)	Determinant	$\lambda_{max}/\lambda_{min}$	λ_{max}
300	1.0	5.05×10^{-7076}	2.60×10^{14}	3.24×10^{2}
300	3.0	8.86×10^{-7036}	3.12×10^{15}	2.24×10^{3}
450	1.0	2.39×10^{-7381}	4.71×10^{13}	9.09×10^{1}
450	3.0	3.59×10^{-7334}	1.94×10^{15}	6.76×10^{2}
450 GRACE	3.0	7.42×10^{-6928}	7.54×10^{13}	1.00×10^{3}

previous case. Figures VII_2_m,n,o,p, and q show a selection of the basis functions, Ψ_i, (6.11) computed from these data and eigenvectors. The same general character of the basis functions is evident. The geometry of the GRACE data set does not seem to be a factor in application of GIT to geoid recovery.
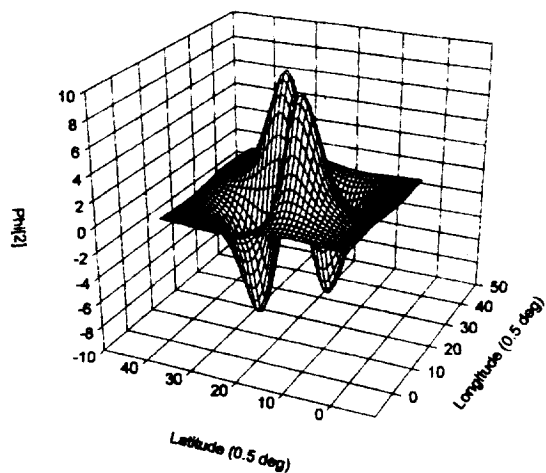
Fig_VII_2_e   Grace Mission Spectrum

GRACE Mission (1135 data)
h=300 km
separation = 3 deg
log(determinant)=-6927.1294
lam(max)/lam(min)=7.57e13

GRACE Mission

Phi[0]

Fig_VII_2_m
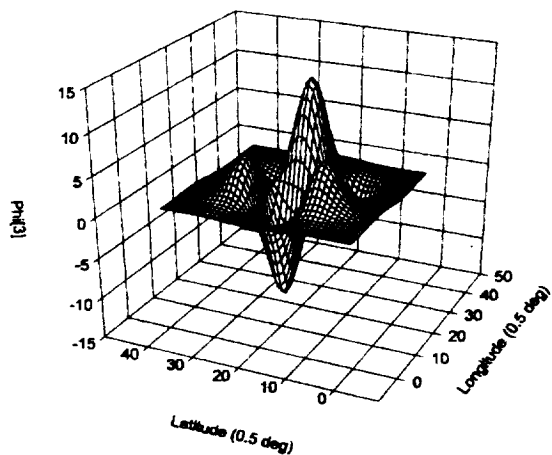
-41-

GRACE Mission
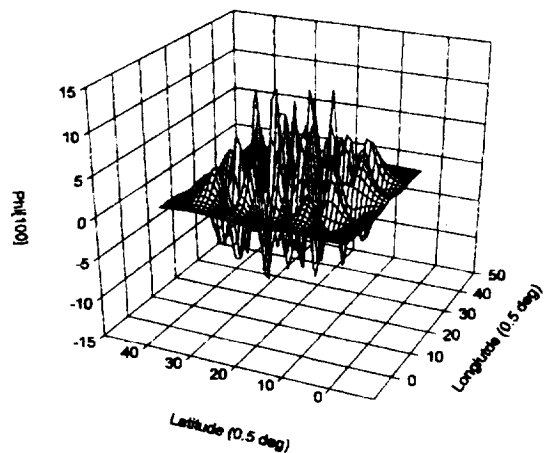
Phi[1]

Fig_VII_2_n

GRACE Mission

Phi[2]

Fig_VII_2_o

GRACE Mission

Phi[3]

Fig_VII_2_p

GRACE Mission

Phi[100]

Fig_VII_2_q

VII_3 Error analysis

Errors in the measurement of potential difference come from two difference sources. First are the inherent measurement errors that will, for this analysis, be assumed to be uncorrelated, zero mean, Gaussian noise with a given standard deviation, σ, i.e. normally distributed errors. The second source is the process of converting the observed velocity difference ($\Delta \, d\rho/dt$) into the potential difference (ΔT). This involves both geometrical corrections (Section V), correction for the dynamical interaction between ΔT and GM/r (section VII_5_3 below), and other unmodeled orbital effects. The first source will be studied in this section. The second will be studied in following sections, and will provide some information about scaling the standard deviation to take these other phenomena in to account in the estimation process.

The data sample described in Table VII_2_1 is used. Potential at satellite positions P,Q is computed using Poissons Integral Formula, (3.1) and the difference used as the observation. Gaussian noise is added, computed using an algorithm from [*Hamming*, (1973), p 143] based on the system random number generator. These data are used to determine the constant C, (6.17) based on the condition (6.18) using the method of Regula Falsi [*Hamming*, (1973), p 65]. Recall, that the GIT SEM can obtain a solution for the expansion coefficients, that exactly matches the observations and has a minimum variance of the model. What we seek is the solution, that only matches the observations to within the observation uncertainty, and has the minimum model variance. For illustrative purposes, three observation uncertainties are used, as given in Table VII_3_1. Also given are the determined value of C/λ_{max}, and C. Choosing C has the same practical effect as removing all $\lambda_i < \approx$ C.

h(km)	Separation (°)	n	σ (m/sec)	C	C/λ_{max}
300	1.0	1000	1.0×10^{-5}	6.44×10^{-1}	1.98×10^{-3}
300	1.0	1000	1.0×10^{-6}	6.73×10^{-2}	2.08×10^{-4}
300	1.0	1000	1.0×10^{-7}	2.56×10^{-3}	7.90×10^{-6}
300	3.0	1000	1.0×10^{-5}	2.71×10^{-1}	1.21×10^{-4}
300	3.0	1000	1.0×10^{-6}	1.81×10^{-2}	8.08×10^{-6}
300	3.0	1000	1.0×10^{-7}	3.86×10^{-4}	1.72×10^{-7}

Figures VII_3_a, VII_3_b, and VII_3_c, show the recovered geoid for these data sets. Clearly, higher accuracy, smaller σ, provides greater resolution.

Figure VII_3_a

Figure VII_3_b

Figure VII_3_c
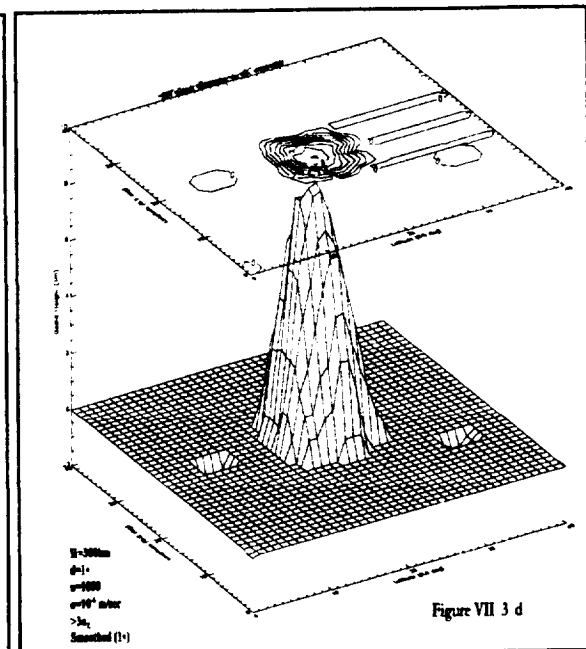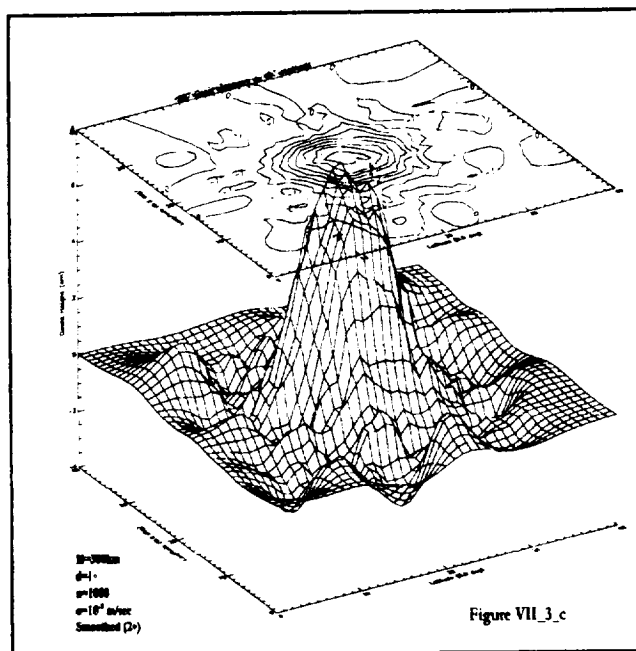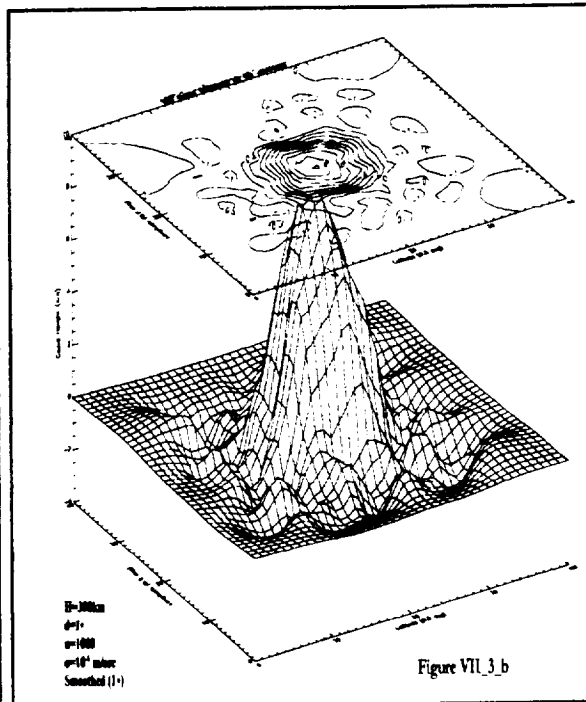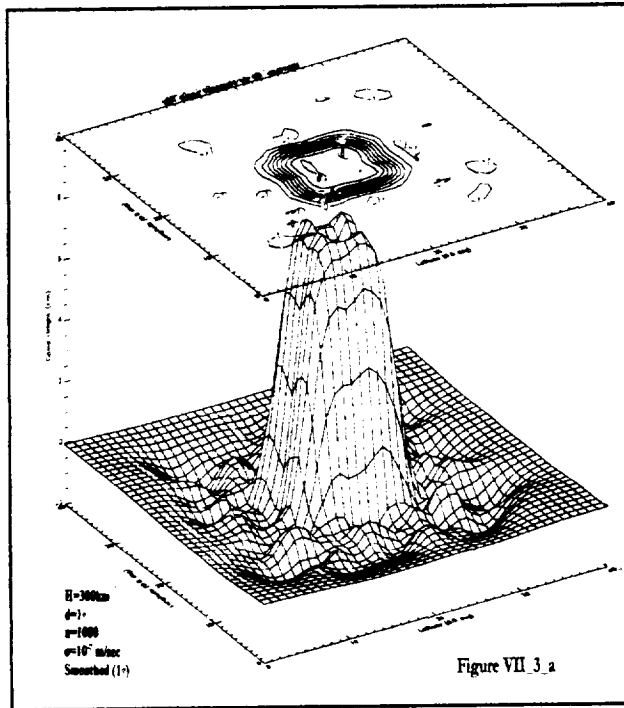
Figure VII 3 d

One important product of the GITSEM process is computation of a formal uncertainty of the model, (equation 6.19). To illustrate this, note that the model has zero signal outside the 5°x 5° geoid anomaly. Figure VII_3_d, is the recovered geoid, where, a zero is plotted when the computed model is less than 3 times the computed uncertainty of the model. The values

-44-

predicted by the model outside the $5°\times 5°$ geoid anomaly are not significantly different from zero, as determined by the model.

Finally, the resolving power of the GITSEM, i.e. the sensitivity and resolution, is investigated as follows. With the analogue of a matched filter, we ask, what fraction of the signal amplitude is recovered? This will depend on the satellite altitude, the satellite separation, the size of the geoid anomaly, and the observation uncertainty. A series of simulations was done with the variables given in Table VI_3_2.

Table VII_3_2 Resolving Power of GITSEM						
Satellite Height (km)	150	200	250	300	350	400
Satellite Spacing (km)	110	220	330			
Anomaly Size (°)	1	2	3	4	5	
Data Accuracy (m/sec)	1.0×10^{-5}	1.0×10^{-6}	1.0×10^{-7}			

Figures VII_3_e and VII_3_f summarize these results. Clearly lower satellite altitude and larger

Figure VII_3_e Attenuation (3 deg spacing)
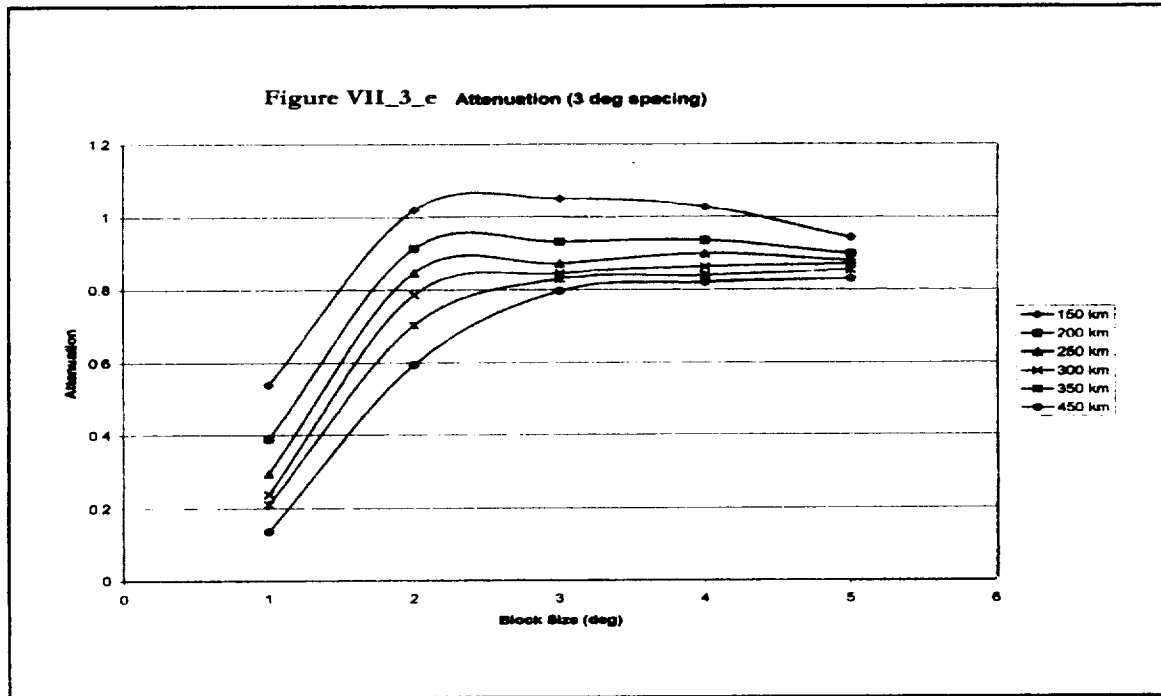
anomaly block size give higher resolution. As seen in numerous previous studies, there is an inherent limitation in recovery of geoid anomalies smaller than the satellite height. There is a

smaller effect of satellite separation, larger separation providing somewhat more sensitivity.

Figure VII_3_f   Attenuation (1 deg spacing)
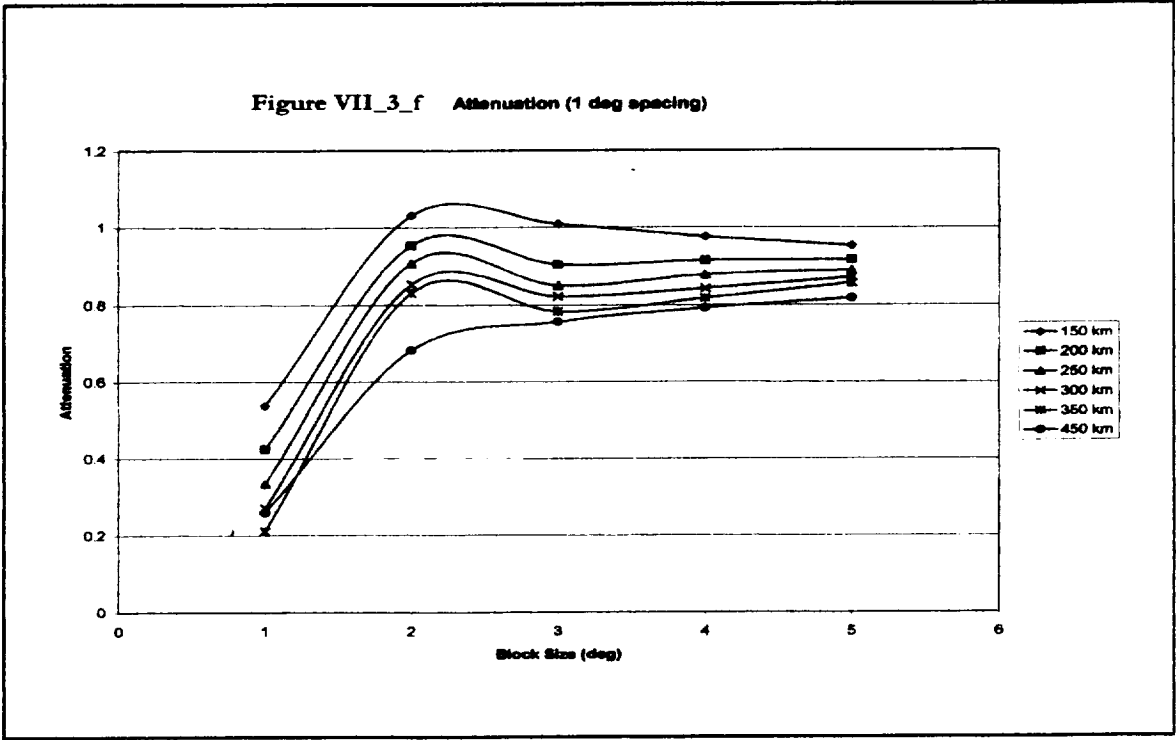
VII_4 Simulation Geoid Block Anomalies

An example is now given with several geoid block anomalies. Four anomalies are created as shown in the cartoon, Fig_VII_4_a and described in Table VII_4_1.

Figure VII_4_a

Geometry of SST Solution
32 cm Geoid height, 1x5 deg anomaly (twice)
-12 cm Geoid height, 1x10 deg anomaly (twice)
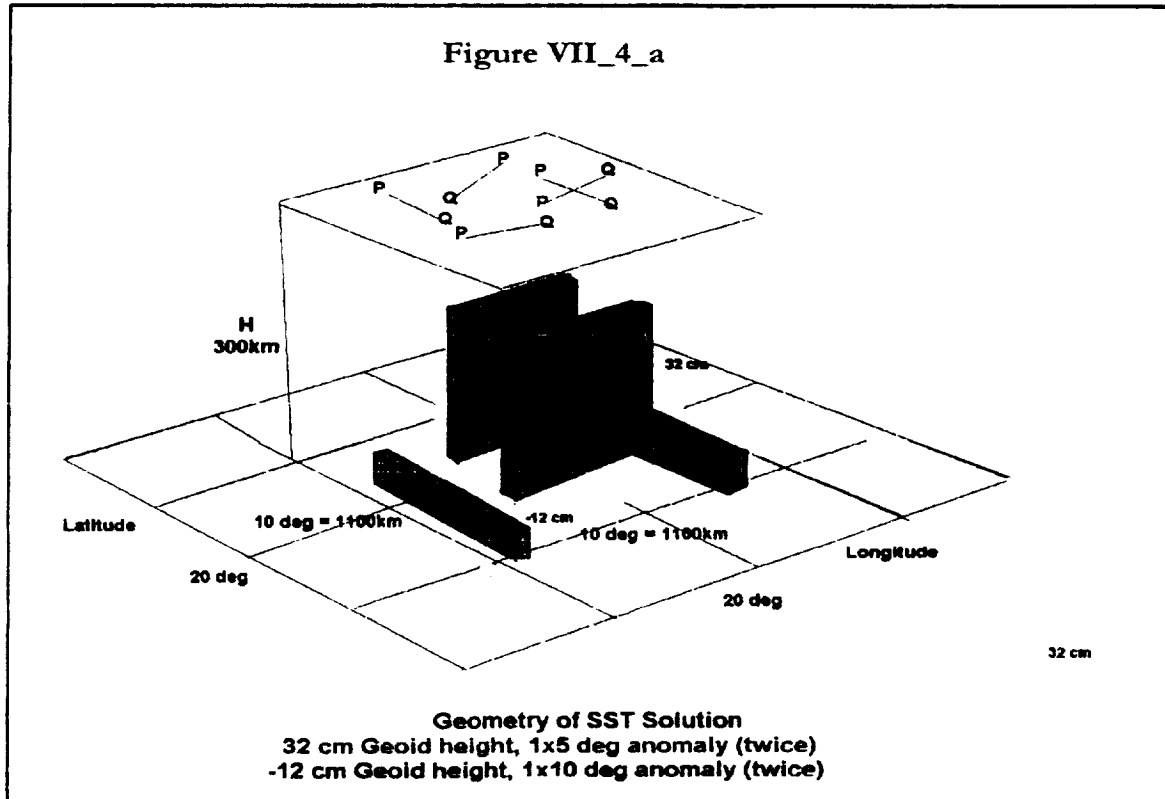
Table VII_4_1 Block Anomaly Simulation	
height (km)	300
separation (°)	1.0
n (data)	1000
σ (m/sec)	1.0×10^{-7}
Anomaly 1 (size,amplitude)	$1° \times 5°$,32 cm
Anomaly 2 (size,amplitude)	$1° \times 5°$,32 cm
Anomaly 3 (size,amplitude)	$1° \times 10°$,-12 cm
Anomaly 4 (size,amplitude)	$1° \times 10°$,-12 cm

As before, the potential at satellite positions (P,Q) is computed using Poissons Integral Formula (3.1) and the difference used as the observation. Gaussian noise is added. The two 32 cm anomalies are resolved. However, only 75% of the amplitude (24 cm) is recovered. Similarly, the -12 cm anomalies are resolved with reduced amplitude (-8 cm).
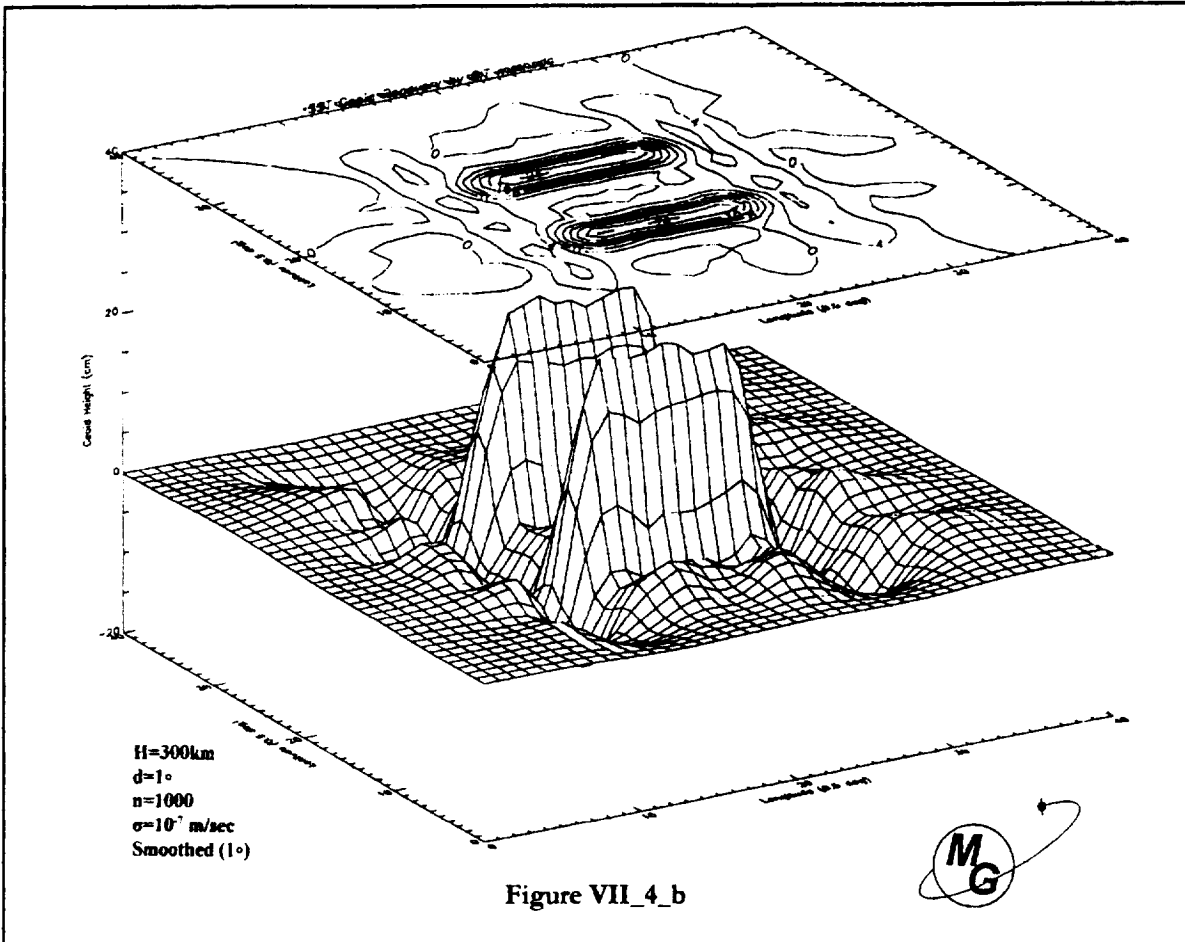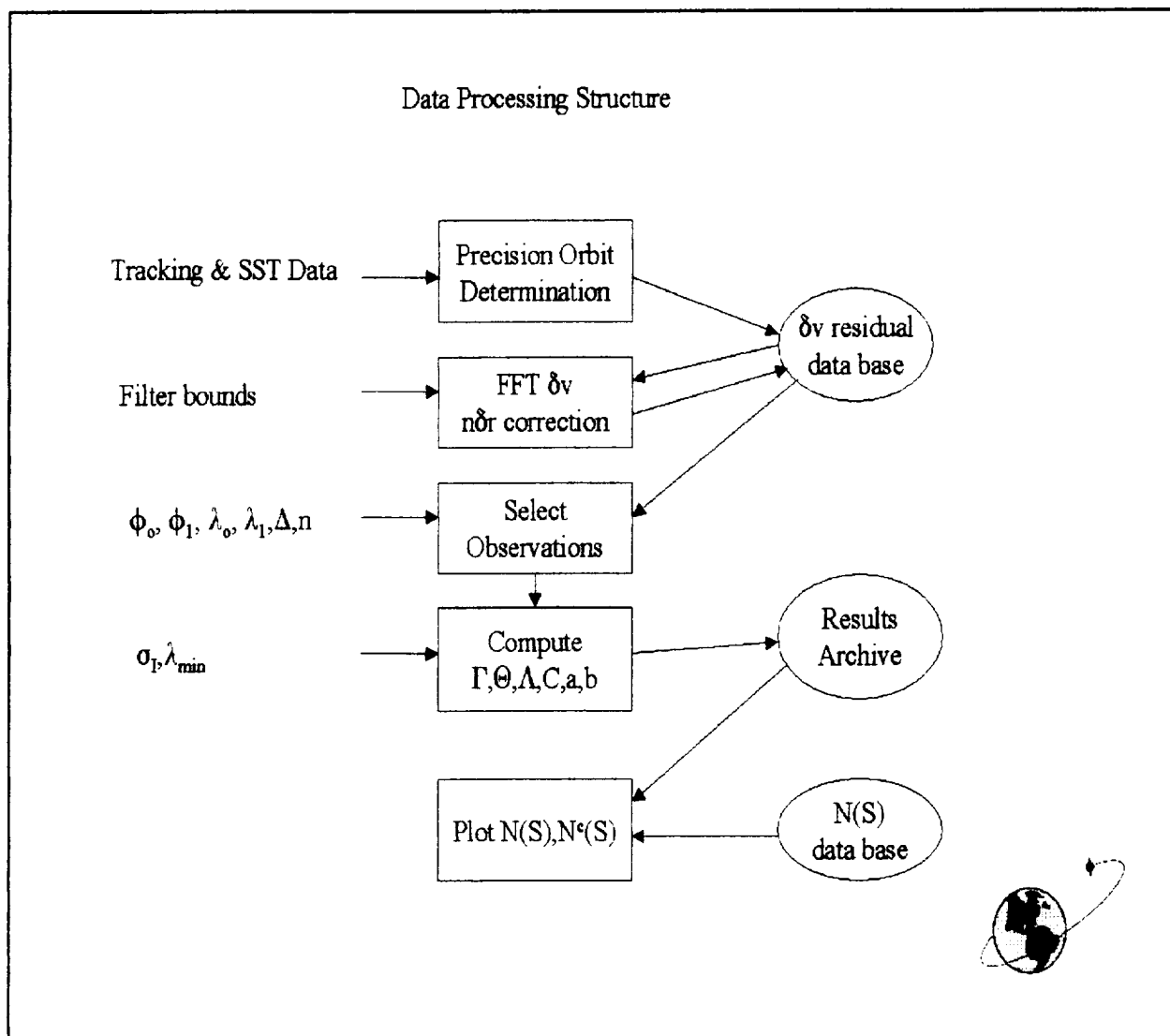

Figure VII_4_b

VII_5 Orbit Simulation

VII_5_1 Introduction

The end to end orbit simulation process is described in figure VII_5_1. It begins with simulated satellite to satellite range rate data. The parameters of the simulations are summarized in Table VII_5_1, and are intended to represent the GRACE mission. The initial state vectors are defined in Table 4.1. However, before reviewing the simulation results, the calculation of the potential difference, ΔT, from the observed satellite to satellite range rate, $d\rho/dt$, must be discussed. Now, we are interested in the contribution of the anomalous potential, T, to the range rate. Therefore, the first step is to perform a Precision Orbit Determination (POD) using the SST data and any other available tracking data – here assumed to be ground based laser tracking – using a chosen reference potential, U, to obtain the orbit residuals, $\Delta\, d\rho/dt$. These residuals contain the desired signal, the interaction terms from $n\delta r$, and other orbital errors due to inadequate force models. Therefore, we now discuss the following three topics: 1) The filter parameters, 2) Calculation of the interaction correction, $n\delta r$, and 3) the geoid database used for calculation and comparison of the results.

<table>
<tr><td colspan="2" align="center">Table VII_5_1 Simulation Parameters</td></tr>
<tr><td>Data Geometry</td><td>400 km altitude, I=87°, 400 km separation</td></tr>
<tr><td>SST Data</td><td>10 second range rate data
60 Day mission</td></tr>
<tr><td>Ground Tracking Stations</td><td>18 laser ranging stations tracking both satellites</td></tr>
<tr><td>Force Model</td><td>Total Geopotential: l=2,70, 2-90, 2-180
Sun, Moon Tides (Ocean Body)
Drag (MSIS), Solar Pressure, Earth Albedo
Reference Potential: l=2-40, 2-90</td></tr>
<tr><td>Orbit Arcs</td><td>1 day
Solve for parameters: drag scale factor</td></tr>
<tr><td>Map Region</td><td>Eastern Mediterranean</td></tr>
<tr><td>Filter parameters</td><td>λ_{low}=800 sec, λ_{high}=30 sec, (5600 km, 47 °)</td></tr>
</table>

VII_5_4 Filter Parameters

To calculate the potential difference (ΔT) from the observed satellite to satellite tracking velocity residuals ($\Delta\, d\rho/dt$) we start with equation (4.33) is used. Recall, the ΔT response of the satellite velocity was local, and takes place immediately. However, the interaction perturbation
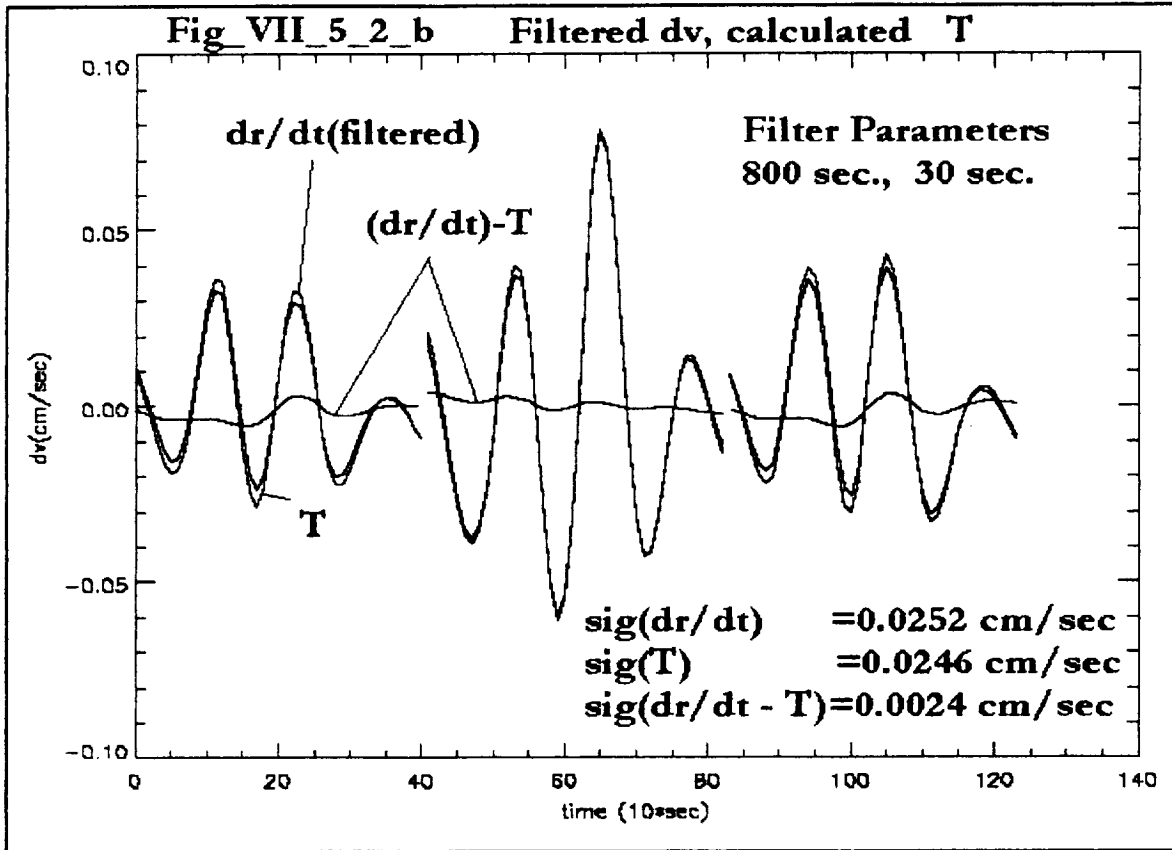
Data Processing Structure

Tracking & SST Data → Precision Orbit Determination

Filter bounds → FFT δv nδr correction

$\phi_o, \phi_1, \lambda_o, \lambda_1, \Delta, n$ → Select Observations

σ_1, λ_{min} → Compute $\Gamma, \Theta, \Lambda, C, a, b$

Plot $N(S), N^c(S)$

δv residual data base

Results Archive

$N(S)$ data base

nδr has an instantaneous component, but also has a cumulative effect, that results in periodic changes with, in fact, the orbital period. Since we are interested in the instantaneous change due only to ΔT we chose to filter out signals with periods longer than the time passing over the region of interest. The satellite traveling at 7.5 km/sec, passes over 40° of latitude (4400 km) in less than 600 seconds. So filtering signals with periods longer than 600 seconds or more, would leave all the instantaneous signals. In fact, the results are not very sensitive to the period cutoff, we experimented with cutoff's of 600, 800, 1200, 1600, 2400, and 4800 seconds, and adopted 800 seconds for all the analysis. The filtering was accomplished using a Fast Fourier Transform Algorithm [Press et al., (1991)]. Each one day arc of residuals (8640 data), was filtered separately. The data were padded with zeros to obtain a sequence of exactly 2^n points. The Fourier coefficients were then convolved with a 10th order Butterworth filter. To mitigate

measurement noise, i.e. high frequency noise, a 30 second short period cutoff was also applied. The resulting Fourier coefficients were then converted back to the time domain. FiguresVII_5_2_a and VII_5_2_b illustrate the result of this filter. The test case has a total

Fig_VII_5_2_a Filtered dr/dt (U+T):(2-70), (U):(2-40)
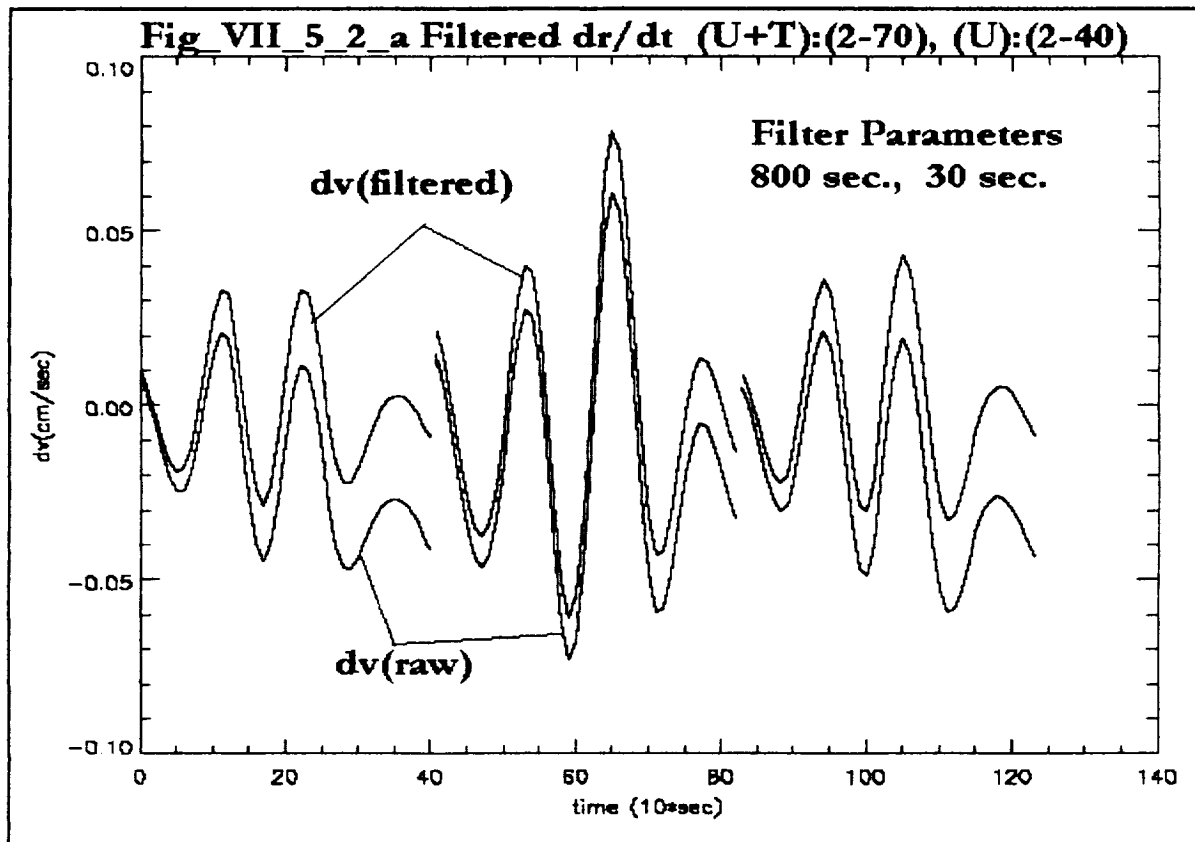
geopotential (U+T) to degree and order 70, and a reference geopotential (U) to degree and order 40. Figure VII_5_2_a shows the computed residual (Δ dρ/dt) and the filtered values (Δ dρ/dt$_{800-30}$) for three passes over the chosen region. Figure VII_5_2_b shows the filtered values of the computed residual (Δ dρ/dt$_{800-30}$) , the computed values of the potential difference (ΔT), and the difference, and the difference (Δ dρ/dt$_{800-30}$ -ΔT). For this comparison, the computed potential difference is converted to velocity using Ψ=U+T=γN=vδv. The variances of the computed residuals (0.0252 cm/sec = 252 μ/sec) and the computed potential difference (0.0246 cm/sec = 246 μ/sec) are nearly the same. The standard deviation of the difference (0.0024 cm/sec) is about 10% of the signal, as predicted in section III. The difference between the computed residual and the potential difference is due to the interaction term, to be discussed in the next section, and other orbital errors.

Fig_VII_5_2_b   Filtered dv, calculated   T

dr/dt(filtered)

(dr/dt)-T

T

Filter Parameters
800 sec., 30 sec.

sig(dr/dt)   =0.0252 cm/sec
sig(T)   =0.0246 cm/sec
sig(dr/dt - T)=0.0024 cm/sec

VII_5_3 Calculation of nδr

If one knows the anomalous potential (T), then we have shown that the correction (nδr) can be computed with sufficient accuracy. Here, this is not the case. Therefore, we develop an approximation based on the available data. Recall that the computed residuals Δ dρ/dt $\approx \Delta T/v = (T(P)-T(Q))/v$. Therefore, if the two satellites are in the same circular coplanar orbit then one can use the computed residuals, Δ dρ/dt, to compute an approximation to the potential along the orbit. This is only approximately true because of the inevitably different evolution of the orbits, and that the earth rotation will result is a different potential at the same orbit position at a different time. We give in Figure VII_5_3_a the potential recovered by this method, expressed as velocity, and the computed anomalous potential, T. Again the case studied is total potential Ψ=U+T complete for l=2-70, the reference potential U:2-40, and the anomalous potential T:41-70. Now, the correction δr depends on the combination 2T+r(∂T/∂r). We obtain the second term as follows. Assume that we have the spherical harmonic expansion for T, i.e.
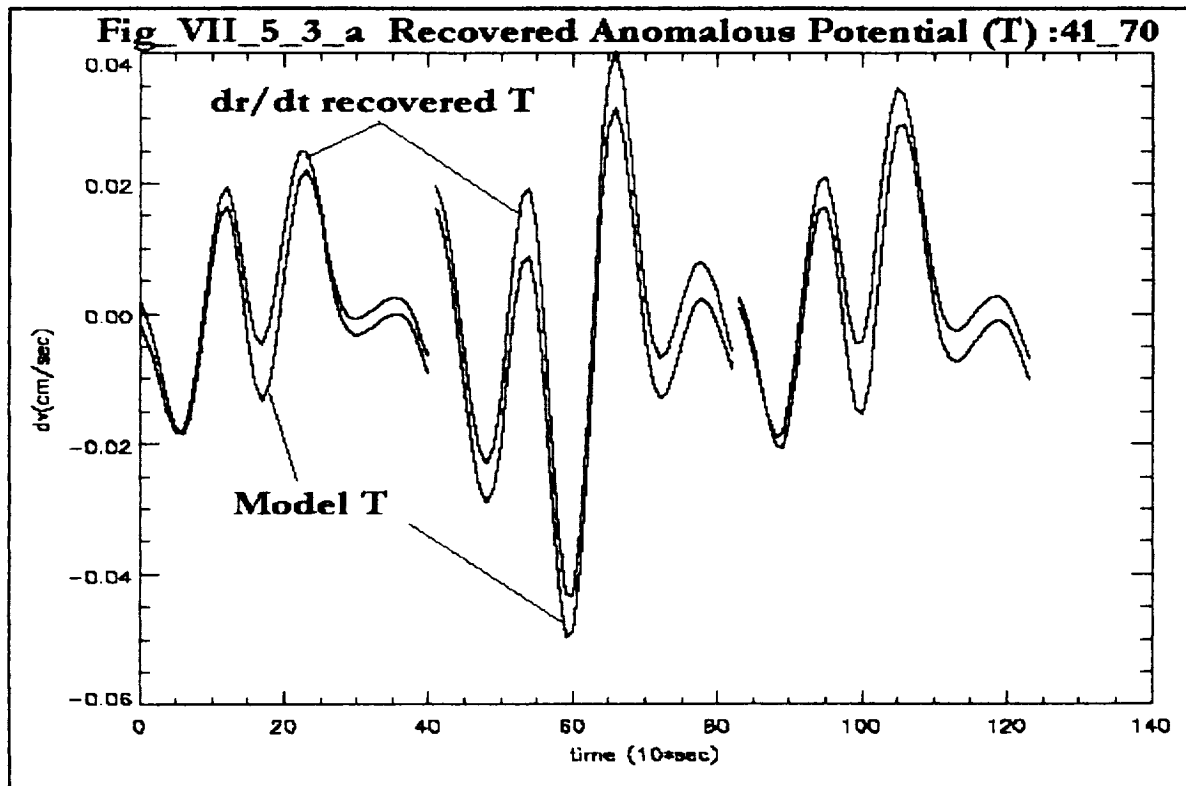
$$T(r,\varphi,\lambda) = \frac{GM}{r}\sum_{l=l\min}^{l=l\max}\left(\frac{R}{r}\right)^{l}\sum_{m=0}^{m=l}\overline{P}_{lm}(\sin\varphi)(\overline{C}_{lm}\cos m\lambda + \overline{S}_{lm}\sin m\lambda) \qquad (7.1)$$

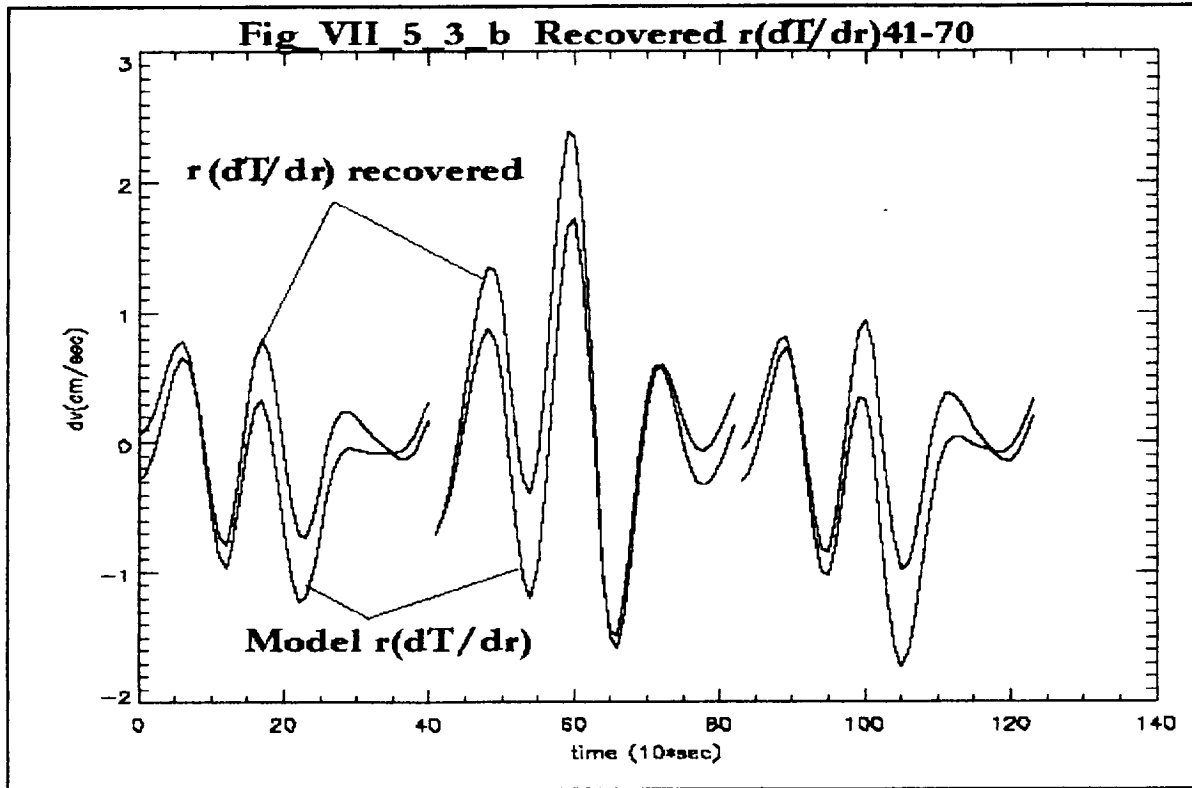$$T(r, \varphi, \lambda) = \sum_{l} \frac{R^{l}}{r^{l-1}} T_{l}(r, \varphi, \lambda) \tag{7.2}$$

and the desiderata

$$r \frac{\partial T}{\partial r} = \sum_{l=l\min} (l+1) \frac{R^{l}}{r^{l+1}} T_{l} \tag{7.3}$$

Consider, an arc, in any orientation on the earths surface containing the point of interest $(\varphi_{o}, \lambda_{o})$ in the orbit subsatellite track. The arc, and $(\varphi_{o}, \lambda_{o})$ define a coordinate system and the spherical harmonics can be transformed to this system. Now, along this arc, the longitude is zero and (7.1) reduces to an expansion in Legendre polynomials. So we take the recovered T, along the arc, and expand it in Legendre polynomials through degree 142. This expansion is centered on the point of interest, $(\varphi_{o}, \lambda_{o})$, and for $-\pi/2$ to $\pi/2$ along the orbit. From this expansion, the sum (7.3) is evaluated at $(\varphi_{o}, \lambda_{o})$. Figure VII_5_3_b shows this gradient is shown as recovered from Δ dρ/dt, and computed from the, in this case, known potential. The same tracks are used as before.

Fig_VII_5_3_a Recovered Anomalous Potential (T) :41_70

Fig_VII_5_3_b Recovered r(dT/dr)41-70

r (dT/dr) recovered

Model r(dT/dr)

The generally good agreeement between the recovered and model values of $r(\partial T/\partial r)$ is satisfactory considering the purpose here is to calculate a 10% correction. The correction is calculated for each satellite separately, and then $n\delta r = n(\delta r(P) - \delta r(Q))$ is computed and added to the observed $\Delta\ dp/dt$ to obtain the estimate of $\Delta T/\gamma$ to be analyzed. Recall, that the calculated δr will introduce long period perturbations. Therefore, the result for δr, will also be filtered before being used, using a 6000 second cutoff period. Figure VII_5_3_c shows the computed values for $n\delta r(P)$ and of $n\delta r$. $n\delta r(Q)$ is not plotted simply because it is shifted in time from $n\delta r(P)$ by $\rho/v \approx 400$ (km)/ (7.5 km/sec) = 53 seconds.

Fig_VII_5_3_c Computed ndr(P), dr=n(dr(P)-dr(Q))
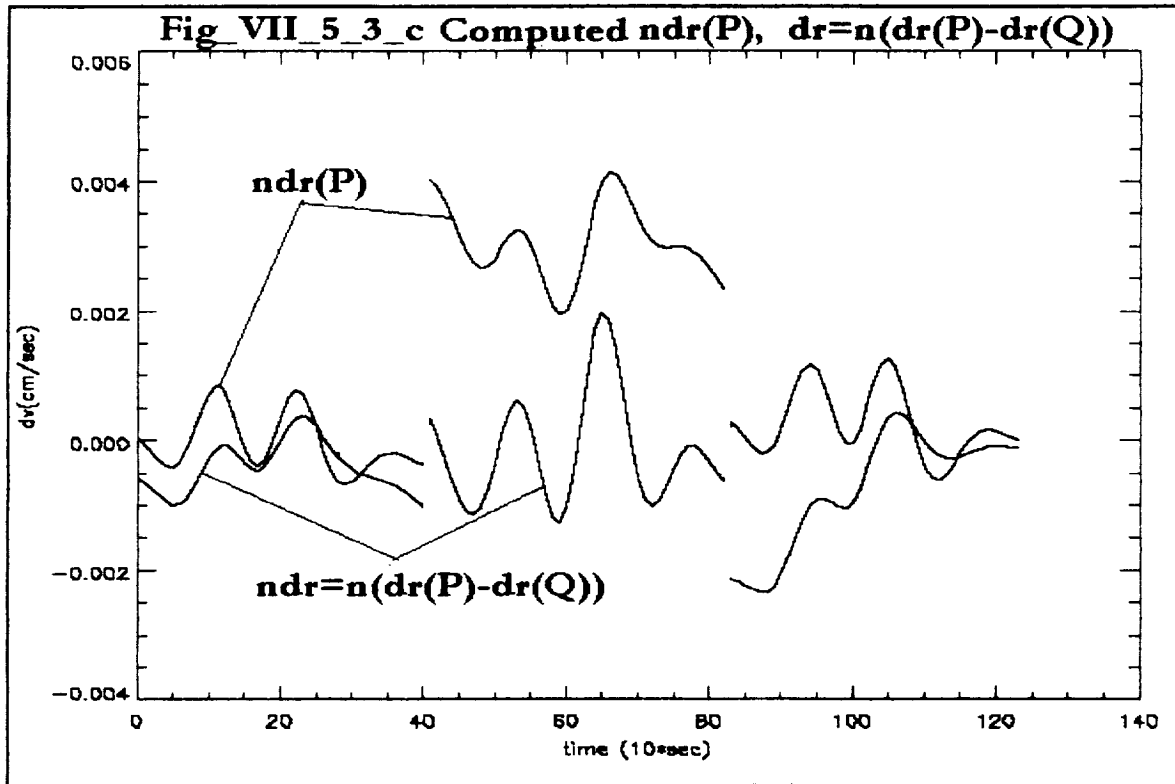
How well does this calculation work? In figure Fig_VII_5_3_d we show the filtered orbit residual $\Delta dp/dt$ minus the computed $dv(model)/dt$, and the calculated $n\delta r$, for the same three tracks used above. One sees the signature of ndr. In addition there is a larger signal due, presumably to other unmodeled effects. Figure VII_5_3_e shows the result of correcting the observed velocity with $n\delta r$.

Examination of many samples of data, give similar results. It is clear, that the conversion of observed range rate residual, $\Delta dp/dt$, to $\Delta T/\gamma$ has remaining unmodeled errors. Though only of the order of 5% to 10% of the desired signal, they limit the accuracy of the recovered geoid, as will be discussed below.

Fig_VII_5_3_d dv(filtered)-dv(model),ndr

Fig_VII_5_3_e dv(filtered)+ndr-dv(model), ndr
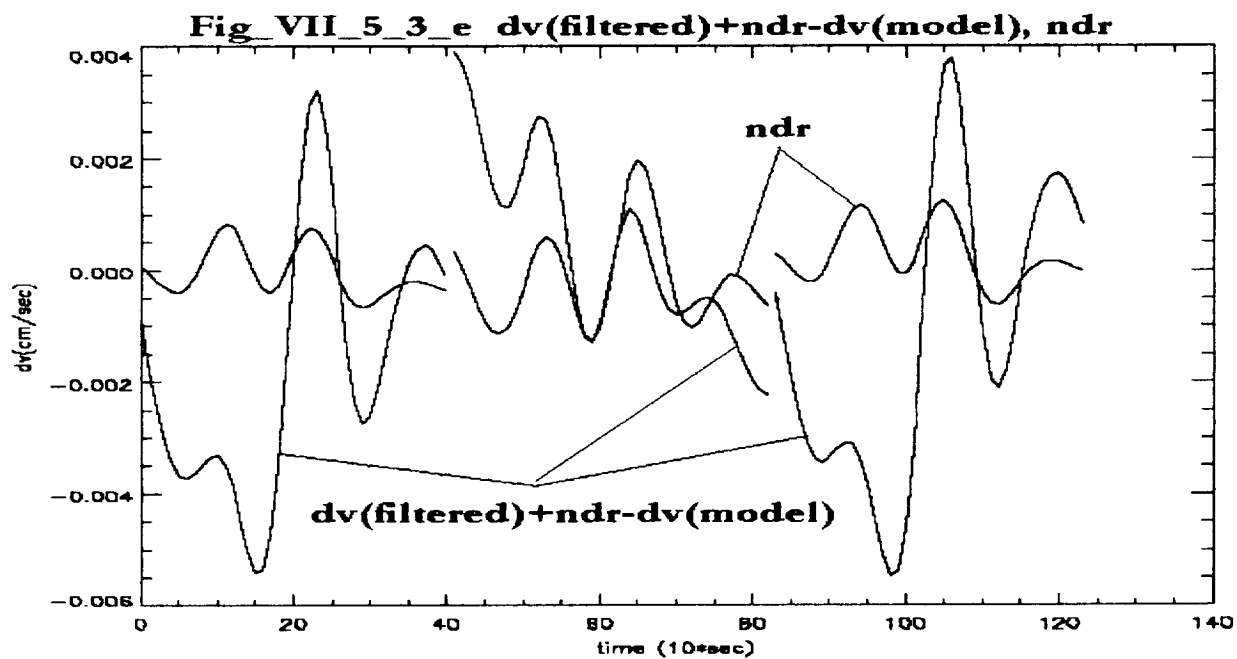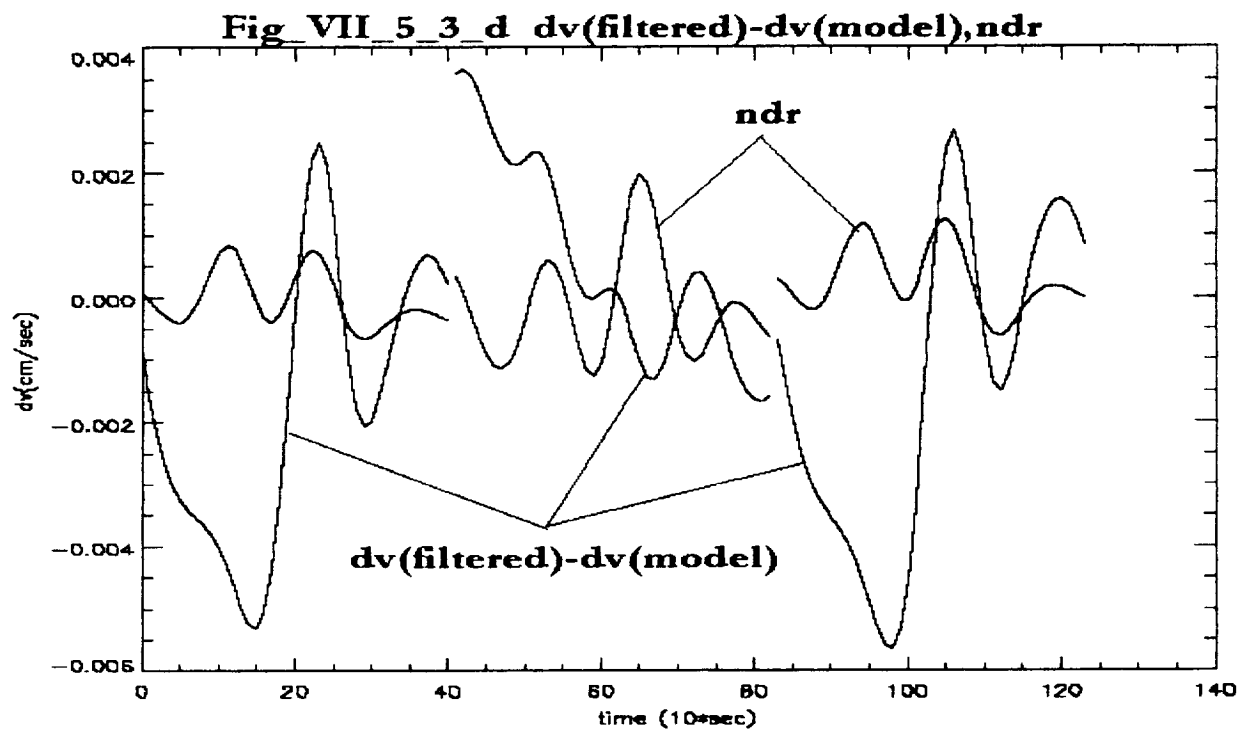
VI_5_5 Geoid Data Base

For facilitating comparison of the recovered geoid, N, with the model geoid, N(model), a geoid data base has been created. The fundamental coordinates used are geodetic latitude and longitude. The surface of the earth is divided into $0.5°$ (55 km), approximately equal area blocks. These blocks are arranged in $0.5°$ latitude bands, with coordinate $\varphi=0.25°\pm k\times0.5°$. Each latitude band is divided into $n=[\cos(\varphi_o)\times 360.0/0.5 + 0.5]$ blocks, where the symbol [x] signifies the integral part of x. The longitude blocks have the size $\Delta\lambda=360.0°/n$. When extracting data in the data base, there are two options. First, is to return the same value for all points within the block. Second, is to use linear interpolation, as a ruled surface, for a point bounded by four data points.

When creating a geoid data base from the potential expressed in spherical harmonics, e.g. the EGM96, we assume that the independent variables are geocentric latitude and longitude. When evaluating the spherical harmonics, for insertion in the geoid data base for a geodetic latitude and longitude, these are converted to geocentric latitude and longitude for the calculation. Note that this is consistent with generation of satellite observation residuals, $\Delta d\rho/dt$. In archiving the satellite residuals the coordinates of the two satellites (P,Q) are archived as height above the reference ellipsoid, geodetic latitude and longitude, as well and the geocentric Cartesian coordinates and velocities.

VII_6 Orbit Simulation

VII_6_1 Introduction

In previous sections, necessary elements of, Potential Theory (III), Orbit Theory (IV), and Geophysical Inverse Theory (VI) to analyze satellite to satellite tracking data for geoid determination have been reviewed. Some numerical experiments were described that illustrate how these elements can be combined, and what sort of results may be expected. These numerical experiments were progressively more complex and complete First the nature of the eigenvalues and eigenfunctions that come from the singular value decomposition were described. These results depend only on the physical geometry of the measurement, and is independent of the measurement itself. Second, some properties of the solution assuming a direct measurement of potential difference: accuracy, resolution, error propagation, and sensitivity were shown. For these analyses, idealized geoid anomalies were used: blocks with a dimension of 1.0 degree and 5.0 degrees were combined. Now a number of orbital simulations will be offered, with increasing complexity in the desired geoid, and other orbital effects. For these the geoid model will be the EGM96 geopotential model [*Lemoine and al.*, (1998)]. EGM96 is a complete Spherical Harmonic representation to degree and order 360. For the illustrative proposes of these demonstrations, the EGM96 model will be truncated, at degree 70, 90 and 180. In addition other physical forces will be included: lunar and solar forces, ocean and solid body tides, atmospheric drag, solar radiation pressure, and earth albedo pressure. The focus of these last simulations will be to demonstrate the recovery of geoid information from satellite to satellite range rate, which involves correcting for the indirect effects (equation 4.33) in the presence of other force model errors, that can only approximately be accounted for in the orbit fit. Exploration of the degradation of the recovered geoid in the presence of these other forces, is a much larger effort than was addressed here, but some limited cases will be shown.

The parameters of the simulations are summarized in Table VII_5_1, and the initial state vectors are defined in Table 4.1. These are intended to represent the GRACE Mission. The end-to-end orbit simulation process is described in Figure VII_5_1. It begins with simulated satellite-to-satellite tracking (SST) range rate data. Now, we need to obtain the contribution of the anomalous potential, T, from the observed range rate. Therefore, the first step is to perform a Precision Orbit Determination (POD) using the SST data and any other available tracking data – here assumed to be ground based laser tracking – using a chosen reference potential, U, to obtain the orbit residuals, Δ dρ/dt. These residuals contain the desired signal, the interaction terms from nδr, and other orbital errors due to inadequate force models. Therefore, the calculation of the potential difference, ΔT, from the observed satellite to satellite range rate, dρ/dt, is accomplished, as described above, using the POD residuals. A number of cases are computed, summarized in Table VII_6_1.

| Table VII_6_1 Parameters of Orbit Simulations						
Case	Total Potential U+T	Reference Potential U	Other Forces	Latitude Range	Longitude Range	Sample POD σ (cm/sec)
1	l=2-70	l=2-40	Sun,Moon,Tides	20°-50°	20°-30°	0.03
2	l=2-180	l=2-90	Sun,Moon,Tides	20°-50°	20°-30°	0.01
3	l=2-90	l=2-40	Sun,Moon,Tides Drag, Solar Pressure, Earth Albedo	20°-50°	20°-30°	0.03
4	l=2-180	l=2-90	Sun,Moon,Tides Drag, Solar Pressure, Earth Albedo	20°-50°	20°-30°	0.01
5	l=2-180	l=2-90	Sun,Moon,Tides Drag, Solar Pressure, Earth Albedo	29°-41°	23°-27°	0.01

VII_6_2 Region of Interest.

The main thrust of using the GITSEM is to obtain local or regional maps of the geoid, from the measurement of SST range rate. We have chosen one region for the simulation: the Eastern Mediterranean Sea. This region is tectonically active, and has a significant signal at all wavelengths. Therefore, it provides a useful geophysical test bed for the method. Figure VII_6_a is a free air gravity anomaly map of the region, centered roughly on the island of Crete.

VII_6_3 Case 1

We begin with the total potential, U+T, complete for degree and order l=2 through 70 and the reference potential, U, complete for l=2 though 40. Therefore, the anomalous potential sought, is complete for l=41 though 70. The 60 day mission is processed, and the observations selected requiring that no positions P or Q are closer than 20 km. This resulted in 1187 observations. The Gram Matrix calculation and Singular Value Decomposition provided the eigenvalues and eigenvectors. Smoothing was achieved by selection of the Lagrange Multiplier, C. Table VII_6_2 gives the values. Figure VII_6_b shows the recovered geoid, and Figure VII_6_c shows the anomalous geoid (l=41 through 70). Also given in Table VII_6_2 are
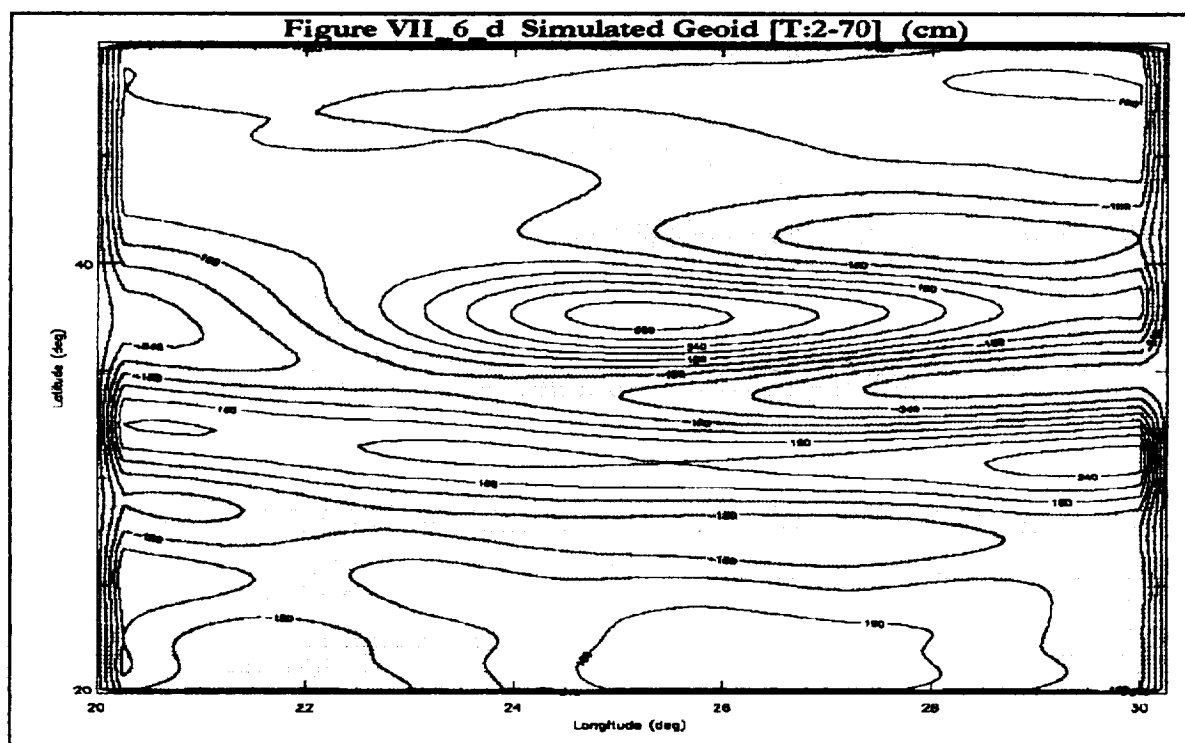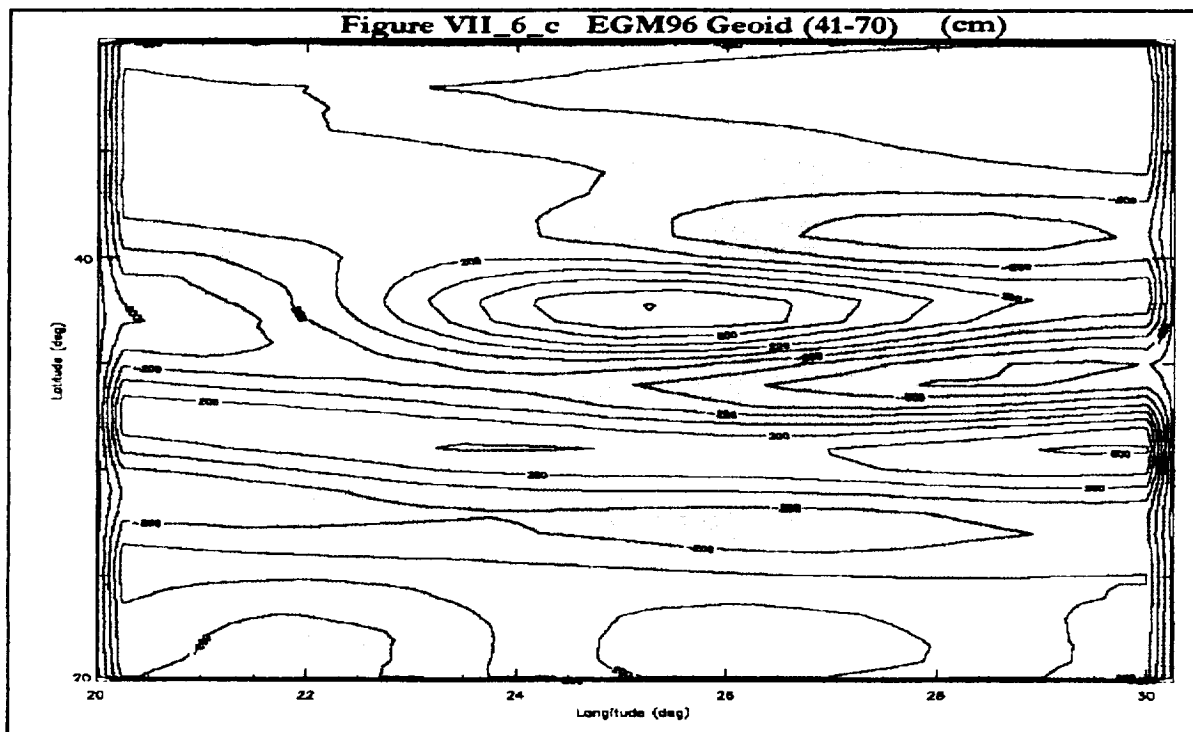
Figure VII_6_a   Eastern Mediterranean
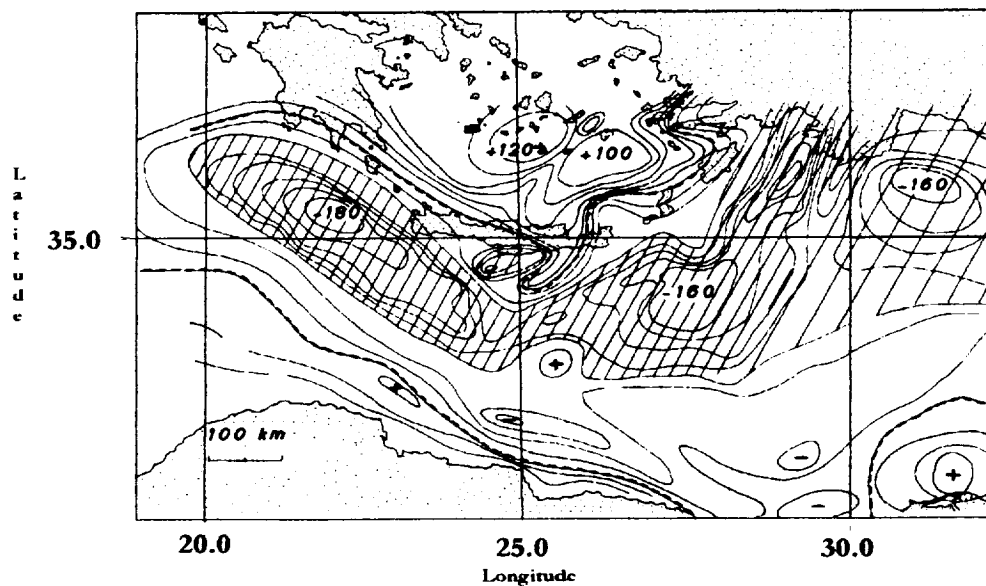
Free Air Gravity Anomalies (milligals)

Figure VII_6_b Recovered Geoid [Total U+T:2-70, Reference U:2_40]   (cm)
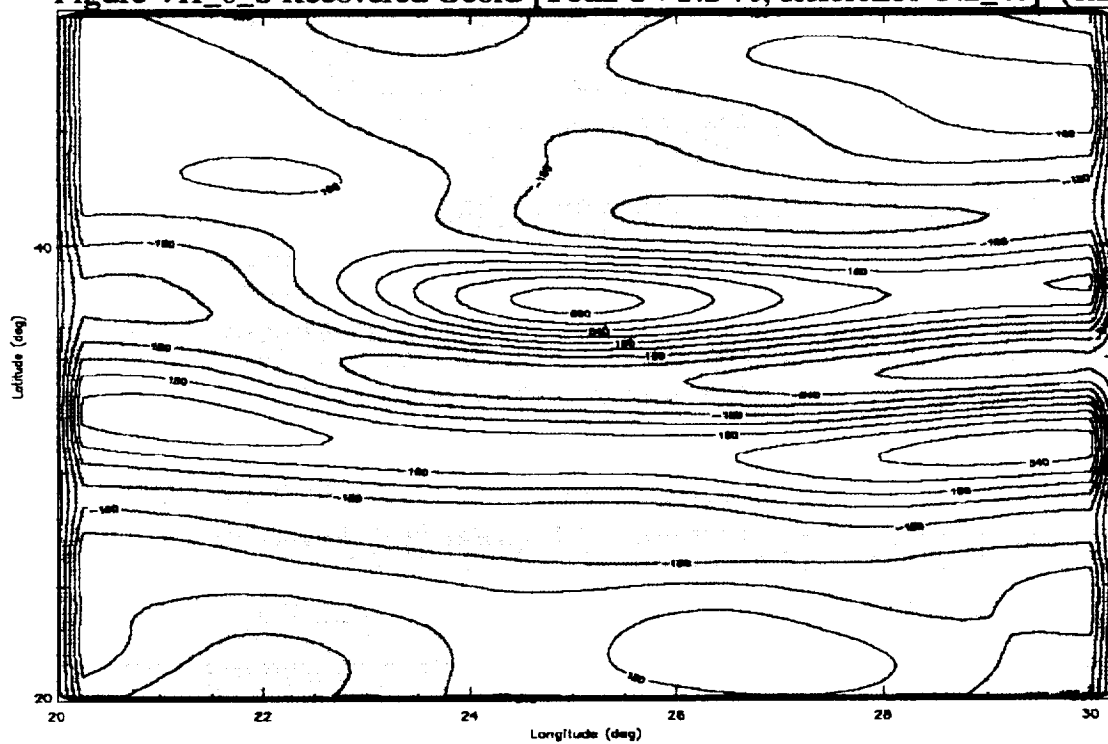
Figure VII_6_c   EGM96 Geoid (41-70)   (cm)

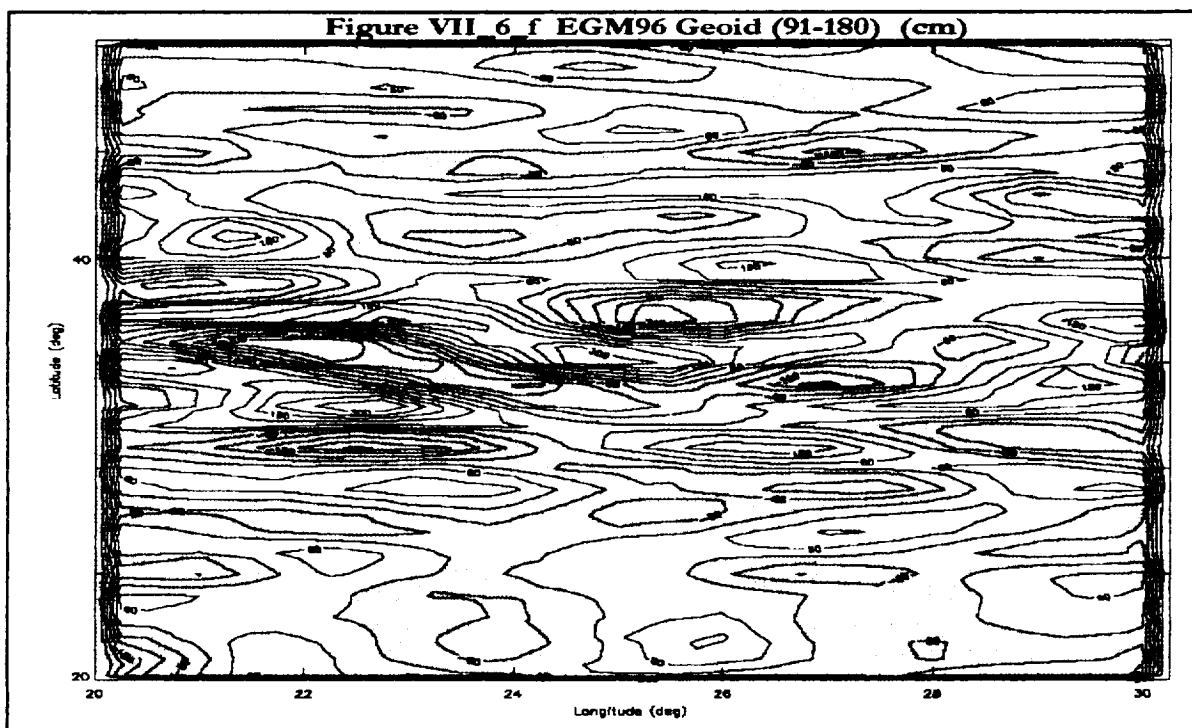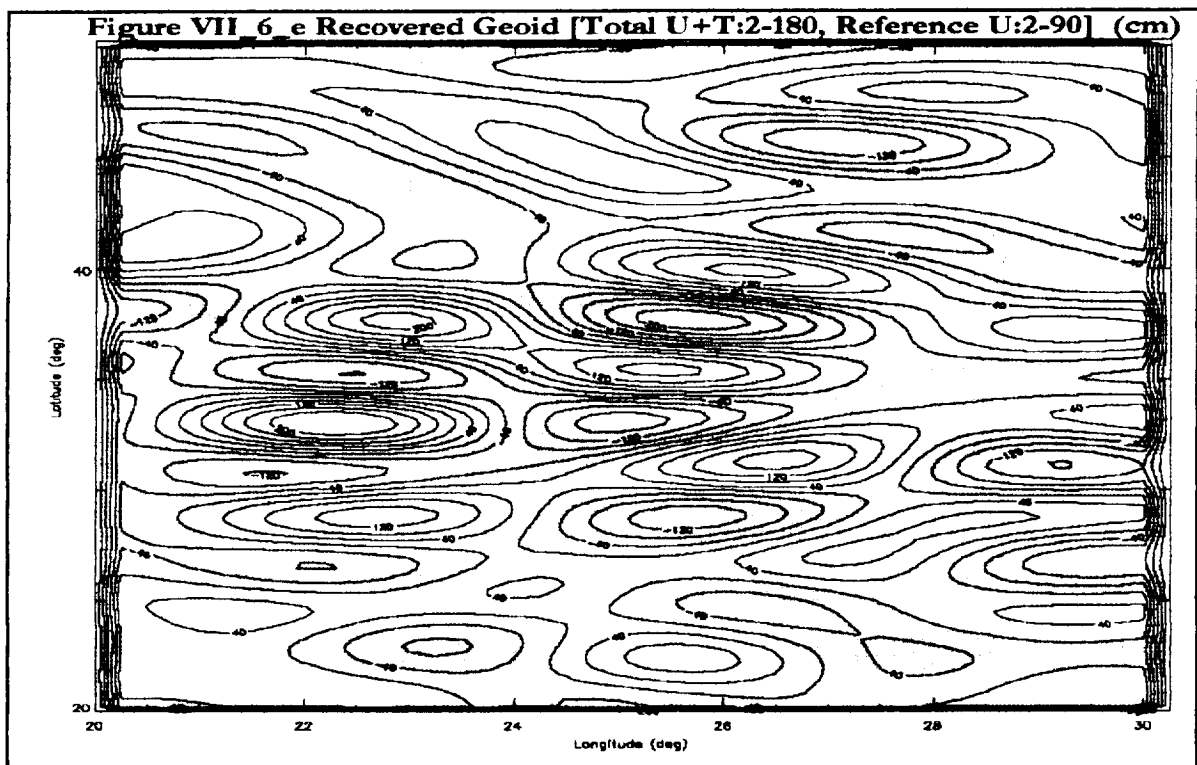Figure VII_6_d Simulated Geoid [T:2-70] (cm)

statistics of the geoid fit. We see the general agreement of features. The statistics of this solution is as follows. The variance of the geoid for the selected region is 268.0 cm. The rms of the geoid fit is 88.2 cm. To identify the error sources in this map, the orbit positions (P,Q) are used, i.e. the same Gram Matrix, and the observed potential difference is calculated from the geoid model using the Poisson Integral formula (3.1). For this calculation the rms of the geoid fit is 23.0 cm. Figure VII_6_d shows this recovered geoid. This calculation is repeated selecting orbit positions with a minimum position difference of 10 km. This results in n=1881 observations, and has an rms of geoid fit of 16.7 cm. This is a marginal improvement considering the increased dimension of the basis functions. A number of remarks are in order. First, it is not possible to obtain exact agreement between the spherical harmonic representation and the GITSEM. This should not be surprising, considering the fact that these use fundamentally different basis functions, and they are finite in dimension. Second, the GITSEM does have the potential to achieve centimeter accuracy in geoid height. Third, errors in the recovered geoid are due to errors in converting the observed range rate residuals, Δ dρ/dt, to potential difference,ΔT.

Table VII_6_2 Summary of Geoid Results							
Case	n	$\lambda_{min}, C/\lambda_{max}$	Obs σ (cm/sec)	Var(Obs) (cm/sec)	Geoid height σ (cm)	Var (geoid) (cm)	Comment
1	1187	$C/\lambda_{max}=10^{-4}$	8.91×10^{-1}	21.85	88.2	268.0	20 km separation
1	1187	$C/\lambda_{max}=10^{-7}$	3.61×10^{-3}	21.97	23.0	268.0	Upward Continuation
1	1881	$C/\lambda_{max}=10^{-9}$	3.18×10^{-4}	20.90	16.7	268.0	10 km separation
2	1186	$10^{-2}(107)$	7.59×10^{-2}	2.67×10^{-1}	64.37	86.38	20 km separation
2	1186	$10^{-6}(402)$	1.61×10^{-4}	2.54×10^{-1}	21.17	86.38	Upward Continuation
2	1913	$10^{-2}(131)$	7.90×10^{-2}	2.68×10^{-1}	69.72	86.38	10 km separation
3	1135	$C/\lambda_{max}=10^{-4}$	8.90×10^{-1}	22.59	85.52	303.2	20 km separation
4	1132	$5\times10^{-4}(173)$	2.92×10^{-2}	2.55×10^{-1}	57.01	86.38	20 km separation
5	271	$C/\lambda_{max}=10^{-6}$	3.01×10^{-2}	3.36×10^{-1}	53.1	124.5	5 km separation Limited Area

VII_6_4 Case 2

In this case we illustrate recovery of smaller scale features of the geoid. Therefore, we begin with the total potential, U+T, complete for degree and order l=2 through 180 and the reference potential, U, complete for l=2 though 90. Therefore, the anomalous potential sought, is complete for l-91 though 180. As before, the 60 day mission is processed, and the observations selected requiring that no positions P or Q are closer than 20 km. This resulted in 1186 observations. The Gram Matrix calculation and Singular Value Decomposition provided the eigenvalues and eigenvectors. Smoothing was achieved by selection of a minimum eigenvalue, λ_{min}. Table VII_6_2 gives the values. For the cases where λ_{min} has been chosen, the number of eigenfunctions used for the model is given in parenthesis. Figure VII_6_e shows the recovered geoid, and Figure VII_6_f shows the anomalous geoid (l=91 through 180). Also given in Table

Figure VII_6_e Recovered Geoid [Total U+T:2-180, Reference U:2-90]   (cm)
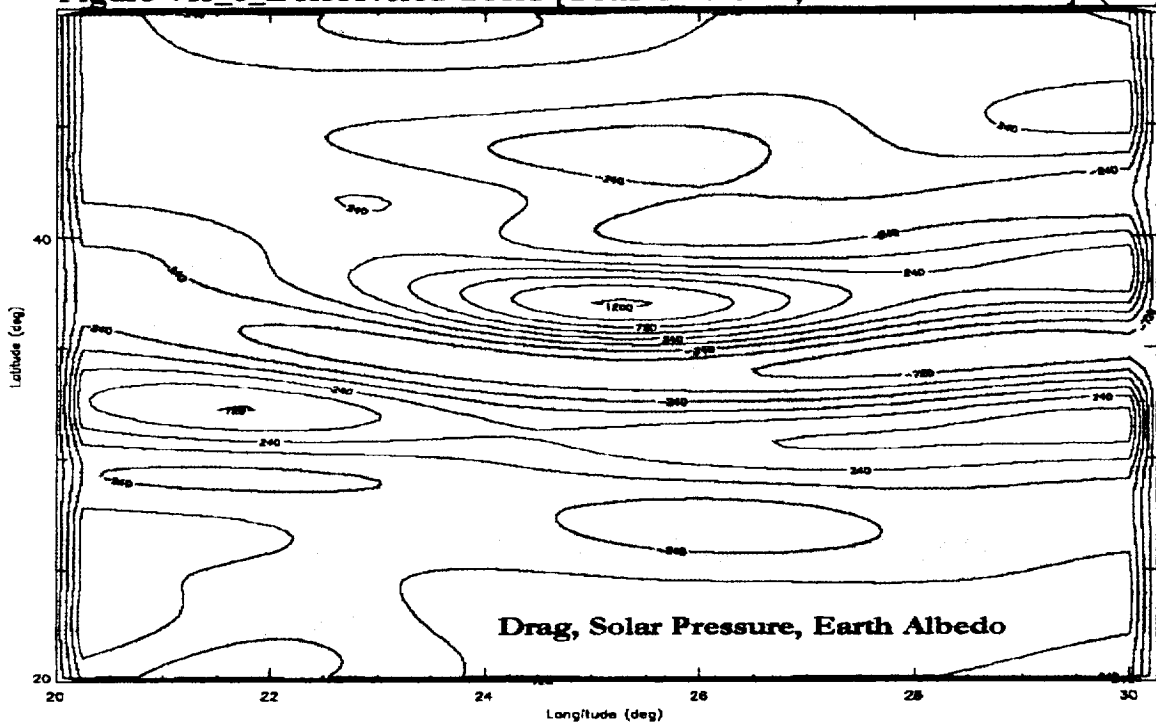

Figure VII_6_f EGM96 Geoid (91-180)   (cm)

VII_6_2 are statistics of the geoid fit. We see the general agreement of features. The statistics of this solution are as follows. The variance of the geoid for the selected region is 86.38 cm. The rms of the geoid fit is 64.37 cm. To identify the error sources in this map, the orbit positions (P,Q) are used, i.e. the same Gram Matrix, and the observed potential difference is calculated from the geoid model using the Poisson Integral formula (3.1). For this calculation the rms of the geoid fit is 21.17 cm. Figure VII_6_g shows this recovered geoid.


Figure VII_6_g Simulated Geoid [T:91-180] (cm)
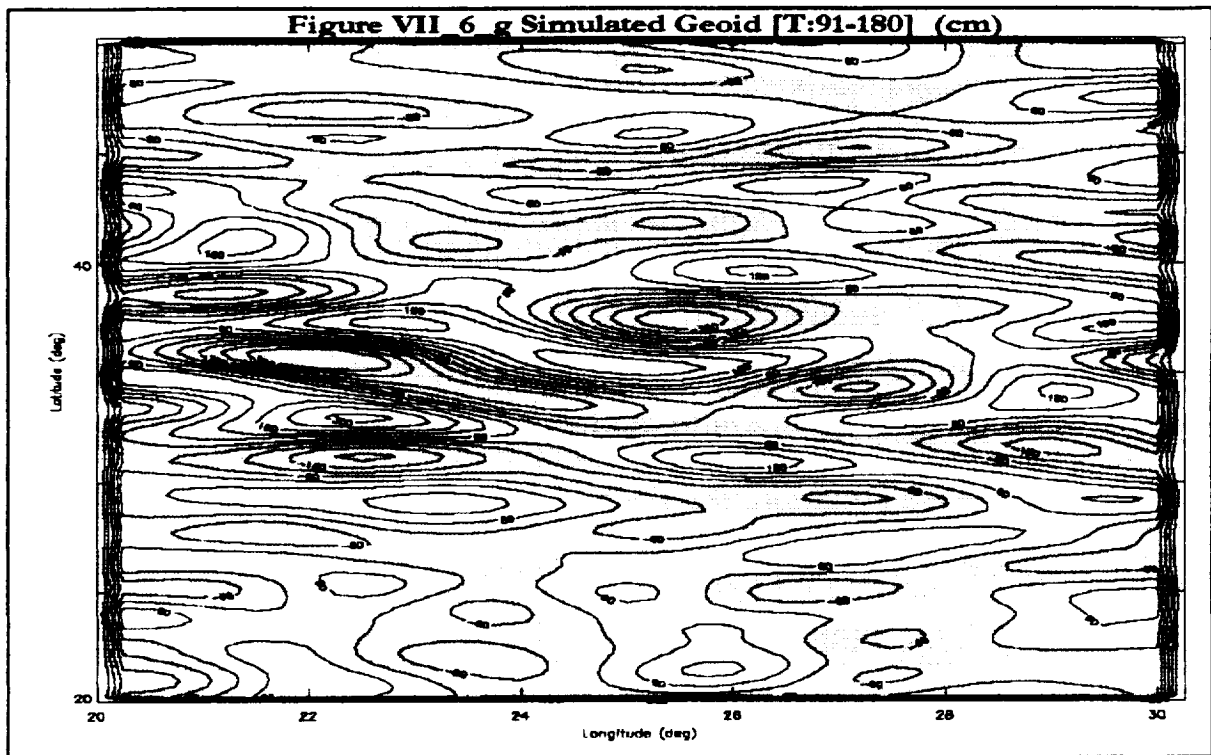
VII_6_5 Case 3

In this case we illustrate geoid recovery in the presence of non gravitational forces, thermosphere drag, solar radiation pressure, and earth albedo pressure. In this case the MSIS thermosphere model is used, a solar pressure model, and an earth albedo pressure model. in generating the simulated data, and in the precision orbit determination (POD). In the POD, a 5% error is introduced in the overall model, and a drag scale "solve for" factor is included. We begin with the total potential, U+T, complete for degree and order l=2 through 90 and the reference potential, U, complete for l=2 though 40. Therefore, the anomalous potential sought, is complete for l-41 though 90. As before, the 60 day mission is processed, and the observations selected requiring that no positions P or Q are closer than 20 km. This resulted in 1135 observations. The Gram Matrix calculation and Singular Value Decomposition provided the eigenvalues and eigenvectors. Smoothing was achieved by selection of a minimum eigenvalue,

## Figure VII_6_h Recovered Geoid [Total U+T:2-90, Reference U:2-40] (cm)

Drag, Solar Pressure, Earth Albedo

Figure VII_6_i EGM96 Geoid (41-90) (cm)
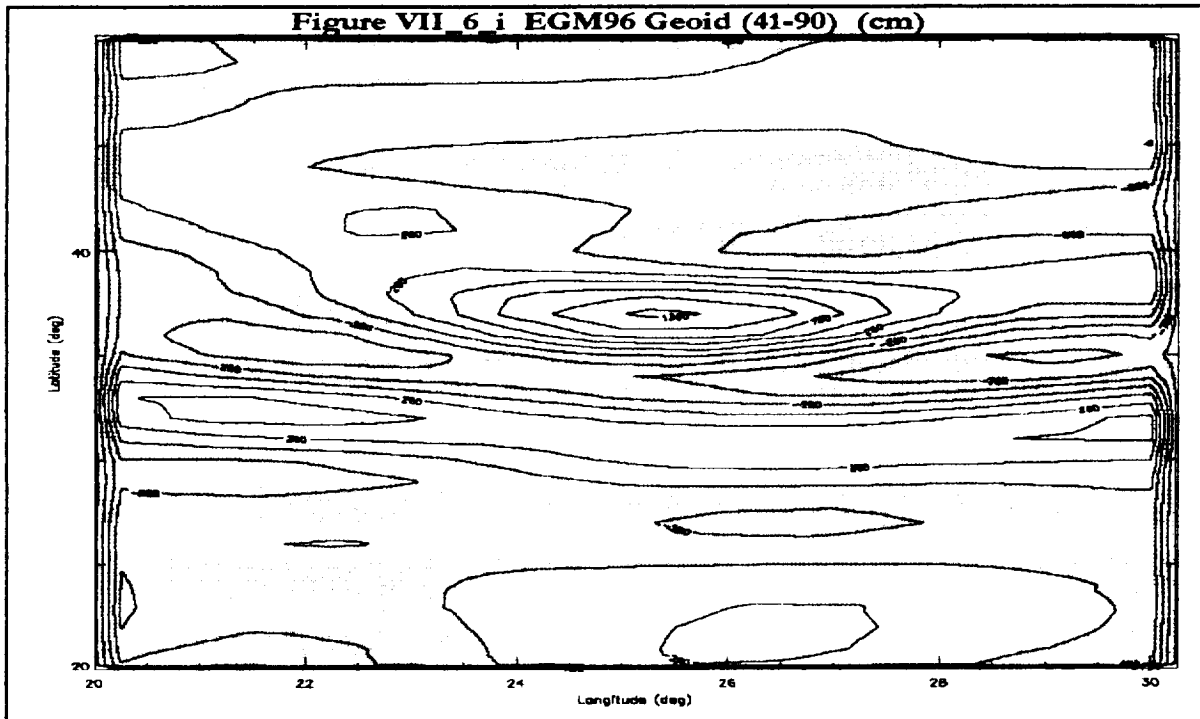
λ_{min}. Table VII_6_2 gives the values. For the cases where λ_{min} has been chosen, the number of eigenfunctions used for the model is given in parenthesis. Figure VII_6_h shows the recovered geoid, and Figure VII_6_i shows the anomalous geoid (l=41 through 90). Also given in Table VII_6_2 are statistics of the geoid fit. We see the general agreement of features. The statistics of this solution as as follows. The variance of the geoid for the selected region is 303.2 cm. The rms of the geoid fit is 85.52 cm. The fact that the results here are so similar to Case 1, is encouraging, in that the presence of nongravitational forces, and errors in modelling them, seem to have a small effect on the geoid recovery. This is consistent with the idea that the effects of, and errors in, drag and solar pressure have quite a different spectral character, and should be separated from the geoid. However, the thermosphere models used here are quite smooth, and do not even attempt to represent small scale thermosphere variations such as gravity waves, winds, etc. No doubt, great care will be necessary in treating these non-gravitational forces.

VII_6_6 Case 4

In this case we continue to illustrate geoid recovery in the presence of non gravitational forces, thermosphere drag, solar radiation pressure, and earth albedo pressure, but for finer scale geoid features. The MSIS thermosphere model, a solar pressure model, and an earth
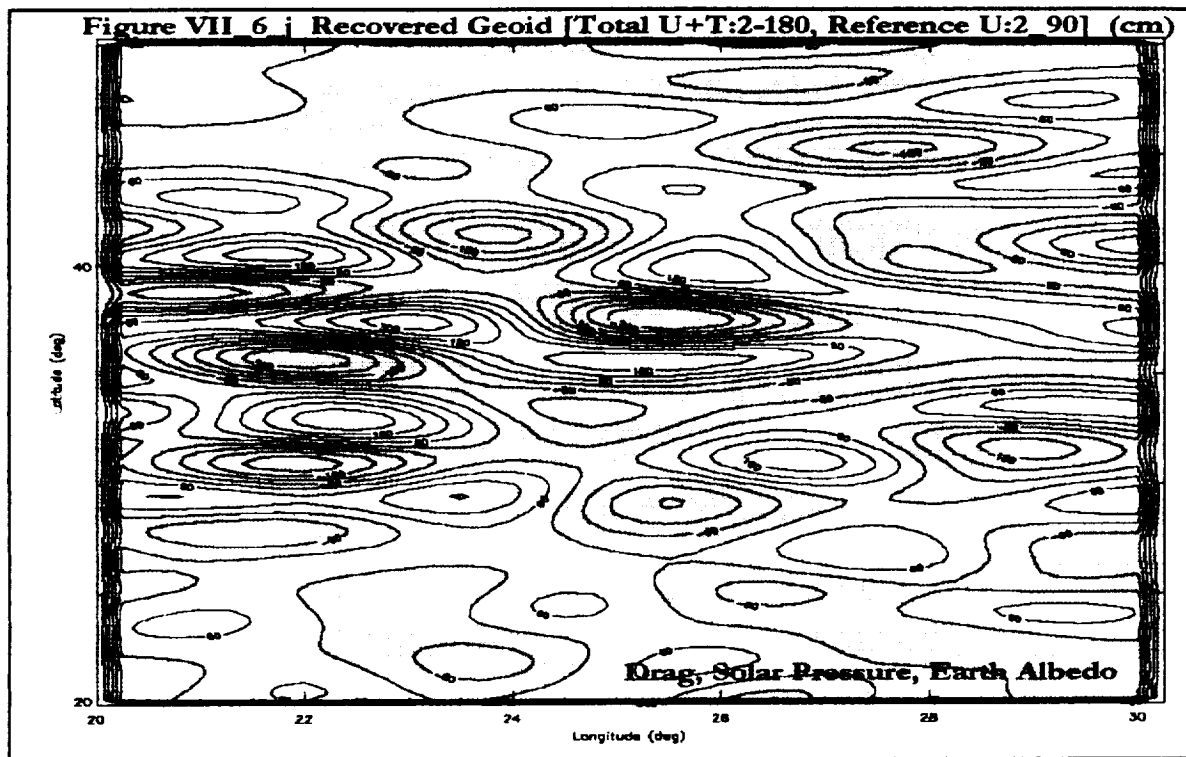
Figure VII_6_i Recovered Geoid [Total U+T:2-180, Reference U:2_90] (cm)

albedo pressure model. are used generating the simulated data, and in the precision orbit determination (POD). In the POD, a 5% error is introduced in the overall model, and a drag scale "solve for" factor is included.   We begin with the total potential, U+T, complete for degree and order l=2 through 180 and the reference potential, U, complete for l=2 though 90.

Therefore, the anomalous potential sought, is complete for 1-91 though 180. As before, the 60 day mission is processed, and the observations selected requiring that no positions P or Q are closer than 20 km. This resulted in 1132 observations. The Gram Matrix calculation and Singular Value Decomposition provided the eigenvalues and eigenvectors. Smoothing was achieved by selection of a minimum eigenvalue, λ_{min}. Table VII_6_2 gives the values. For the cases where λ_{min} has been chosen, the number of eigenfunctions used for the model is given in parenthesis. Figure VII_6_j shows the recovered geoid. Also given in Table VII_6_2 are statistics of the geoid fit. We see the general agreement of features. The statistics of this solution as as follows. The variance of the geoid for the selected region is 86.38 cm. The rms of the geoid fit is 57.01 cm.

Figure VII_6_k Recovered Geoid [Total U+T:2-180, Reference U:2-90] (cm)
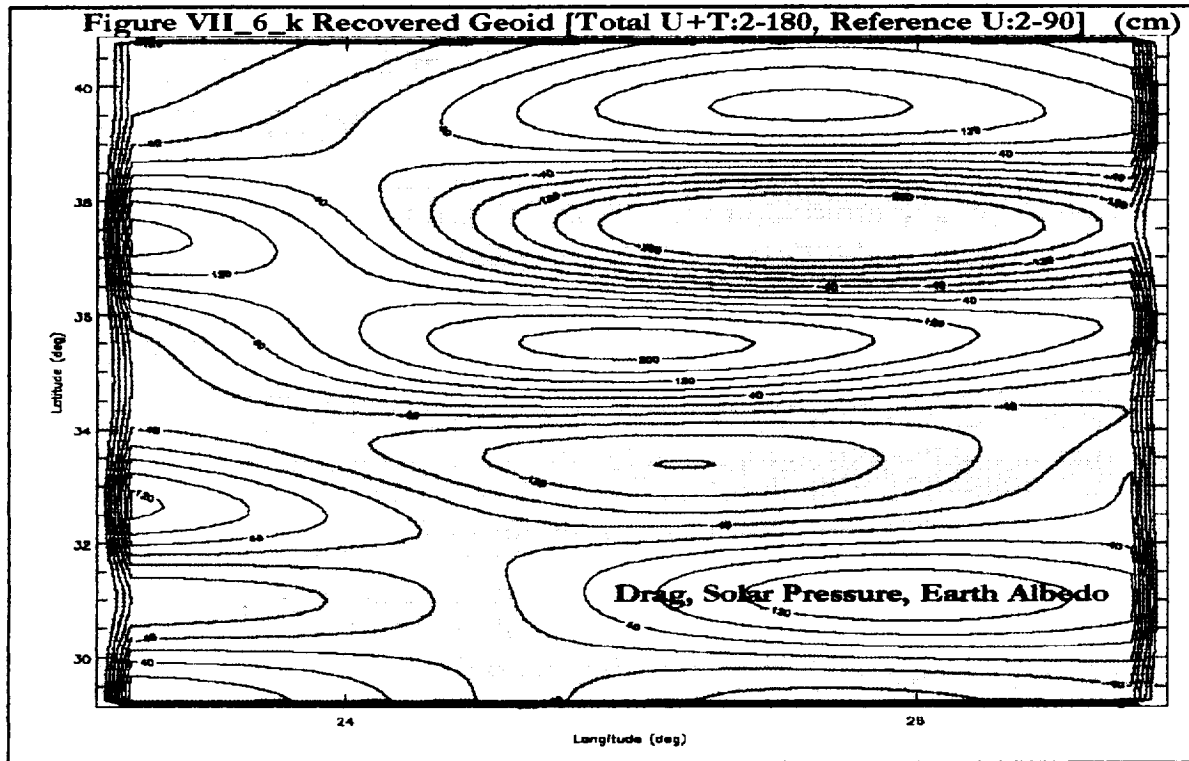
VII_6_7 Case 5

In this case we continue to illustrate geoid recovery in the presence of non gravitational forces, thermosphere drag, solar radiation pressure, and earth albedo pressure, for finer scale geoid features. Here, we reduce the area of interest, and decrease the minimum distance between points (P or Q), to see if this would increase the recovered geoid resolution. As above, the MSIS thermosphere model, a solar pressure model, and an earth albedo pressure model. are used generating the simulated data, and in the precision orbit determination (POD). In the POD, a 5% error is introduced in the overall model, and a drag scale "solve for" factor is

included.   We begin with the total potential, U+T, complete for degree and order l=2 through 180 and the reference potential, U, complete for l=2 though 90. Therefore, the anomalous potential sought, is complete for l-91 though 180.   As before, the 60 day mission is processed, and the observations selected requiring that no positions P or Q are closer than 5 km. This resulted in 271 observations. The Gram Matrix calculation and Singular Value Decomposition provided the eigenvalues and eigenvectors. Smoothing was achieved by selection of a minimum eigenvalue, λ_{min}.   Table VII_6_2 gives the values. For the cases where λ_{min} has been chosen, the number of eigenfunctions used for the model is given in parenthesis. Figure VII_6_k shows the recovered geoid and Figure VII_6_l shows the anomalous geoid (l=91 through 180). Also given in Table VII_6_2 are statistics of the geoid fit. We see the general agreement of features. The statistics of this solution as as follows. The variance of the geoid for the selected region is 124.5 cm. The rms of the geoid fit is 53.1 cm.

Fig_VII_6_l EGM96 Geoid (91-180) (cm)
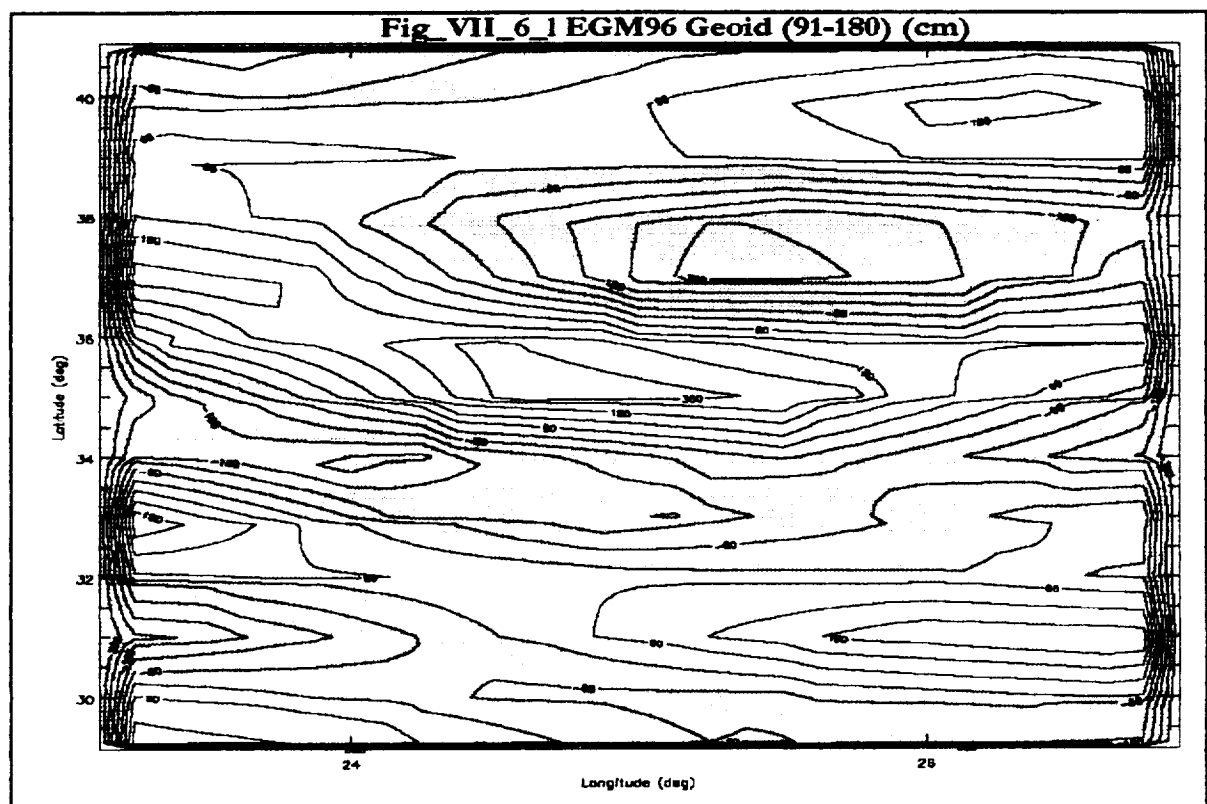
VIII   Discussion

The geoid recovered in all cases represents the major features of the model geoid.
It is not possible to obtain exact agreement between the spherical harmonic representation and
the GITSEM. This should not be surprising, considering the fact that these use fundamentally
different basis functions, and they are finite in dimension. Second, the GITSEM does have the
potential to achieve centimeter accuracy in geoid height. Third, errors in the recovered geoid
are due to errors in converting the observed range rate residuals, Δ dp/dt, to potential
difference, ΔT

The present accuracy of the orbital simulation, does not meet the objective of achieving
0.5 μ/sec range rate residuals, and centimeter accuracy short wavelength geoid height.. Due to
limited scope of this analysis, refinements of calculating the potential difference ΔT, from the
range rate residuals, Δ dp/dt, could not be explored. The current method has an error of ~5%.
There are a number of avenues to be investigated. First would be use of short arc calculation to
obtain the residuals. Since we believe that the remaining error is due to unmodeled orbital
errors, this could reduce these errors. The second would be to use an iterative method. Taking
the first solution for the geoid, calculate a correction to the residuals, and repeat the GIT geoid
estimate to obtain a correction. A third method would be to develop a recursive digital filter,
based on the orbit model, to improve the correction estimate.

In a careful and detailed analysis Jekeli, [*Jekeli*, (1981)] has shown two critical results.
Jekeli combines the error of representation (3.20) and the error of omission (3.19 suitably
generalized for r<R as 3.17) as the downward continuation error – the error of commission is
not included. Jekeli, with $\bar{n} = 300$, finds (tables 3 and 4) that the DCE largest near the poles
$\sigma(\varepsilon_r)$ <0.090 mgals (0.290 mgals max) gravity anomaly and $\sigma(\varepsilon_r)$ <0.042 cm (0.14 cm max)
geoid height. Second, by seeking anomalies averaged over a spherical cap of about 1.4 degrees
(tables 6 and 7), the DCE – again largest at the poles, is estimated to be $\sigma(\varepsilon_r)$ <0.004 mgals
(0.014 mgals max) gravity anomaly and $\sigma(\varepsilon_r)$ <0.0020 cm (0.0066 cm max) geoid height.
Therefore the conclusion of Jekeli [*Jekeli*, (1981), p 127] "The downward continuation errors
depicted in tables 3 through 7 are completely insignificant with respect to anticipated
measurement accuracies of 1 mgal and 10 cm in the gravity anomaly and geoid undulation,
respectively." And, " .. the estimation of point or mean gravity anomalies and geoid
undulations (height anomalies) using the outer series expansion to degree 300 anywhere on the
earth's surface is practically unaffected by the divergence of the total series." We believe that
using a spherical approximation for the anomalous potential, has sufficient accuracy for our
geoid estimate.

We turn now to the question of computer resources needed for this analysis. This study
has been done on an INTEL Pentium II, 233 Mhz PC. Storage on this class of machine is quite
adequate. However, the processor speed limits the analysis. There are two major steps in the
computation: 1) the Precision Orbit Determination (POD) and 2) calculation of the Gram
Matrix. For this analysis, we use the canonical 60 day mission. The POD is accomplished in
less that 1 day, the exact amount of time, of course, depending on the force model complexity,

and the number of iterations (i.e. on the amount of bad data to be screened). This is not limiting. The algorithms developed for calculating the Gram Matrix, require about 0.2 sec per matrix element on this machine. Being a symmetric matrix the time for each region would be 0.2×n×(n+1)/2 seconds. So for n=1000, we need about 28 hours of processor time. This is the bottleneck. Assuming the regional dimension used in this analysis, 20×30=600 square degrees, there would be 70 such regions for the whole earth. Presumably, for global analysis, one would want to use the classical spherical harmonic analysis anyway. In addition, the PC processor used here is now obsolete: there are 1 Ghz processors on the market now. A factor of 10 improvement in running time is easily achieved with PC architecture today, and greater speed is available with more advanced and expensive computer architectures. If desired, once set up, one could produce a global set of geoid maps in a few days. It seems that this approach is feasible.

References

anon., "*Report on a dedicated gravitational satellite mission.*", Panel on Gravity and Sea Level of the Committee on Geodesy, National Academy of Sciences/National Research Council,Washington DC,Report No. 53 pp,(1979).

anon., "*Satellite Gravity and the Geosphere*", National Research Council/National Academy of Sciences,Washington D.C.,Report No. 112 pp,(1997).

Backus, G., and F. Gilbert, "Numerical applications of a formalism for geophysical inverse problems", *Geophys. Journ. Roy. Astron. Soc.*, *13*,pp. 247-276, (1967).

Backus, G., and F. Gilbert, "The resolving power of gross earth data", *Geophys. Journ. Roy. Astron. Soc*, *16*,pp. 169-205, (1968).

Backus, G., and F. Gilbert, "Uniqueness in the inversion of inaccurate gross earth data", *Phil. Trans. Roy. Soc. London, Ser. A, 226*,pp. 343-344, (1970).

Backus, G.E., "Application of a nonlinear boundary-value problem for Laplace's equation to gravity and geomagnetic intensity surveys", *Q.J. Mech. Appl. Math, 21*,pp. 195-221, (1968).

Bettadpur, S.V., B.E. Schutz, and J.B. Lundberg, "Spherical harmonic synthesis and least squares computation in satellite gravity gradiometry", *Bulletin Geodesique, 66* (2),pp. 261-272, (1992).

Brouwer, D., and G.M. Clemence, "*Methods of Celestial Mechanics*", 598 pp., Academic Press, New York, (1961).

Bullard, E.C., and R.I. Cooper, "The determination of the masses necessary to produce a given gravitational field.", *Proc. Roy. Soc. London Ser. A, 194*,pp. 332-347, (1948a).

Colombo, O., "*Global Geopotential Modelling From Satellite-To-Satellite Tracking*", The Ohio State University,Columbus Ohio,Report No. 317,137 pp,(October 1981)

Gaposchkin, E.M., "*Satellite dynamics*", Smithsonian Astrophysical Obs.,Cambridge MA 02138,Report No. 353,85-192 pp,(1973)

Golub, G.H., and C. Reinsch, Singular Value Decomposition and Least Squares Solutions, in *Handbood for Automatic Computation, Volume II, Linear Algebra*, edited by J.H. Wilkinson, and C. Reinsch, pp. 134-151, Springer-Verlag, New York Heidelberg Berlin, (1971).

Hamming, R.W., "*Numerical Methods for Scientists and Engineers*", 721 pp., McGraw Hill, New York, (1973).

Heiskanen, W.A., and H. Moritz, "*Physical Geodesy*", 364 pp., W.H. Freeman, San Francisco, (1967).

IAU, "*Proceedings of the Eighteenth General Assembly Patras 1982*", , Reidel, Dordrecht, Holland, (1983).

Jeffreys, H., and B.S. Jeffreys, "*Methods of Mathematical Physics, 3rd edition*", 714 pp., Cambridge University Press, Cambridge, (1956).

Jekeli, C., "*The Downward Continuation to the Earth's Surface of Truncated Spherical and Ellipsoidal harmonic Series of the Gravity and Height Anomalies*", The Ohio State University,Columbus, Ohio,Report No. 323,140 pp,(December 1981)

Jekeli, C., "The Determination of Gravitational Potential Differences from Satellite-to-Satellite Tracking", *Celestial mechanics and Dynamical Astronomy, 75* (2),pp. 85-101, (1999).

Kaula, W.M., Global harmonic and statistical analysis of gravity, in *Extension of Gravity Anomalies to Unsurveyed Areas*, edited by H. Orlin, pp. 58-67, American Geophysical Union Monograph, (1966).

Kaula, W.M., "Inference of Variations in the Gravity Field from Satellite-to-Satellite Range-Rate", *Journ. Geophys. Res.*,pp. 17, (1982).

Kaula, W.M.chairman, *"The Terrestrial Environment: Solid Earth and Ocean Physics"*, Massachusetts Institute of Technology,Cambridge MA,Report No. NASA CR 1579,152pp pp,(1970)

Kellog, O.D., *"Foundations of Potential Theory"*, 384 pp., Dover, New York, (1953).

Lemoine, F.G., and e. al., *"The development of the joint NASA GSFC and National Imagery Mapping Agency NIMA geopotential model EGM96,"*, NASA Goddard Space Flight Center,Greenbelt, Maryland,Report No. TP-1998-206861,600 pp,(1998).

Moritz, H., "Least Squares Collocation", *Rev. Geophys. Space. Phys., 16*,pp. 421-430, (1978).

Moritz, H., *"Advanced Physical Geodesy, 2nd ed."*, 500 pp., Abacus Press Wichmann Verlag, Karlsruhe, (1980,1989).

Muller, P.M., and W.L. Sjogren, "Mascons: Lunar mass concentrations", *Science, 161*,pp. 680-684, (1968).

Nerem, R.S., C. Jekeli, and W.M. Kaula, "Gravity field determination and characteristics: Retrospective and prospective", *Journ. Geophys. Res., 100* (B8),pp. 15053-15074, (1995 Aug 10).

Parker, R.L., "Understanding Inverse Theory", *Ann. Rev. Earth & Planetary Science, 5*,pp. 35-64, (1977).

Parker, R.L., *"Geophysical Inverse Theory"*, vi+386 pp., Princeton Univ. Press, Princeton, New Jersey, (1994).

Press, W.H., S.A. Teukolsky, W.T. Vetterling, and B.P. Flannery, *"Numerical Recipes in C: The Art of Scientific Computing (2nd Edition)"*, 994 pp., Cambridge Univ. Press, Cambridge, UK, (1991).

Rummel, R., *"Downward continuation of gravity information from satellite tracking or satellite gradiometry in local areas."*, Ohio State Univ.,Columbus Ohio,Report No. 221,50 pp,(1975)

Rummel, R., C. Reighber, and K.H. Ilk, "the Use of satellite-t-satellite tracking for gravity parameter recovery", in *Space Oceanography Navigation and Geodynamics Workshop*, European Space Agency, (1978).

Vonbun, F.O., W.D. Kahn, W.T. Wells, and T.D. Conrad, "Gravity anomalies determined from tracking the Apollo-Soyuz", *Journ. Geophys. Res.*,pp. 30, (1978).

Wang, Y.M., "On the error of analytical downward continuation of the earth's external gravitational potential on and inside the earth's surface", *Journ. of Geodesy, 71* (2),pp. 70-82, (1997).

Wilkinson, J.H., and C. Reinsch, *"Handbook for Automatic Computation, Volume II, Linear Algrbra"*, 439 pp., Springer-Verlag, New York Heidelberg Berlin, (1971).

Wolf, M., "Direct measurements of the earth's gravitational potential using a satellite pair", *Journ. Geophys. Res., 74*,pp. 5295-5300, (1969).

REPORT DOCUMENTATION PAGE

Public reporting burden for this collection of information is estimated to average 1 hour per response, including the time for reviewing instructions, searching existing data sources, gathering and maintaining the data needed, and completing and reviewing the collection of information. Send comments regarding this burden estimate or any other aspect of this collection of information, including suggestions for reducing this burden, to Washington Headquarters Services, Directorate for Information Operations and Reports, 1215 Jefferson Davis Highway, Suite 1204, Arlington, VA 22202-4302, and to the Office of Management and Budget, Paperwork Reduction Project (0704-0188), Washington, DC 20503.

1. AGENCY USE ONLY *(Leave blank)*	2. REPORT DATE August 2000	3. REPORT TYPE AND DATES COVERED Final Report 22 February 1999 - 30 June 2000

4. TITLE AND SUBTITLE Geoid Recovery using Geophysical Inverse Theory Applied to Satellite to Satellite Tracking Data	5. FUNDING NUMBERS NASA Contract NAS5-99123
6. AUTHORS E.M.Gaposchkin	

7. PERFORMING ORGANIZATION NAME(S) AND ADDRESS(ES) Mathematical Geosciences Inc. 55 Farmcrest Ave. Lexington MA 02421	8. PERFORMING ORGANIZATION REPORT NUMBER MG-103

9. SPONSORING/MONITORING AGENCY NAME(S) AND ADDRESS(ES) National Aeronautics and Space Asministration Goddard Space Flight Center Greenbelt, MD 20771	10. SPONSORING/MONITORING AGENCY REPORT NUMBER

11. SUPPLEMENTARY NOTES

12a. DISTRIBUTION/AVAILABILITY STATEMENT See Handbook NHB-2200.2	12b. DISTRIBUTION CODE

13. ABSTRACT *(Maximum 200 words)*

This report describes a new method for determination of the geopotential. The analysis is aimed at the GRACE mission. This Satellite-to-Satellite Tracking (SST) mission is viewed as a mapping mission. The result will be maps of the geoid. The elements of potential theory, celestial mechanics, and Geophysical Inverse Theory are integrated into a computation architecture, and the results of several simulations presented. Centimeter accuracy geoids with 50 to 100 km resolution can be recovered with a 30 to 60 day mission.

14. SUBJECT TERMS Geodesy, Geoid, Celestial Mechanics, Geophyscial Inverse Theory, Potential Theory, GRACE mission, SST data.		15. NUMBER OF PAGES 74
		16. PRICE CODE

17. SECURITY CLASSIFICATION OF REPORT UNCLASSIFIED	18. SECURITY CLASSIFICATION OF THIS PAGE UNCLASSIFIED	19. SECURITY CLASSIFICATION OF ABSTRACT UNCLASSIFIED	20. LIMITATION OF ABSTRACT UNCLASSIFIED